Bio-inspired Iron Complexes for Shape-Selective Hydrocarbon Oxidations

A THESIS SUBMITTED TO THE FACULTY OF THE GRADUATE SCHOOL OF
THE UNIVERSITY OF MINNESOTA
BY

Anusree Mukherjee

IN PARTIAL FULFILLMENT OF THE
REQUIREMENTS FOR THE DEGREE OF DOCTOR OF PHILOSOPHY

Prof. Lawrence Que Jr., Advisor

August 2011

ACKNOWLEDGEMENTS

My journey in graduate school would have not been completed without a network of personal & professional support for which I remain grateful. The mainspring of this journey was the immense support that I received from my advisor Prof. Lawrence Que. Jr., whom I would define as a cornerstone of my career. My decision of joining his lab as a graduate student has left a huge impression on me both professionally and personally. Over the years, my scientific thoughts matured. From an inquisitive student I transformed to an independent scientist. Prof. Que had been immensely supportive throughout this transformation. He gave me the inspiration along with the independence to be a critical thinker, and did not hesitate to provide his valuable opinion when I needed it. His criticisms along with the valuable insights have been very helpful, as they always pushed me to perform better. Apart from all this, I would like to thank him personally for his support during the last year, as my journey during 2010 took an rough turn. The kind gesture along with the supportive attitude at that tumultuous time makes me feel obliged to him for the rest of my life.

There have been many other people who have helped my journey possible. I might forget their names, but the people of the Department of Chemistry have always provided a great support, whether that is a help with fixing my computer, or help with an instrument, or just mere discussion. But the people who deserve the most thanks are my co-workers. As the Que group is always evolving place, I had the fortune of meeting many people with diverse skill sets and interacting together to exchange opinions; moreover their presence inspired me a lot. Two people who have contributed significantly to my professional development are two previous graduate students Dr. Eric Klinker and Dr. Erik Farquhar, to whom I owe a lot. When I joined the Que group, Eric was in his fourth year, and during my initial days he helped me to learn many details in aspect of experimental details or instrumentation techniques. Apart from being a great mentor, Eric made those days very memorable by his jovial nature and charming personality. I also had the opportunity to interact with Erik Farquhar, whom I admired for his profound knowledge. Our casual discussion over coffee or just in the hallway or in the lab always opened doors to new ideas. Erik also taught me how to use various softwares,

whether to obtain a protein picture or simply to use Adobe Photoshop. We overlapped for a long time as he was only one year senior to me and during this time he provided many valuable insights. We had shared many ideas and thoughts over coffees, discussing about our professional goals and also how science as a field is growing or mere random topics. The other people from Que group whom I thank graciously include Dr Tim Jackson, Dr. Adam Fiedler, Dr. Kathy van Heuvelen, Dr. Jason England, Dr. Ken Xue, Dr. Praneeth V. and the list goes on. All of these great scientists helped me to enrich my knowledge by sharing their valuable opinions and science in group meetings or in person. Few other names which must not be forgotten are Dr. Kallol and Iweta Ray and most importantly Partha Das. I basically have no words to thank Kathy and Iweta for their friendship and co-operation that they have extended to me during the journey. My journey with Partha started from our under-graduate days and it will be too little to say that his friendship I value the most.

I will also like to thank my collaborators, Prof. Münck of Carnegie Mellon University and Prof. Fujisawa for their help in this project. I would also like to thank all of my teachers who have taught me to enjoy science. Prof. Swapan Sengupta and Prof. Jyotsna Choudhury are two of my previous professors who have helped me to find out the joy and created interest to go further in the field of inorganic chemistry.

Above all I sincerely convey my gratitude to all of my committee members for being so supportive all through out my journey. Your good self have been very helpful, not only you have agreed to serve in my committee, but also addressed my queries and concerns with your valuable opinions.

Finally, the most important people, to whom I dedicate my thesis is my family. I would not have been able to come to this place of my career, without their support. My parents' blessings gave me the courage to continue this journey. Above all, the values they taught me have helped me to reach the place where I reached today. I am truly blessed to have such a supportive family and wish that I can live up to my parents' expectations and fulfill their dreams.

Abstract

Shape-selective hydrocarbon oxidation is highly important in many industrial processes particularly in petrochemical refining, but is very difficult to achieve under mild conditions. On the other hand, Nature often performs selective hydrocarbon oxidations under ambient conditions. Inspired by Nature we are interested in synthesizing complexes that can perform such shape-selective hydrocarbon oxidations and also identifying the responsible species that discriminates among substrates based on their shape. My work in particular involves modeling a class of iron enzymes, α-ketoglutarate-dependent dioxygenases.

α-Ketoglutarate-dependent dioxygenases are a nonheme iron enzymes that perform oxygen activation under mild conditions and oxidizes hydrocarbons selectively. The best model complex reported so far involves an iron center supported by a tridentate ligand and an α-ketocarboxylate, but no C-H bond oxidation (primary action of enzyme) has been observed. The intent of this research is to generate new model complexes of α-ketoglutarate-dependent dioxygenases that can perform oxygen activation along with selective C-H bond oxidation.

Iron complexes supported by the tridentate nitrogen donor Tp ligand (where Tp is hydrotris(pyrazolyl)borate) and various α-ketocarboxylates are synthesized. Substituents on the pyrazolyl rings of the Tp are modified to generate iron complexes with different steric and electronic requirements. All of these complexes are studied for oxygen activation and their reactions with hydrocarbons are explored. It is observed that this class of complexes is very efficient in oxygen activation and can perform hydrocarbon oxidation. One of the complexes also exhibits shape-selectivity towards small, flat cyclic hydrocarbons. Oxygen activation at low temperatures is also performed to observe and characterize intermediates.

Table of Contents

List of Tables

List of Schemes and Figures

List of Abbreviations

α-KG	α-ketoglutarate
TauD	Taurine/α-ketoglutarate dioxygenase
TPA	Tris(2-pyridylmethyl)amine
6-Me_3TPA	tris(6-methyl-2-pyridylmethyl)amine
N4Py	*N,N*-bis(2-pyridylmethyl)bis(2-pyridyl)methylamine)
TMC	1,4,8,11-tetramethyl-1,4,8,11-tetraaza-cyclotetradecane
DAOCS	Deacetoxycephalosporin C synthase
CAS	Clavaminate synthase
CarC	Carbapenem synthase
TauD	Taurine/α-ketoglutarate dioxygenase
EXAFS	Extend X-ray absorption fine structure
NMR	Nuclear paramagnetic resonance
BPMCN	*N,N'*- bis-(2-pyridylmethyl)-*N,N'*-dimethyl-*trans*-1,2-diaminocyclohexane
Bn-TPEN	*N*-benzyl-*N,N',N'*-tris(2-pyridylmethyl)-1,2-diaminomethane
TMG_3-TREN	1,1,1-tris[2-N^2-(1,1,3,3-tetramethylguanidino)ethyl]amine
Tp^{Ph2}	Hydrotris(3,5-diphenylpyrazol-1-yl)borate
Tp^{Me2}	Hydrotris(3,5-dimethylpyrazol-1-yl)borate
Tp^{tBu}	Hydrotris(3-*tert*butylpyrazol-1-yl)borate
Tp^{iPr2}	Hydrotris(3,5-di*iso*propylpyrazol-1-yl)borate
OBz	Benzoate
BF	Benzoylformate

PRV	Pyruvate
MLCT	Metal to ligand charge transfer band
LMCT	Ligand to metal charge transfer band
THT	tetrahydrothiophene
GC	Gas-chromatography
DHA	9,10-dihydroanthracene
DHN	1,2-dihydronaphthalene
BDE	Bond dissociation energy
DFT	Density functional theory
2,3-HPCD	Homoprotocatechuate-2,3-dioxygenase
4NC	4-nitrocatechol
EPR	Electron paramagnetic resonance
MIOX	*myo*-inositol oxygenase
IPNS	isopenicillin N synthase
HEPD	hydroxyethylphosphonate dioxygenase
ESI-MS	Electrospray ionization mass spectrometry
rR	Resonance Raman
Py5	2,6-bis(bis(2-pyridyl)methoxymethane)pyridine
N-Et-HPTB	anion of *N,N,N′,N′*–tetrakis(2-benzimidazolylmethyl)-2-hydroxy-1,3-diaminopropane
TBP	2,4,6-tri-*tert*-butylphenol
MMO	Methane mono oxygenase
RNR	Ribonucleotide reductase

L^{Ph4}	*N,N,N¢,N¢*-tetrakis[(1-methyl-2-phenyl-4-imidazolyl)methyl]-1,3-diamino-2-propanolate

Chapter 1

Introduction to the α-Ketoglutarate-Dependent Dioxygenases

1.1. Introduction

The key reaction involved in many biologically important transformations is the selective functionalization of organic molecules, and this is accomplished by enzymes under benign conditions.[1] In most cases, the selective functionalization involves the oxidation of organic molecules by oxygen. Although regioselective oxidation of organic molecules is a thermodynamically favorable process, it is kinetically less favored.[2] Since atmospheric oxygen has a triplet ground state and organic molecules usually have a singlet ground state, spontaneous oxidation of organic molecules by oxygen is spin-forbidden.[2,3] The advantageous consequence of this process is the prevention of the uncontrolled combustion of organic materials to carbon dioxide and water. This spin-mismatch also results in the sluggish reactivity of oxygen towards hydrocarbons.[3-6] But the question that has intrigued the chemists and biochemists is how oxygen is incorporated in a biological molecule with such high specificity from atmospheric O_2 under ambient conditions. The answer to this question has fundamental importance and also can have wide applications, including the design of catalysts for the conversion of abundant molecules for fuels and synthons.[1,7]

The kinetic barrier to the low oxygen reactivity can be overcome by activating oxygen to one of its reduced active states by complexation with a paramagnetic metal ion, as simple inversion of an oxygen electron to yield the singlet state directly is highly endothermic.[7] Nature chose this elegant pathway, in the form of metalloenzymes to harness the strong oxidizing potential of oxygen to sustain life. Another advantage of using metal ions in order to regulate biological oxidations is their availability of multiple redox states.[2,3,7] The metalloenzymes responsible for substrate oxidation by activating

dioxygen contain mainly copper (Cu) and iron (Fe) in their active sites.[8,9] This chapter will focus on the iron-based enzymes responsible for oxygen activation.

Iron-containing enzymes that are involved in dioxygen activation can be subdivided into two classes based on their active site structures. One widespread and well studied class involves iron with a porphyrin prosthetic group, known as heme enzymes, a classic example being cytochrome P450 (Figure 1.1).[10] The other class of iron-based enzymes that are rapidly emerging involves iron without the porphyrin prosthetic group, and are therefore known as non-heme iron enzymes.[6,7,11,12] The non-heme iron enzymes can be further subdivided into two classes based on the number of iron atoms present in the active site, mononuclear and dinuclear iron enzymes. A remarkable enzyme of the latter class is methane monooxygenase (MMO), which converts methane, a recalcitrant substrate, to methanol that synthetic chemists find difficult to reproduce.[13]

The mononuclear non-heme enzymes have drawn significant attention recently due to the diverse oxidative transformations they accomplish.[6] Due to the recent availability of the crystal structures of many different enzymes, it has now been established that all of these enzymes share a common structural motif in the active site. This structural motif consists of a mononuclear iron(II) center that is facially coordinated by two histidines and one carboxylato ligand, either an aspartate or a glutamate residue, from the protein backbone. This structural motif has been coined as the '2-His-1-carboxylate facial triad'.[11,14,15]

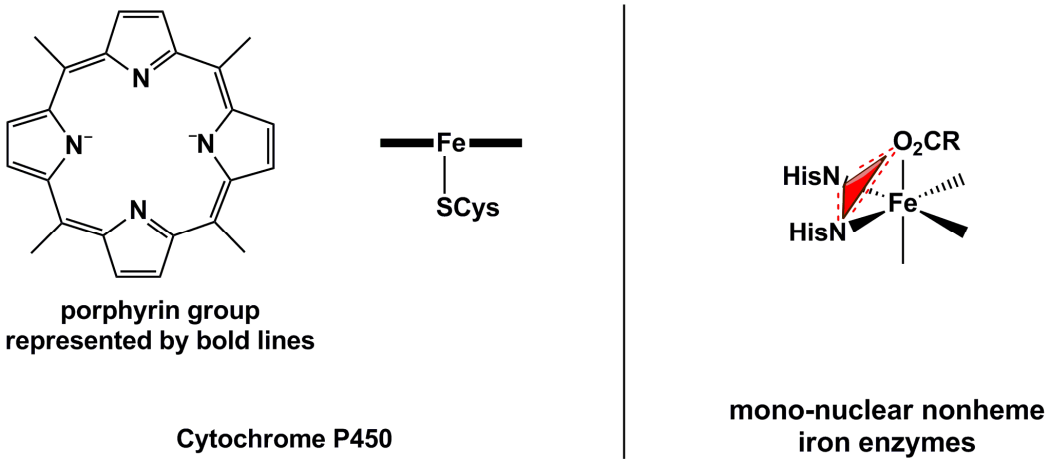

Figure 1.1. Structural motifs of heme and non-heme iron enzymes. Red triangle shows schematic representation of the facial triad.

The largest sub-family of mononuclear nonheme iron enzymes that carry out diverse physiological transformations is known as the α-ketoglutarate (α-KG)-dependent dioxygenases.[3,6,16,17] This class of enzymes requires a sacrificial co-substrate in order to activate oxygen and in the end both of the oxygen atoms derived from dioxygen are incorporated into the products. (Figure 1.2) In the next section few important examples of such reactions will be discussed briefly. This class of enzyme has been implicated in various metabolic pathways, the repair of nuclei acids, and the synthesis of many important biomolecules.

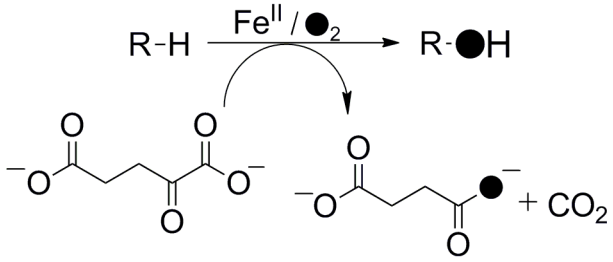

Figure 1.2. The most common type of reaction performed by α-KG-dependent dioxygenases

1.2. Biological Roles of α-KG-dependent Enzymes

Many α-KG-dependent dioxygenases catalyze the hydroxylation of side chains of the proteins, resulting in the modification of proline, lysine, aspartic acid, and asparagine residues.[16] Prolyl 4-hydroxylase catalyzes the hydroxylation of proline at the 4-position to yield the *trans*-4-hydroxyprolyl group (Figure 1.3). In mammals, this transformation is essential for the post-translational modification of procollagen, which is important to the formation of fibrous tissues.[6,18] Aspartyl (asparaginyl) β-hydroxylase modifies the β-carbon of specific aspartic acid or asparagine residues in the epidermal growth factor-like domains of coagulation factors.[19] The modified residues form calcium binding sites, likely to be important for protein-protein interactions.

The most significant role performed by α-KG-dependent dioxygenases that has intensified attention to this class of enzymes is their involvement in the hypoxia response.[19-21] Oxygen deprivation, or hypoxia, occurs during many diseases, such as ischemia, diabetes, and cancer. Hypoxia inducible factor (HIF) is responsible for regulating the mammalian response to hypoxia. HIF hydroxylases have been implicated in this hypoxic response and are therefore interesting targets for therapeutic purposes. HIF hydroxylases are closely related to procollagen prolyl-4-hydroxylase and they hydroxylate two conserved proline residues (Pro402 and Pro564 in HIF-1α) at their 4-positions.[22,23] In subsequent studies the source of the hydroxyl oxygen in the hydroxylated HIF was shown to derive from dioxygen.[24]

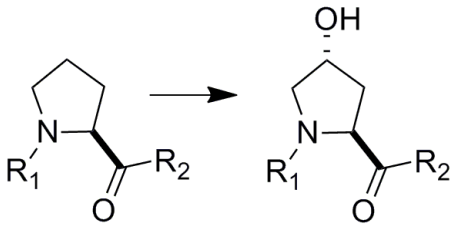

Figure 1.3. Hydroxylation of the prolyl ring at the 4-position by prolyl-4-hydroxylase.

Another medicinally important reaction performed by this class of enzymes is the demethylation of nucleic acids and histones.[25] Irreversible alkylation of the pyrimidine or purine bases of DNA and RNA results in lesions that are both cytotoxic and mutagenic. *Escherichia coli* AlkB and the homologous human enzyme ABH3 repair the lesions by hydroxylating the alkyl group of the pyrimidine or purine ring, and spontaneous deformylation of the hydroxylated alkyl group regenerates the unmodified base.[25-27]

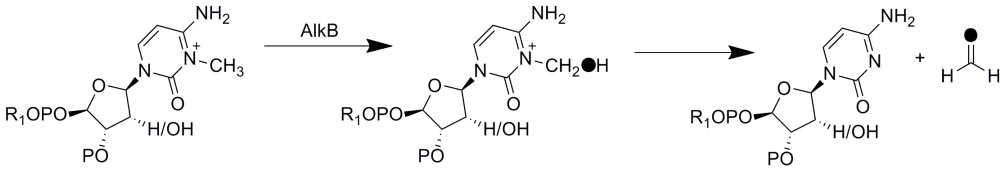

Figure 1.4. Regeneration of the nucleotide by the enzyme AlkB.

Antibiotic synthesis is another important biological transformation performed by α-KG-dependent dioxygenases. Deacetoxycephalosporin C synthase (DAOCS) catalyzes cephalosporin synthesis by performing the ring expansion of the thiazolidine ring of the penicillin N nucleus followed by desaturating the same ring as shown in Figure 1.5.[28,29] Desaturation has been manifested by other α-KG-dependent enzymes, particularly by

clavaminate synthase (CAS), which catalyzes three separate oxidative steps in the synthesis of clavulanic acid. Carbapenem synthase (CarC) exhibits similar desaturation reaction as CAS.[30,31]

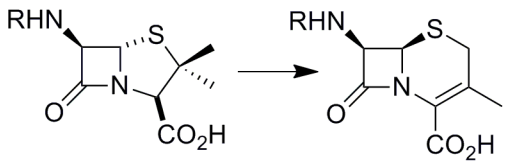

Figure 1.5. Bio-synthesis of the antibiotic Cephalosporin performed by the α-KG-dependent Deacetoxycephalosporin C synthase.

Apart from the aforementioned biologically relevant transformations, these classes of enzymes are also involved in the biosynthesis of plant products and in lipid metabolism.[16] The elegance of all these diverse reactions is that they all involve the same active site structure, 2-His-1-carboxylate facial triad that is retained throughout the catalytic process, and these reactions require the sacrificial co-substrate α-ketoglutarate.

Very recently a new group of non-heme mononuclear iron enzymes has been discovered that requires α-ketoglutarate, dioxygen and chloride for activity, but instead of performing substrate hydroxylation they catalyze halogenation of an aliphatic C-H bond. Many natural products are known in biology that contain a carbon-halogen bond, most often a chloride or a bromide. The enzyme SyrB2 was the first enzyme in the α-KG-dependent family that was discovered to perform such a reaction.[32] The enzyme SyrB2 generates the 4-chloro-L-threonine residue that is incorporated into the framework of the non-ribosomal lipopeptidolactone syringomycine (Figure 1.6). Since the discovery

of SyrB2, non-heme iron enzymes have been identified as being responsible for the biosyntheses of coronatine, barbamide, and dichloroaminobutyrate.[32-34]

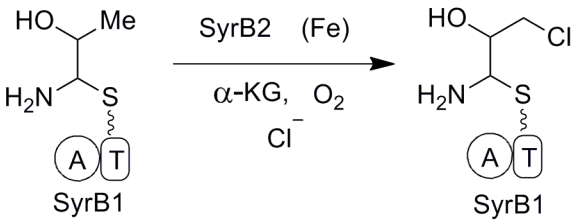

Figure 1.6. Halogenation reaction performed by the enzyme SyrB2, an α-KG-dependent halogenase.

1.3. Mechanism of α-KG-dependent Enzymes

The large body of crystallographic data, together with spectroscopic studies and computational calculations, has led to the proposal of a common mechanism for the α-KG-dependent dioxygenases.[4,35-37] In the resting state of the metalloenzyme, iron is present in its +2 oxidation state in an octahedral geometry and is bound by two histidines, one carboxylate residue and three water molecules[38-40] The proposed mechanism involves an ordered sequential binding of α-KG, substrate and oxygen. The co-substrate α-KG binds in a bidentate fashion, with displacement of two water molecules[31,41-44] (Figure 1.7B), to generate a characteristic UV-vis spectrum with λ_{max} near 500 nm region.[45] The substrate docks near the active site, displacing the third water molecule and making the iron center five-coordinate and primed for the activation of dioxygen (Figure 1.7C).[43,46] The conversion of the coordination sphere from six to five in the presence of native substrates has been crystallographically established in different enzymes.[43,46] It has been

observed in TauD that the rate of the dioxygen activation is notably enhanced for the ternary Fe^{II}-TauD-αKG-taurine complex over the binary Fe^{II}-TauD-αKG complex.[45,47] The enhancement of reactivity toward oxygen after substrate binding is significant as it favors generation of reactive intermediates only in the presence of target substrates and prevents deleterious side reactions. In the presence of substrate, oxygen binding to the metal results in the formation of an iron(III)-superoxo radical species (Figure 1.7D), which is supported by DFT calculations.[48,49] The terminal superoxo oxygen then nucleophilically attacks the carbonyl group of the α-ketoacid to form a putative iron(IV)-peroxo intermediate (Figure 1.7E). This peroxo intermediate then undergoes heterolysis of the O-O bond to generate an iron(IV)-oxo species (Figure 1.7F) concomitant with the de-carboxylation of the α-ketoacid to succinate and CO_2. The iron(IV)-oxo species or ferryl intermediate is thought to be responsible for substrate oxidation.

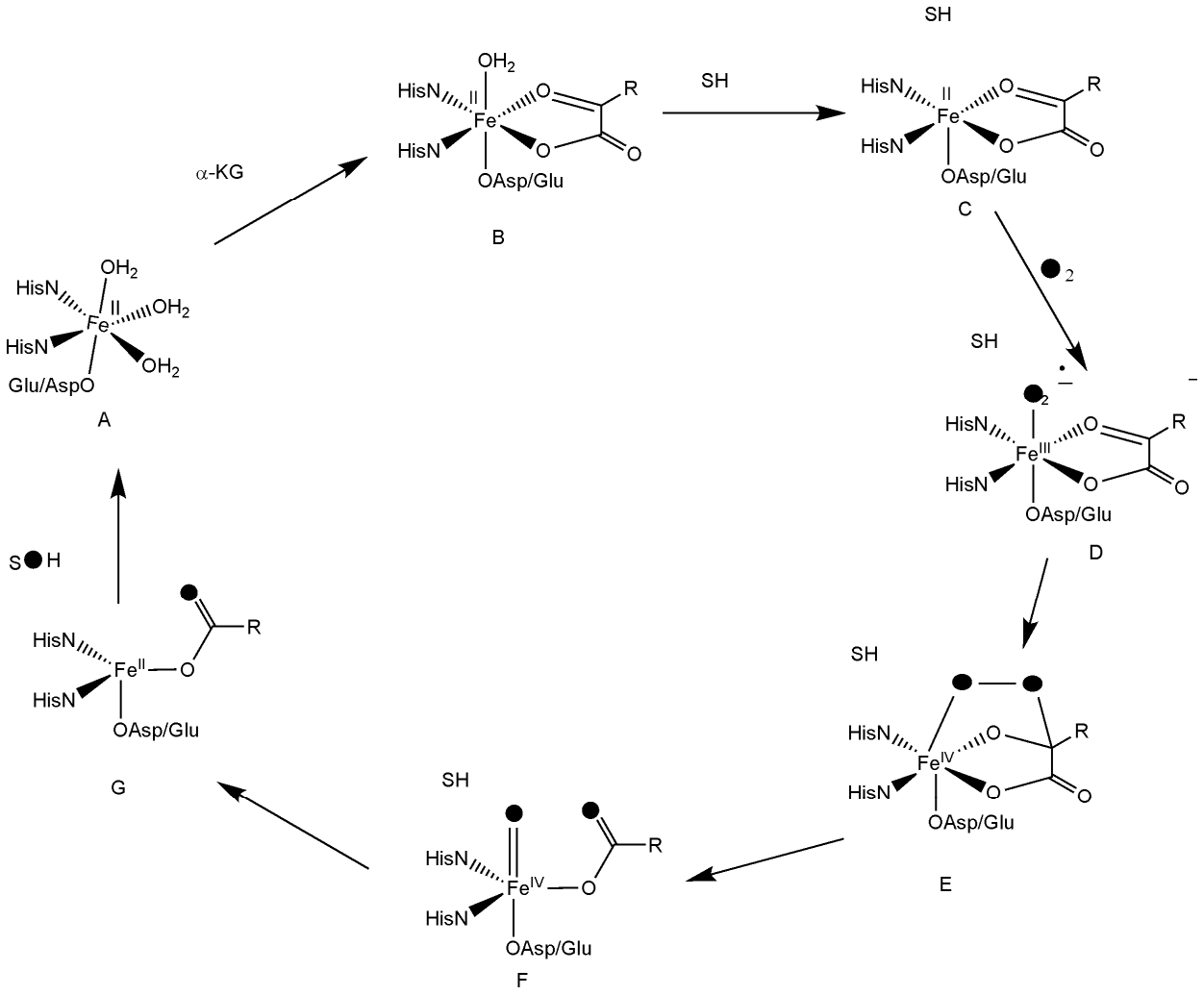

Figure 1.7. Common mechanism proposed for the enzyme α-KG-dependent dioxygenases based on spectroscopic and computational studies.

The competence of the iron(IV)-oxo species for substrate hydroxylation has been supported by recent studies of TauD.[50] Stopped-flow studies on the oxygenation reaction of the ternary Fe^{II}-TauD-αKG-taurine complex shows an intermediate that forms with a λ_{max} of 318 nm, which develops to its maximum extent within 20-25 ms and then decays within ~600 ms.[50] Mössbauer analysis of this intermediate shows that it has an integer

spin ground state with $S \geq 2$. The intermediate, termed as intermediate **J** (Figure 1.8), has an isomer shift of 0.31 mm/s. The fact that cryoreduction of the intermediate gives high spin iron(III) suggests that the species with an isomer shift of 0.31 mm/s should have oxidation state higher than +3. Hence it was concluded that this intermediate contains high spin iron(IV). EXAFS analysis of this intermediate shows a 1.62 Å iron-oxygen interaction indicative of oxoiron(IV).[51] A resonance Raman study on the intermediate shows an oxoiron(IV) vibration at 821 cm^{-1}, supporting the proposed iron(IV)-oxo intermediate.[52] This high-valent species is directly responsible for hydrogen abstraction.[53] Decay of the iron(IV)-oxo species in the presence of deuterated taurine gives rise to a kinetic isotopic effect of *ca* 35, strongly suggesting that it is the key oxidant.[54] The ferryl intermediate observed in TauD gave the first direct evidence of involvement of an iron(IV) intermediate in the reaction catalyzed by α-KG-dependent enzymes.[55] Since then ferryl intermediates have been identified in at least 4 different enzymes belonging to this class.[34,56-58] These results support the mechanism of the α-KG-dependent dioxygenases shown in Figure 1.7.

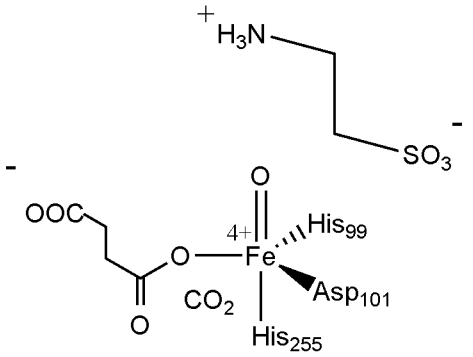

Figure 1.8. Coordination environment of the ferryl intermediate, intermediate **J,** trapped and characterized from the enzyme TauD.

Once the ferryl intermediate is generated, the chemistry of each enzyme diverges and different subsequent steps result in different chemical transformations that this subgroup catalyzes. For TauD and other hydroxylases, the mechanism for this substrate oxidation has a close resemblance to that suggested for cytochrome P450 (Figure 1.9).[59] The ferryl intermediate abstracts a hydrogen atom from the substrate taurine, which is hydroxylated once the coordinated hydroxyl group rebounds to the substrate-derived radical. After oxidizing the substrate the high valent iron(IV)-oxo intermediate returns to the resting state.

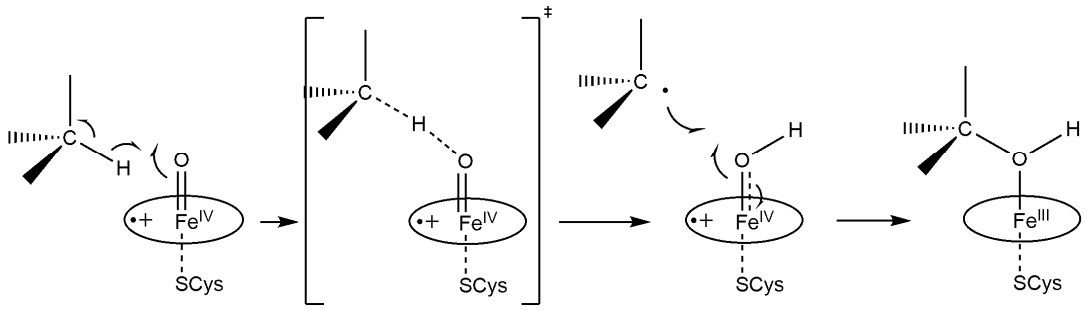

Figure 1.9. Schematic representation of the mode of substrate oxidation by the enzyme cytochrome P450.

For α-KG-dependent halogenases, the proposed mechanism is very similar to that of TauD or prolyl-4-hydroxylase, but the halogenase active site structure is slightly different from that of the α-KG-dependent dioxygenases. (Figure 1.10) In the active site of the halogenases, the aspartate/glutamate residue of the facial triad was replaced by a halide ion.[3,34,60,61] Therefore once the ferryl intermediate abstracts the hydrogen atom from the unactivated C-H bond, the substrate-derived radical preferentially undergoes rebound to the halide ion rather than the hydroxyl ion (Figure 1.11).[33]

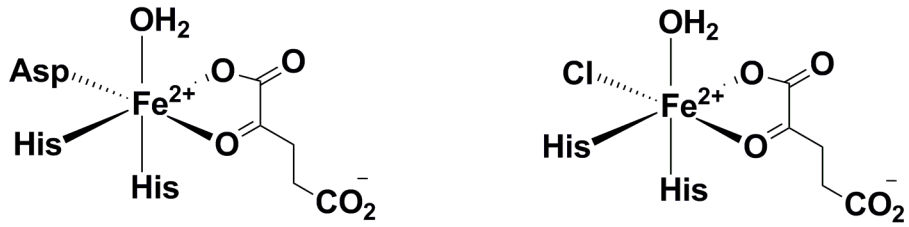

Figure 1.10. Active site comparisons of the two closely related enzymes. (Left) α-KG-dependent dioxygenases (Right) α-KG-dependent halogenases.

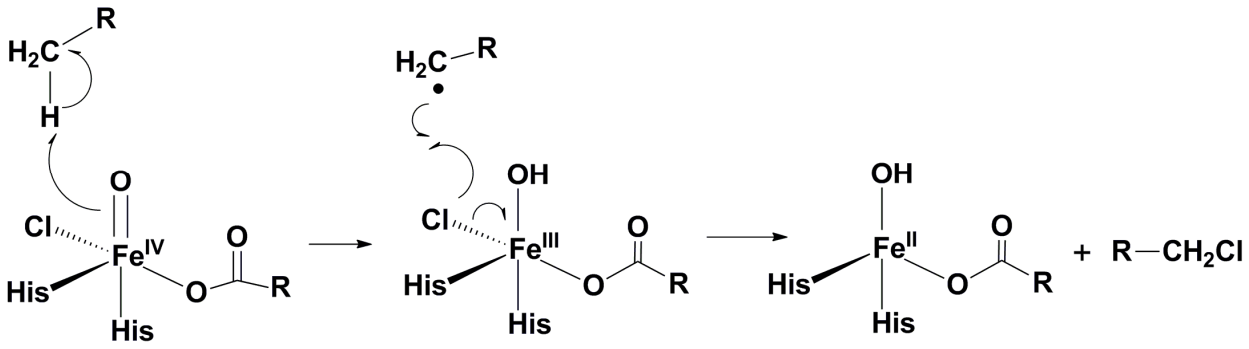

Figure 1.11. Proposed mechanism for halogenation of substrates by the non-heme ferryl intermediate of the α-KG-dependent halogenases.

As mentioned before, some α-KG-dependent enzymes perform desaturation reactions.[38] The proposed mechanism for desaturation involves the same initiation step by the ferryl intermediate, (Figure 1.7F) that is abstraction of the hydrogen atom from the substrate. The reaction mechanism is not clearly established after this first step. In one hypothesis it is proposed that this radical get further oxidized to carbocation followed by a proton transfer to generate the alkene.[62] But the other mechanism shown in Figure 1.12., suggests that the Fe(III)-hydroxyl intermediate abstracts the second hydrogen from the vicinal C-H bond to generate the desaturated compound.[63,64]

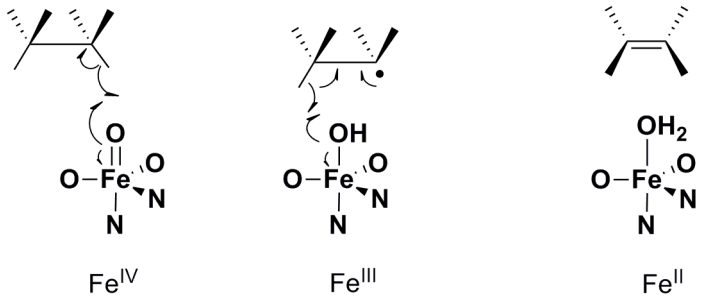

Figure 1. 12. **.** Proposed mechanism for the desaturation of substrates by the non-heme ferryl intermediate of the α-KG-dependent enzymes.

1.4. Modeling α-KG-dependent Enzymes

1.4.1 Structural Modeling

Modeling the enzyme active site is a way to understand the chemistry behind the transformations performed by the enzyme. The goal is to understand electronic structure, reactivity, and chemical mechanism. As the properties of the metal are expected to be the same, studies of small molecules as analogues of enzyme active sites will be helpful in understanding complex proteins. The iron coordination geometry and ligand environment of these model systems can be systematically varied in ways that are not feasible biochemically. Attempts have been made to mimic α-KG-dependent dioxygenases by synthetic model complexes, in order to gain a clear understanding of the mechanism.

Bio-mimetic studies of the α-KG-dependent dioxygenases have evolved in two directions. One of them focuses on the design of structural models that retain the two-nitrogen-one-oxygen coordination sphere of the enzyme active site and the other on preparing functional models of enzymes mainly based on nitrogen rich ligands. Different approaches have been adopted to reproduce the facial coordination mode of the 2-His-1-carboxylate triad. Burzlaff and co-workers have studied the iron coordination mode of the bis(pyrazolyl)acetates.[65] Bis(pyrazolyl)acetates (Figure 1.13) belong to the family of monoanionic *N,N,O*-heteroscorpionate ligands. The ligands are easy to synthesize and steric properties of the ligand can be easily varied by introducing different substituents in the pyrazolyl moiety. Depending on the steric demands of the ligand, different complexes have been obtained, but most commonly they are of the [ML_2] type.[65,66] A ruthenium complex with bis(3,5-dimethylpyrazol-1-yl)acetate with the bidentate α-keto acid, benzoyl formate, has been reported to be the closest model of the mononuclear α-KG-

dependent dioxygenases.[67] However, the nitrogen donor atoms in these model complexes are pyrazoles, not imidazoles as observed in the enzymes. Therefore, in order to obtain a closer resemblance to the active site in terms of size and electronic properties, a new type of ligand system was developed by Gebbink and co-workers.[68] The ligand 3,3-bis(1-alkylimidazole-2-yl)propionate incorporates the biologically relevant 1-methylimidazole and the carboxylato donor group into a tripodal monoanionic framework. Unfortunately, these ligands also result in coordinatively saturated [FeL_2] complexes that lack activity.[3,68,69]

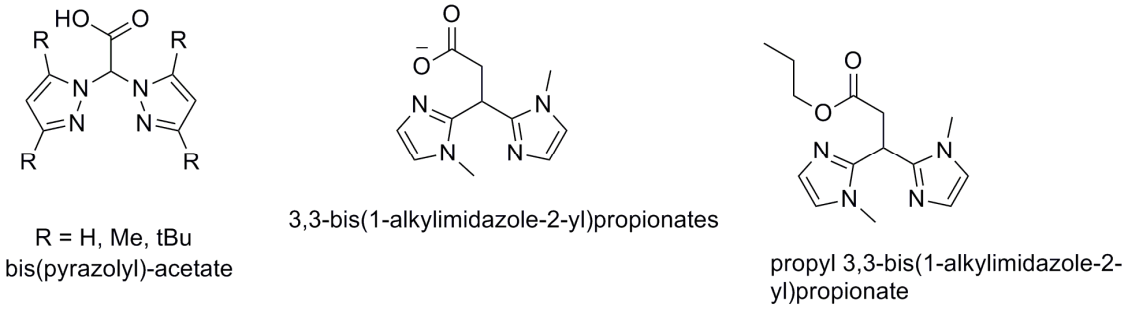

Figure 1.13. Ligands used in structural modeling the 2-His-1-carboxylate facial triad platform of the enzymes.

1.4.2. Functional Modeling: Making Oxoiron(IV) Intermediates

Efforts to make functional model complexes of non-heme mononuclear enzymes have been rewarding and provided considerable insight into the mechanistic details of the enzymes under scrutiny.[70] These functional model complexes mostly focused on using nitrogen rich ligands. The key intermediate responsible for substrate oxidations in the non-heme iron enzyme family is an oxoiron(IV) intermediate.[58] Therefore, many oxoiron(IV) compounds have been synthesized, mostly using alternative oxidants, and they provided valuable insights about the mechanisms of the enzymes. The first example of a non-heme oxoiron(IV) intermediate came from the Weighardt lab using a cyclam-acetato ligand. The oxoiron(IV) species was generated by ozonolysis of a $[Fe^{III}$(cyclam-acetate)(OTf)$]^+$ complex at -40 °C in a water/acetone solvent mixture. The compound was stable for an hour and was characterized by Mössbauer spectroscopy with isomeric shift δ = 0.01 mm/s and ΔE_Q = 1.37 mm/s, but the yield was only 25%, preventing more detailed characterization by other techniques.[71]

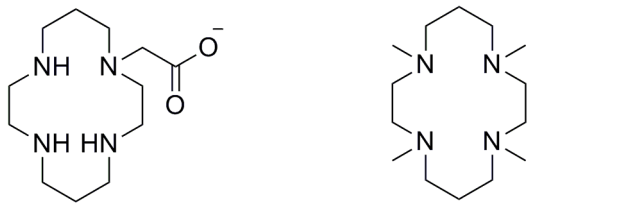

cyclam acetate tetramethylcyclam

Figure 1.14. Macrocyclic ligands that supported initial high valent ferryl intermediates.

The groundbreaking success in synthesizing a non-heme oxoiron(IV) compound comes from the Que and Nam groups, using the macrocyclic TMC ligand platform

(Figure 1.14). When [Fe(TMC)(OTf)](OTf) complex was treated with PhIO at – 40 °C in MeCN, a green solution was generated with λ_{max} at 820 nm (ε = 400 M^{-1} cm^{-1}). The green species was characterized by Mössbauer spectroscopy and identified as an iron(IV) complex with parameters δ = 0.17 mm/s and ΔE_Q = 1.24 mm/s, corresponding to an S = 1 spin state.[72] The complex $[Fe(O)(TMC)(CH_3CN)]^{2+}$ was stable at – 40 °C allowing it to be crystallographically characterized. After this seminal work, Que group and others have contributed significantly to the development of multiple oxoiron(IV) complexes, supported by diverse ligands. [Figure 1.15 and Table 1.1] They all have a short iron-oxygen bond and their Mössbauer parameters suggest an S = 1 ground electronic state. However, the electronic ground state of these oxoiron(IV) complexes is significantly different from the S = 2 ground state of intermediate **J** and other oxoiron(IV) compounds observed in enzymes.[9,58,70]

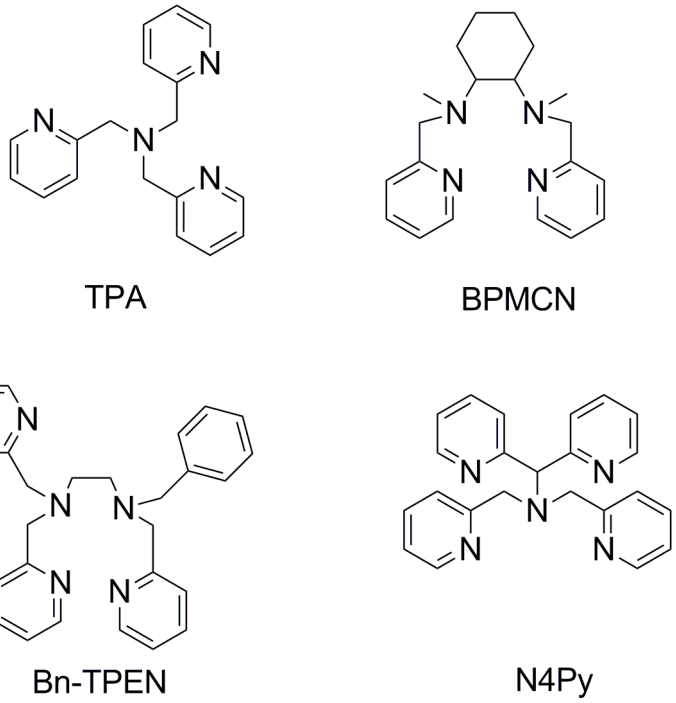

Figure 1.15. Examples of synthetic ligands used to generate high-vaent oxo-iron complexes.

Table 1.1 Properties of some representative examples of oxo-iron(IV) complexes

	r(Fe-O) (Å)*	λ_{max} (nm)	δ (mm/s)	ΔE_Q (mm/s)	Ref
$[Fe(O)(TMC)(NCMe)]^{2+}$	**1.646(3)**	282 820	0.17	1.24	[72]
$[Fe(O)(TPA)(NCMe)]^{2+}$	1.67	724	0.01	0.92	[70]
$[Fe(O)(N4Py)]^{2+}$	**1.639(5)**	695	0.04	0.93	[70]
$[Fe(O)(Bn\text{-}TPEN)]^{2+}$	1.67	739	0.01	0.87	[70]
$[Fe(O)(BPMCN)(NCMe)]^{2+}$	1.66	753	0.07	1.02	[70]
*Intermediate **J***	*1.62*	*318*	*0.31*	*-0.88*	[58]
$[Fe(O)(TMG\text{-}TREN\text{-}d_{36})]^{2+}$	***1.661(2)***	*825*	*0.09*	*-0.29*	[73]
$[Fe(O)(OH_2)_5]^{2+}$			*0.38*	*-0.33*	[74]

*Distance obtained from crystallography shown in bold; high spin (S = 2) systems are shown in italics

The preparation of an isolable synthetic oxoiron(IV) complex with an S = 2 ground electronic state continued to stymie synthetic chemists until 2009. This is not surprising as DFT predicts that a high-spin ferryl intermediate will be very reactive.[75-77] Examples of ferryl intermediates known till that date have intermediate spin states (S = 1) due to the strong ligand field environment exerted by N-rich octahedral ligand. The only known example of an oxoiron(IV) complex in a high spin ligand environment was $[Fe(O)(OH_2)_5]^{2+}$ but its very short lifetime at 25 °C prevents its isolation.[74] The first high-yield generation of a ferryl intermediate in a high-spin state came from the Que group in

2009. Strategic design of the ligand and sufficient steric bulk in the ligand framework stabilized the ferryl intermediate at low temperature in a trigonal-bi-pyramidal geometry (Figure 1.16). This ferryl intermediate was also generated from the iron(II) precursor at low temperature in MeCN by the use of an oxo-transfer agent, a soluble iodosyl arene. Upon deuteration of the ligand, Que and coworkers were also able to obtain the diffraction quality crystals of the ferryl intermediate that led to a crystal structure of the complex.[73,78]

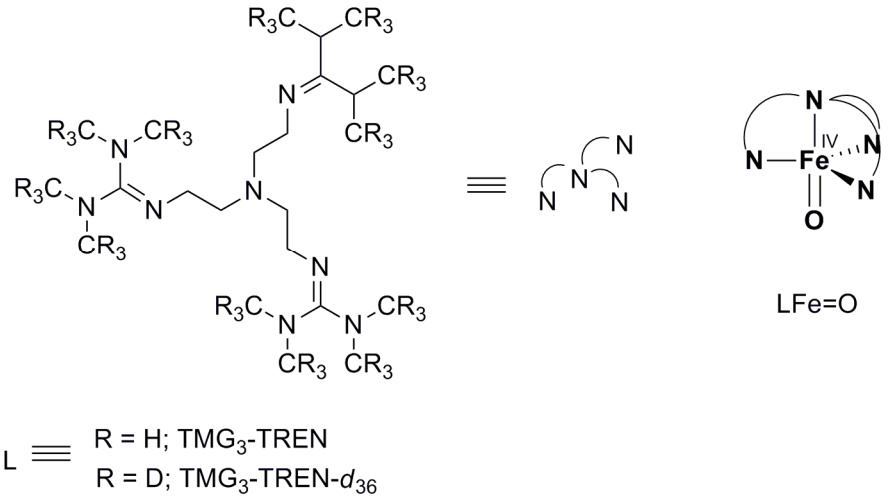

Figure 1.16. Ligand that supported the high-spin ferryl intermediate in trigonal-bi-pyramidal geometry.

1.4.3. Modeling the Reactivity of the α-KG-dependent Enzymes

In parallel to the generation of ferryl complexes to model enzymatic reactions, there has also been an effort to make iron complexes supported by α-ketoacids to test their reactivity with oxyen. Early attempts were made using both the tris-(2-

pyridylmethyl)amine (TPA) and tris-(6-methyl-2-pyridylmethyl)amine ($6Me_3$-TPA) ligands. [Fe^{II}(TPA)(BF)] and [Fe^{II}($6Me_3$-TPA)(BF)] complexes were synthesized using sodium benzoylformate (NaBF) as an α-ketoacid co-substrate and it was found that they both react with oxygen under ambient conditions in acetonitrile.[79,80] The crystal structure of [Fe^{II}($6Me_3$-TPA)BF] showed that the α-ketoacid is bound in a bidentate fashion. This bidentate complex has a characteristic blue-purple (λ_{max} = 544 nm) color due to the metal-to-ligand charge transfer transition. However, the [Fe^{II}(TPA)(BF)] complex is yellow (λ_{max} = 385 nm) in color and the absence of the characteristic blue-purple color suggests that BF is not bound in a bidentate fashion, even in the solution state.[79] Both of these complexes perform oxygen activation but at different rates. [Fe^{II}($6Me_3$-TPA)BF] takes one week to give a quantitative yield of oxygen-incorporated benzoate (produced from decarboxylation of BF), whereas the Fe^{II}(TPA)BF complex takes two days to react completely.[79,80] The slow rate of oxygenation can be attributed to the coordination environment around the metal. In both of these complexes, the iron center is coordinatively saturated. Hence oxygen binding to the metal center, a very important step for oxygen to get reduced, is highly disfavored. Moreover, the difference in the rate of oxygenation suggests that the ligand environment plays some role in dioxygen activation.

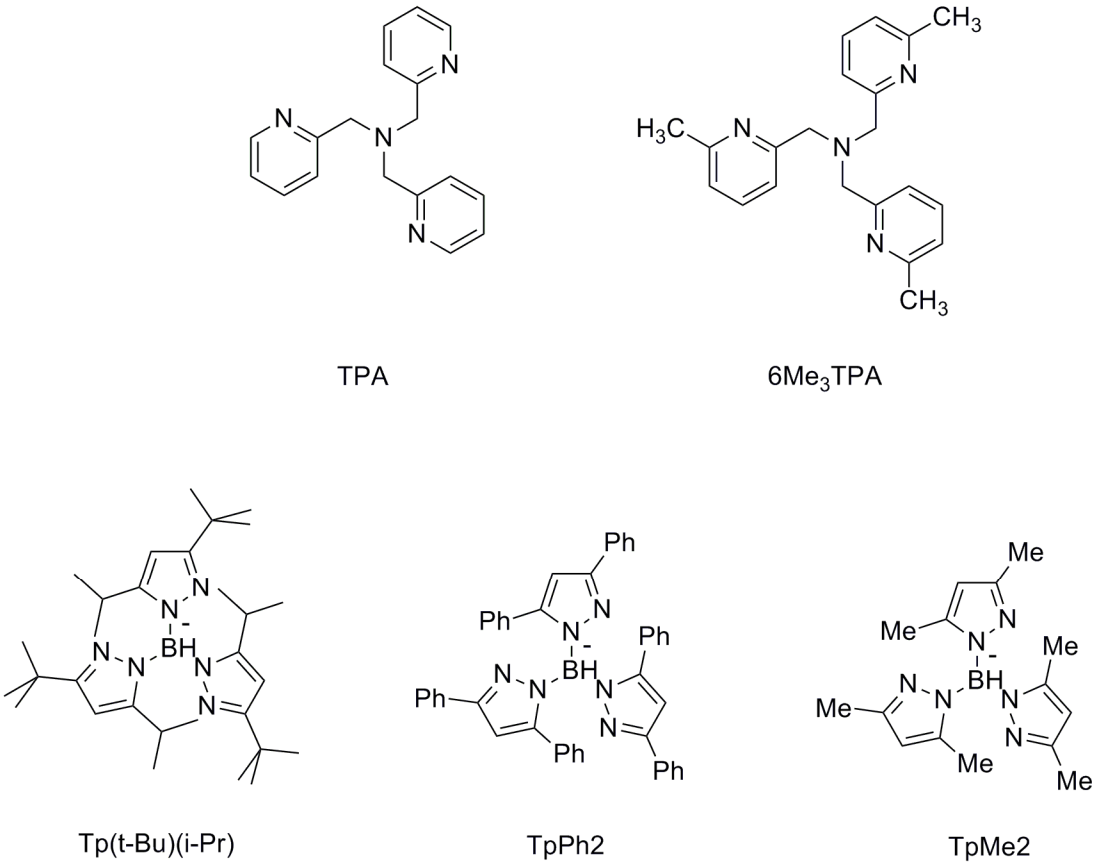

Figure 1.17. Synthetic ligands used to mimic the oxygen activation reaction performed by the α-KG-dependent dioxygenases.

Although iron complexes of both TPA and $6Me_3$-TPA ligand were successful in modeling activation of oxygen, albeit slowly, tridentate ligands were subsequently utilized in order to enhance the rate of oxygenation. Hydrotris-3,5-dimethylpyrazolylborate (Tp^{Me2}) and Hydro(tris-3,5-diphenylpyrazolyl)borate (Tp^{Ph2}) ligands (Figure 1.17) have also been used in enzyme modeling. It has been observed that these [$Fe^{II}Tp^{RR}$(BF)] complexes also have a blue-purple color, suggesting that the BF binds in a bidentate mode.[81] The first successful substrate oxygenation using a Fe(II) complex having a Tp ligand motif and an α-ketoacid was observed by Valentine *et al.*

who showed that [$Fe^{II}Tp^{Me2}$(BF)] performs alkene epoxidation. The complex [$Fe^{II}Tp^{Me2}$(BF)] can epoxidize cyclohexene and *cis*-stilbene but not *trans*-stilbene, suggesting that the reaction between the substrate and the oxidant proceeds through an associative pathway. This is claimed to be the first successful model of an α-ketoacid dependent enzyme, as it can oxygenate both the α-ketoacid cofactor and a substrate. In a related study a hindered structural model of α-KG-dependent enzymes was synthesized by Kitajima using the [$Tp^{(tBu)(iPr)}$] ligand. This [$Fe^{II}(Tp^{(tBu)(iPr)})$(BF)] complex successfully mimicked the enzyme structurally but proved inert towards dioxygen activation.[82] The inertness of this complex is attributed to steric congestion around the metal center.

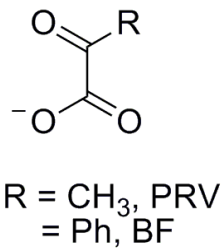

Figure 1.18. α-ketoacids used in the synthetic model complexes.

The dioxygenase nature of the α-ketoacid dependent enzyme is mimicked by [$Fe^{II}(Tp^{Ph2})$(BF)] complex. [$Fe^{II}(Tp^{Ph2})$(BF)] also produces a red-violet chromophore (λ_{max} = 531 nm), suggesting the bidentate coordination mode of the benzoylformate and the crystal structure of the complex shows a five-coordinate iron center.[83] [$Fe^{II}(Tp^{Ph2})$(BF)] can activate dioxygen, but intramolecular hydroxylation of the ligand occurs along with benzoate formation as shown in Figure 1.19. The oxygenation of the [$Fe^{II}(Tp^{Ph2})$(BF)] complex generates the iron(II) phenol product that undergoes rapid

oxidation by excess oxygen to the green iron(III)-phenolate complex.[83,84] The green chromophore arises from a phenolate-to-Fe(III) charge transfer transition of the product. This species was further characterized by resonance Raman spectroscopy, which showed vibrations associated with the Fe-O stretch and C-C stretch of the phenolate ring. Diffraction quality crystals of the product were obtained, providing crystallographic confirmation of the hydroxylated product [Fe(Tp^{Ph2*})(BF)] shown in Figure 1.19.[84]

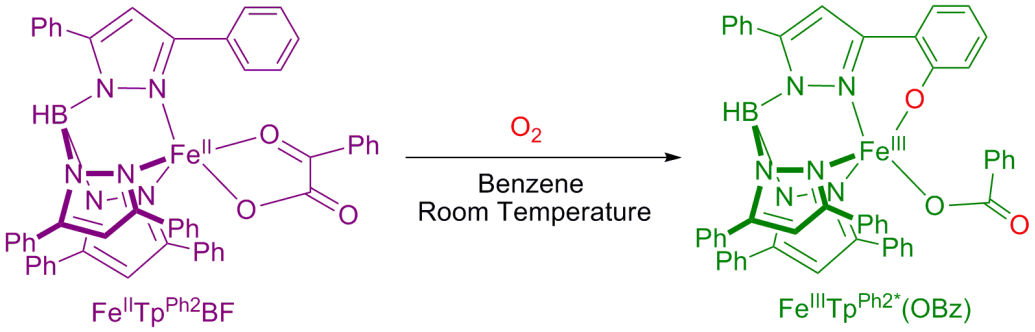

Figure 1.19. Oxygenation of the [$Fe^{II}(Tp^{Ph2})(BF)$] complex results in self-hydroxylation of ligand.

Investigations of the rate of oxygenation of [$Fe^{II}(Tp^{Ph2})(BF)$] with a series of substituted BF complexes suggest that the reaction between the iron complex and dioxygen proceeds through an associative pathway. This intramolecular hydroxylation occurs within one hour at room temperature in benzene.[84] The [$Fe^{II}(Tp^{Ph2})$(benzoate)] complex was also synthesized and the rate of oxygenation was investigated. This complex was found to also react with dioxygen but requires two to three days for completion. Hence it was concluded that the α-ketoacid moiety highly facilitated oxygen activation by the model complex. Isotope labeling studies with $^{18}O_2$ showed that one oxygen atom was incorporated into the benzoate while the other was incorporated into the hydroxylated arene.

Although [$Fe^{II}(Tp^{Ph2})(BF)$] is successful in mimicking the active site of α-ketoacid dependent enzymes structurally and functionally, the mechanism of the reaction remains to be established. The potent oxidant is not yet identified and the oxidation

ability of the oxidant is not fully explored, providing wide scope for further exploration of this reaction mechanism.

1.5. Aim and Scope of the Thesis.

In this thesis, efforts to understand oxygen activation performed by the α-KG-dependent dioxygenases by studying model complexes will be discussed. Chapter 2 describes a functional model complex of the enzyme and its ability to oxidize external substrates. Substrate oxidation was used as a tool to identify the nature of the active oxidant. Oxo-transfer reactions and H-atom abstraction from hydrocarbons with strong C-H bonds clearly suggest that the active oxidant generated in situ from the model complex and oxygen is as powerful as that in α-KG-dependent dioxygenases. The unique selectivity depicted by the model complex in Chapter 2 strongly resemblance that of the encumbered nature of the active site. Chapter 3 explores the reactivity of a related model complex of the α-KG-dependent dioxygenases at low temperature. The results described in chapter 3 gave us the first credible evidence for the existence of an iron-superoxo intermediate in the mechanism of the α-ketoglutarate-dependent enzymes. Chapter 4 describes how oxygen is activated in a model complex that lacks the α-ketoacid.

This thesis significantly enhances our understanding of the mechanism of the α-KG-dependent dioxygenases, and highlights another way to investigate the reaction mechanism, using chemical substrates as a probe. This work also enabled us to identify a functional model complex of the α-KG-dependent dioxygenases that can selectively oxidize substrates based on their access to the active site, quite like the enzymes.

Chapter 2

Selective Oxidation of Hydrocarbons by an Oxygen Derived Oxidant Supported by A Bio-mimetic Iron Complex

A part of the content of this chapter was published in *Angew. Chem. Int. Ed*. **2009**, *49*, 1780-1783

Reproduced in part with permission from *Angew. Chem. Int. Ed.* **2009**, *49*, 1780-1783

Compound Abbreviations

1 = [Fe(Tp^{Ph2})(BF)]

2 = [Fe(Tp^{Ph2*})(OBz)]

3 = [Fe(Tp^{Me2})(BF)]

4 = [Fe(Tp^{tBu})(BF)]

2.1 Introduction

Regioselective oxidation of hydrocarbons or selective functionalization of an unactivated C-H bond is a challenging task and had gained considerable interest in the last few decades.[1,7,85] The catalysts available for attempting such transformations are often degraded by undergoing self-oxidation[86] or cost-ineffective, as they require multiple steps and employ high temperatures and harsh conditions that lead to low reaction selectivity.[87] Nature, on the other hand, unequivocally performs regioselective oxidation of strong C-H bonds, responsible for many important biological transformations.[1] This is accomplished by enzymes under benign conditions, and such selectivity arises due to discrimination of substrates at the enzyme active site based on substrate shape, and size, as well as the access of the substrate towards the active site.[88] Many attempts have been made to generate a compound synthetically that will enable 'shape-selective' oxidation of hydrocarbons.[89] Metalloporphyrin complexes were made to mimic the enzymatic action of the cytochrome P450, an enzyme responsible for regioselective oxidation of hydrocarbons.[59] Although they were able to perform selective epoxidation of hydrocarbons,[89-92] only few examples were known for regioselective hydroxylation of alkanes.[93-95] Suslick and co-workers, was able to hydroxylate straight

chain alkane(s) using metallo-caged porphyrin, also known as bis-pocket porphyrin,[88] but even in that case specific oxidation of the primary methyl group was not observed. Selective oxidation of unactivated hydrocarbons using non-metalloporphyrin complexes was rare,[96-98] even though many nonheme enzymes execute hydrocarbon oxidation selectively.[6]

α-Ketoglutarate-dependent iron enzymes comprise the largest sub-family of dioxygen activating nonheme iron enzymes that share a common active site motif, and perform a diverse array of biological functions, including the biosynthesis of collagen, oxygen sensing in cells, DNA and RNA repair, and the demethylation of histones.[3,6,16] Dioxygen activation occurs at the iron(II) active site in concert with α-ketoglutarate to generate a high-spin iron(IV)-oxo intermediate that effects substrate oxidation.[34,50,53,56,58]

To date, there are only few functional synthetic models for this class of enzymes. In 1995, Valentine and co-workers reported the *in situ* generation of [Fe(Tp^{Me2})(BF)], which upon exposure to O_2 carries out the epoxidation of *cis*-stilbene (but not *trans*-stibene).[81] More recently, Mehn *et al.* reports the isolation of [Fe(Tp^{Ph2})(BF)] (**1**) and its crystallographic characterization.[84] Complex **1** reacts with O_2 in benzene at ambient temperature to form in 70% yield green [Fe^{III}(Tp^{Ph2*})(OBz)] (**2**) that results from oxidative decarboxylation of the benzoylformate (BF) ligand and the hydroxylation of one of the phenyl rings of the Tp^{Ph2}. These examples demonstrate that iron(II)-α-keto acid complexes and O_2 react to generate an oxidant, presumably an iron(IV)-oxo species by analogy to the enzyme results, that can attack olefins and arenes, but there is no example where C-H bonds are cleaved, which is the principal reactivity exhibited by the α-ketoglutarate-dependent iron enzymes.[16] In this chapter, we report experiments

showing that the oxidant generated in the reaction of **1** with O_2 can be intercepted intermolecularly by added hydrocarbons, resulting in the dehydrogenation of the latter. We find that the extent of trapping is governed by both the strength of the C-H bond and the shape of the hydrocarbon. Moreover, it is also observed that the oxidant responsible for such transformation can attack strong C-H bonds. Further exploration reveals that this selectivity is intrinsic to the putative oxidant [Fe(O)(Tp^{Ph2})(OBz)], and how the rudimentary 'pocket' of the [Fe(O)(Tp^{Ph2})(OBz)] allows the complex **1** to be the first bio-mimetic pre-oxidant to perform selective ω-oxidation of a linear alkane.

2.2 Experimental Section

Materials and methods

All reagents and solvents were purchased from commercial sources and used without further purification unless otherwise stated. Preparation and handling of air-sensitive materials were carried out under inert atmosphere using standard Schlenk techniques or a glovebox. The ligands $K(Tp^{Ph2})$, $K(Tp^{Me2})$, $Tl(Tp^{tBu})$ were prepared as previously reported.[99] Sodium benzoylformate was purchased from Aldrich. The complex $[Fe(Tp^{Ph2})(BF)]$ was prepared as previously reported.[83] 9,10-dihydroanthracene was purchased from Aldrich and recrystallized from ethanol prior to use.[100] The complex $FeTp^{Me2}BF$ was also prepared by modifying the published procedure slightly.[81]

Synthesis of $[Fe(Tp^{Me2})(BF)]$ (3)

To a mixture of KTp^{Me2} (0.074 g, 0.25 mmol) and $Fe(OTf)_2$ 2MeCN (0.10 g, 0.25 mmol) in dichloromethane/MeCN (3 mL), sodium benzoylformate (0.043 g 0.25 mmol) was added, resulting in an immediate color change of the solution from colorless to bluish-purple. This cloudy solution was stirred for an hour at room temperature. The solid was then filtered and dried in vacuo. The complex has a similar UV- vis that like **1** with the peak at 555 am along with a shoulder at 610.

Synthesis of $[Fe(Tp^{t\text{-}Bu})(BF)]$ (4)

To a mixture of $TlTp^{t\text{-}Bu}$ (0.146 g, 0.25 mmol) and $Fe(OTf)_2$ 2MeCN (0.10 g, 0.25 mmol) in dichloromethane (3 mL), sodium benzoylformate (0.043 g 0.25 mmol) was added resulting in an immediate color change of the solution from colorless to bluish-purple. This cloudy solution was stirred for an hour at room temperature. The solution was then filtered and dried in vacuo. Anal. Calcd for **3**, $C_{30.4}H_{41.6}BCl_2FeN_{6.2}O_3$

[$C_{29}H_{39}BFeN_6O_3$•CH_2Cl_2•0.2CH_3CN], (678.41 g/mol): C, 53.74; H, 6.17; N, 12.78. Found: C, 53.68; H, 6.13; N, 12.72. UV- vis [λ_{max}, nm in Benzene]: 505 (sh), 550, 610 (sh).

Physical Methods

UV-vis spectra were recorded on a HP 8452A diode-array spectrometer with a temperature controlled bath set to 25 °C. Electrospray ionization mass spectral experiments were carried out on a Bruker BioTOF II mass spectrometer using the following conditions: spray chamber voltage = 4000 V; gas carrier temperature = 200 °C. GC product analyses were performed on a Perkin-Elmer Sigma 3 gas chromatograph (AT-1701 column, 30 m) with a flame ionization detector. For *n*-alkane oxidations GC experiments were carried out using naphthalene as an internal standard, on an Varian Star 3400 CX gas chromatograph (Restek column, Rxi-1ms, 1.0 micrometer film thickness) with a Varian Saturn 3 GC/MS detector.

2.3 Oxygenation of Complex 1 in the Presence of Thioethers

When the oxygenation reaction of **1** was carried out in the presence of thioanisole, the green chromophore was not observed; instead the red-violet chromophore of **1** faded to a colorless solution. (Figure 2.1). ESI-MS analysis of the resulting solution revealed one prominent peak at m/z 865.1, corresponding to the $[Fe(Tp^{Ph2})(PhS(O)CH_3)]^+$ ion. GC analysis found that methyl phenyl sulfoxide was in fact formed in 70% yield, while Mössbauer spectroscopy showed that all the iron in the oxygenated sample was in the high-spin iron(II) state with 75% of the iron having an isomer shift and a quadrupole splitting identical to that of a sample derived from the addition of $PhS(O)CH_3$ to $[Fe(Tp^{Ph2})(OBz)]$ (Figure 2.2).[101] Monitoring the reaction by ^{1}H-NMR showed the disappearance of paramagnetically shifted features associated with **1** and their replacement by features of $[Fe^{II}(Tp^{Ph2})(OBz)]$, so oxidative decarboxylation occurred. (Figure 2.3). Addition of 1 equiv PhSMe was sufficient to suppress the 650 nm chromophore by 65%, and addition of 10 equiv PhSMe completely prevented its appearance. Thus PhSMe is capable of fully intercepting the oxidant generated in the reaction of **1** with O_2 and preventing the intramolecular hydroxylation of a ligand phenyl group.

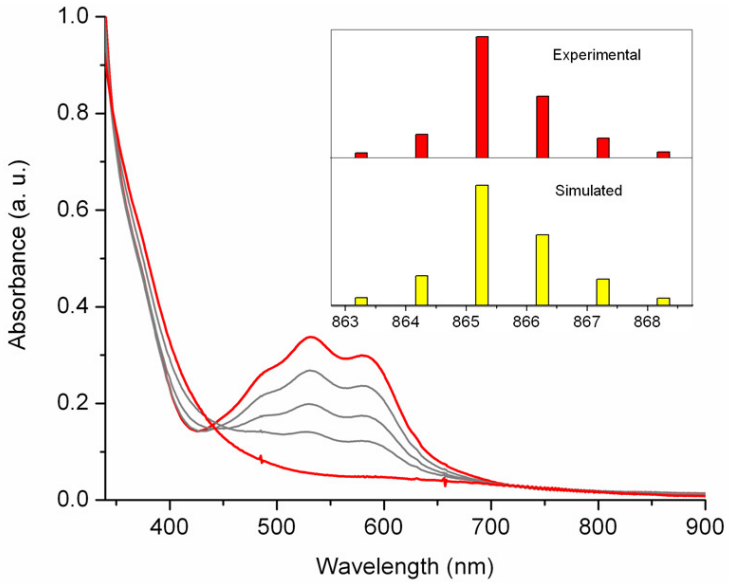

Figure 2.1. Spectral changes monitored when oxygenation of **1** (~1.25mM in benzene, l = 0.5 cm) was performed in the presence of excess thioanisole. Inset: ESI-MS analysis of the colorless solution generated at the end of the reaction showed a peak with *m/z* = 865.

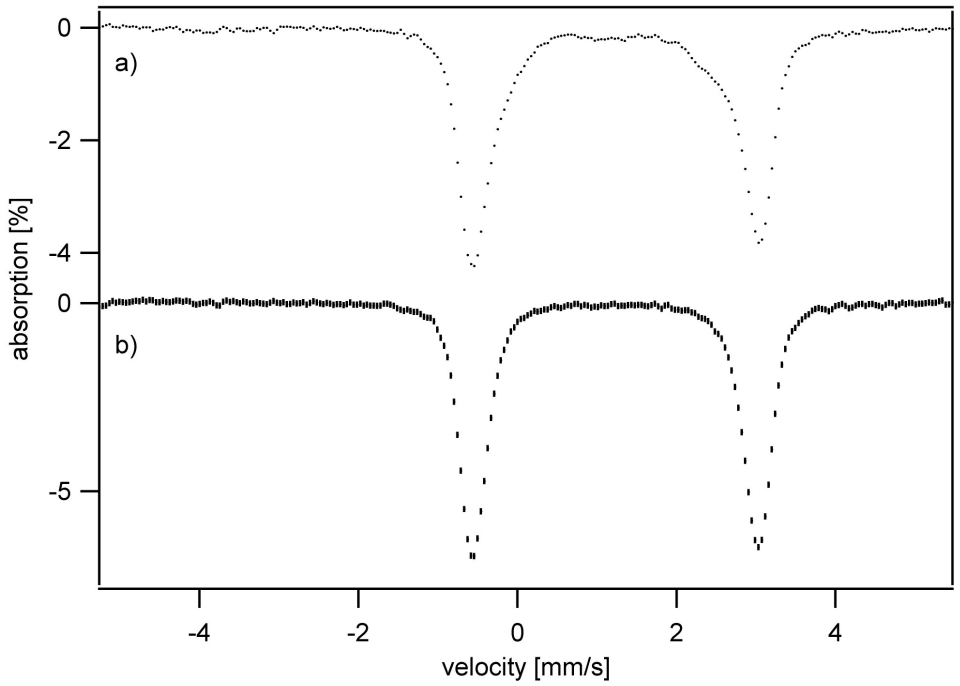

Figure 2.2. (a) Mössbauer spectrum at the end of the reaction of **1** and oxygen in the presence of thioanisole. Isomeric shift of the major species was observed at 1.22 mm/s with ΔE_Q = 3.6 mm/s (75%) (b) Mössbauer spectrum of separately prepared [$FeTp^{Ph2}$(PhSOMe)(OBz)], with isomeric shift 1.23 mm/s and ΔE_Q = 3.58 mm/s. Sincere thanks to Prof. Münck and his group at Carnegie Mellon University for their help in Mössbauer measurements.

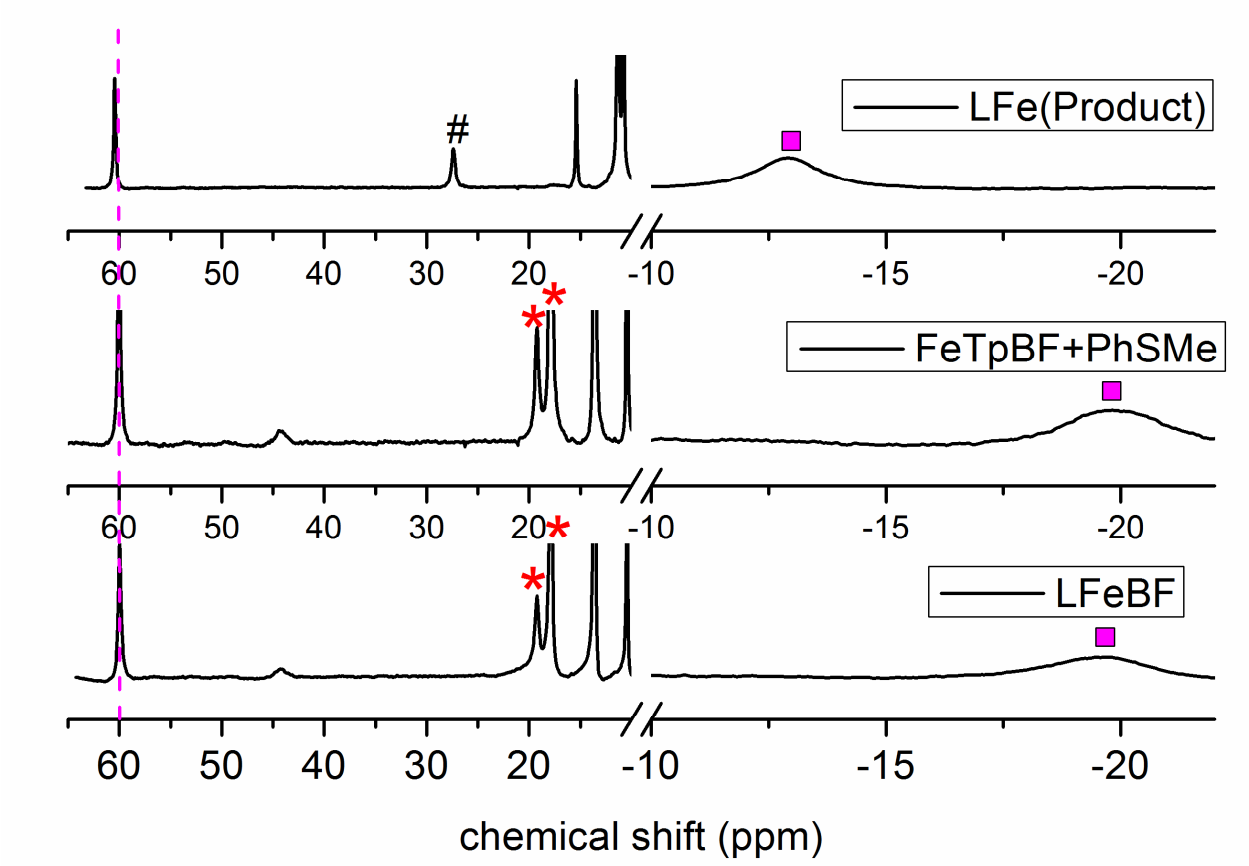

Figure 2.3: A) ^{1}H-NMR spectrum of FeTp^{Ph2}BF complex. The broad peak at – 20 arises from the *ortho*-proton of 3-phenyl group of the ligand, and is marked by the filled square. Protons from benzoylformate (BF) were shown by asterick (*) at 20-10 ppm. B) ^{1}H-NMR spectrum of the FeTp^{Ph2}BF complex with excess thioanisole (PhSMe). Addition of thioanisole resulted in no observable change in the NMR spectrum. C) ^{1}H-NMR spectrum after bubbling dioxygen to a solution of FeTp^{Ph2}BF and thioanisole. A different spectrum was obtained. Peaks associated with BF were gone, and the high field peak at – 20 ppm was shifted to – 12 ppm. C has peak similar to FeTp^{Ph2}OBz[84] peaks corresponding to benzoylformate were gone and benzoate peaks were observed (marked with #). This suggests successful decarboxylation of the benzoylformate upon

oxygenation in the presence of thioanisole. The shift observed for the *ortho*-proton of the 3-phenyl group (marked by filled square) of the ligand Tp^{Ph2}, suggest binding of PhSOMe to the iron center. This binding might result in decrease in the paramagnetic interaction between the *ortho*-proton and the Fe(II).

Reaction with other thioethers occured in a similar fashion and ESI-MS spectrum supported formation of sulfoxide adducts as major products. Tetrahydrothiophene (THT) led to full interception when the reaction was carried out with 0.1 M of substrate (Figure 2.4), and ESI-MS analysis of the resulting solution revealed one prominent peak at m/z 829.1, corresponding to the $[Fe(Tp^{Ph2})[(CH_2)_4SO]]^+$ ion. When the reaction was performed in the presence of diphenyl sulfide, the product diphenyl sulfoxide was also characterized by ESI-MS and a 74% yield was determined by GC.

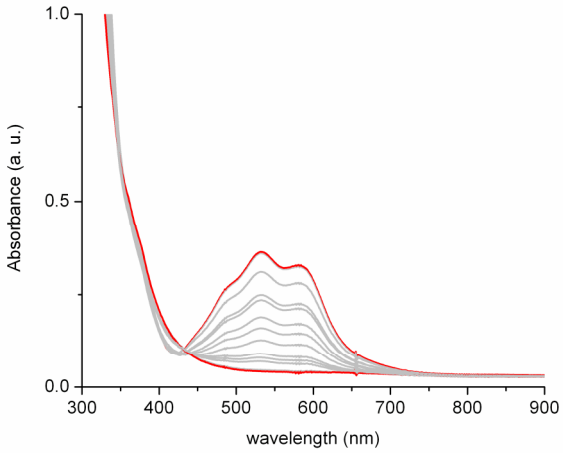

Figure 2.4. Spectral changes monitored when oxygenation of **1** (~1.25 mM in benzene, l = 0.5 cm) was performed in the presence of excess tetrahydrothiophene.

As mentioned earlier, all thioethers were very efficient in complete prevention of the ligand hydroxylation when used in excess. However, when stoichiometric amounts of the different thioethers were used, the amounts of interception varied. Figure 2.5 illustrates the difference in the extent of ligand hydroxylation when tetrahydrothiophene and diphenylsulfide were used as substrates. Diphenylsulfide, a thioether with two bulky phenyl substituents, showed only 40% interception, whereas tetrahydrothiophene showed 90% interception. The amount of interception with thioanisole was 65% under stoichiometric conditions. When 4-nitrothioanisole or 4-methoxythioanisole was used as substrates, the percent of interception remained comparable to that of thioanisole.

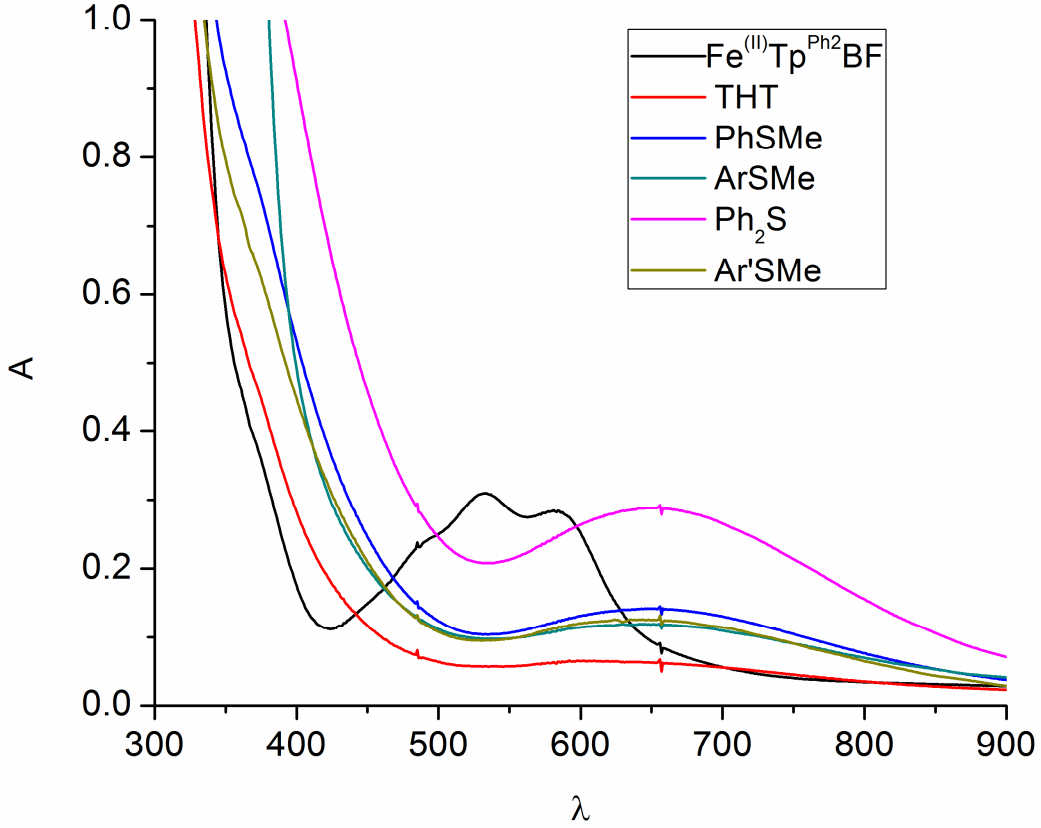

Figure 2.5. . UV-vis spectral changes monitored when oxygenation of **1** was performed in the presence of 1 mM of thioethers in a 0.5-cm cell. Legends for each thioether: pink: diphenyl sulfide, blue: thioanisole. green: 4-nitrothioanisole (ArSMe), olive: 4-methoxythioanisole (Ar′SMe), red: tetrahydrothiophene.

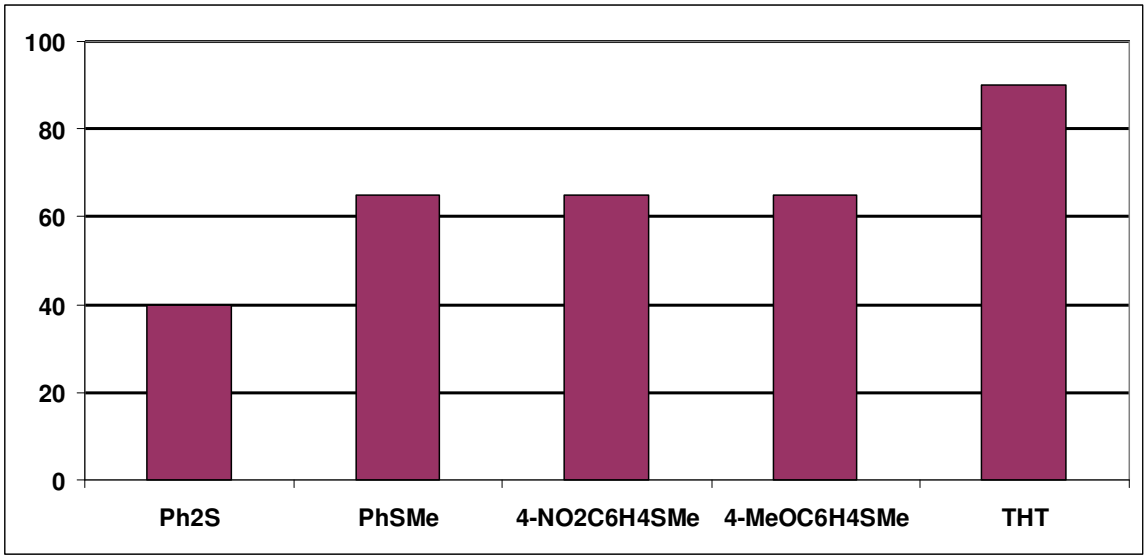

Figure 2.6. Different amounts of interception in the reaction of **1** and O_2 in the presence of stoichiometric amounts of thioethers in benzene at 25 °C. Each thioether has different steric and electronic properties. The Y-axis represents the amount of interception. A gradual enhancement in the amount of interception was observed when oxo-philicities of the thioethers were enhanced, and steric properties were reduced.

The interception trend among thioethers could be explained considering their steric and electronic properties. Tetrahydrothiophene was the most efficient in preventing ligand hydroxylation at 1 mM concentration and the Ph_2S was the least. (Figure 2.6) Thioanisoles and *para*-substituted thioanisoles showed similar amounts of interception.

2.4 Oxygenation of 1 in the Presence of Hydrocarbons

The thioether oxidations performed by the oxidant generated in situ from **1** and O_2 paved our way to investigate whether hydrocarbons could also intercept this oxidant. Figure 2.7 shows the reaction of **1** with O_2 in the presence of 0.1 M 9,10-dihydroanthracene (DHA). Anthracene was formed as a product, as indicated by the appearance of its three characteristic sharp peaks at 379, 357, and 339 nm after a period of 1 hr. UV quantification after removal of iron showed an anthracene yield of 35%, while the residual absorbance at 650 nm suggested that **2** was formed at only 20% of its original level.[101] Initial success with oxidation of DHA, by the putative oxidant generated from **1,** prompted us to further investigate an array of added substrates with different C-H bond strengths, sizes, and shapes. Figure 2.8 shows ligand hydroxylation was prevented in the presence of 1,2-dihydronaphthalene (DHN) as a substrate (0.1 M). Under these conditions, 80% of the ligand hydroxylation was prevented and the spectrum at the end showed a band at 350 nm along with minor absorbance at 650 nm. GC analyses of the solution at the end after removal of iron showed naphthalene as the product (30% yield with nitrobenzene as internal standard). Similar results were obtained with 0.1 M cyclohexene, where the amount of **2** formed decreased by a factor of 4. Cyclohexadiene was obtained in 40% yield, and neither 2-cyclohexenol nor 2-cyclohexenone was observed as products. Thus, under these conditions, DHA, DHN and cyclohexene were capable of intercepting about 75-80% of the oxidant responsible for the self-hydroxylation reaction.

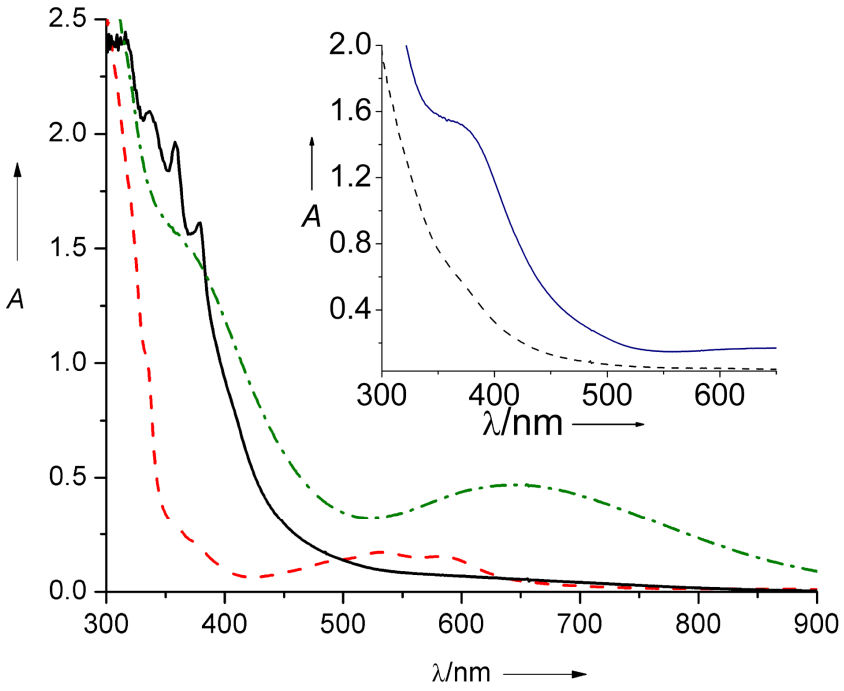

Figure 2.7. Spectral changes observed in the reactions of **1** (1 mM) with O_2 saturated in benzene at room temperature in a 0.5-cm cell after 1 h. Main plot: dashed line, **1** alone; dashed-dotted line, **1** + O_2; solid line, **1** + O_2 + 0.1 M DHA. Inset: solid line, **1** + O_2 + 0.1 M cyclohexene; dashed line, **1** + O_2 + 0.1 M thioanisole.

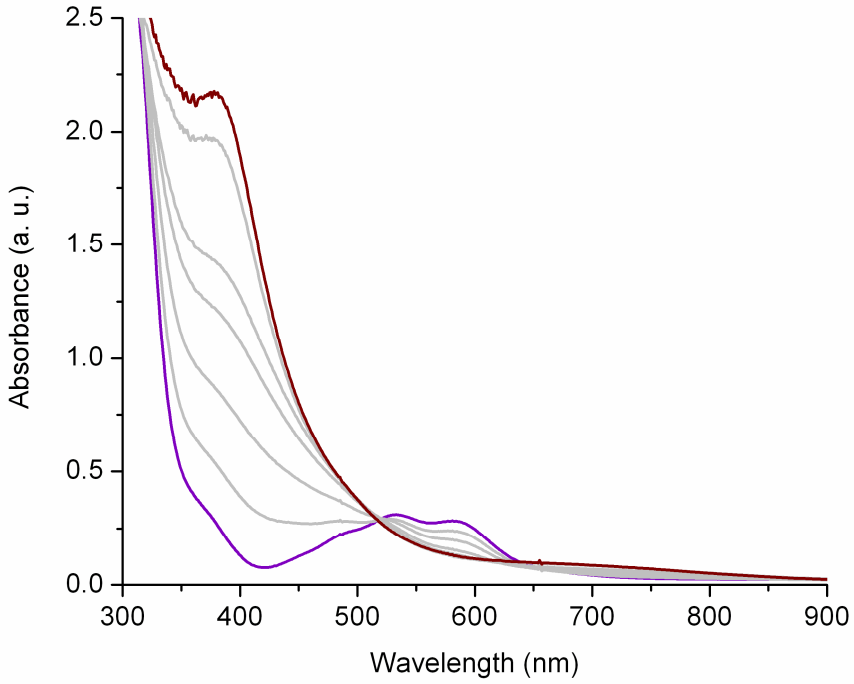

Figure 2.8. Spectral changes observed in the reactions of **1** (1 mM) with O_2 in the presence of 1,2-dihydronaphthalene in benzene at room temperature in a 0.5-cm cell after 1 hour.

Scheme 2.1 shows some of the representative examples of added substrates that were also capable of intercepting the O_2-derived oxidant at a concentration of 0.1 M. Besides DHA and cyclohexene, cyclopentane and cyclooctane also reacted with the [Fe=O] oxidant, but their trapping efficiency was significantly lower, probably due to their stronger C-H bonds. On the other hand, cyclohexane did not affect the ligand hydroxylation at all, under these conditions. For other substrates the dehydrogenation product was obtained consistently. The only exception was fluorene, absence of a vicinal C-H bond in the fluorene allowed the carbon-centered radical to float away and be

trapped by the excess oxygen to generate the hydroxylated product, which undergoes further oxidation to fluorenone.

***Scheme* 2.1**. Hydrocarbon substrates studied to intercept the putative Fe^{IV}=O oxidant. % values indicate the extent to which the green chromophore was decreased in the presence of 0.1 M substrate; values in parentheses are the bond dissociation energies in kcal/mol[102] for the weakest C-H bond in each substrate.

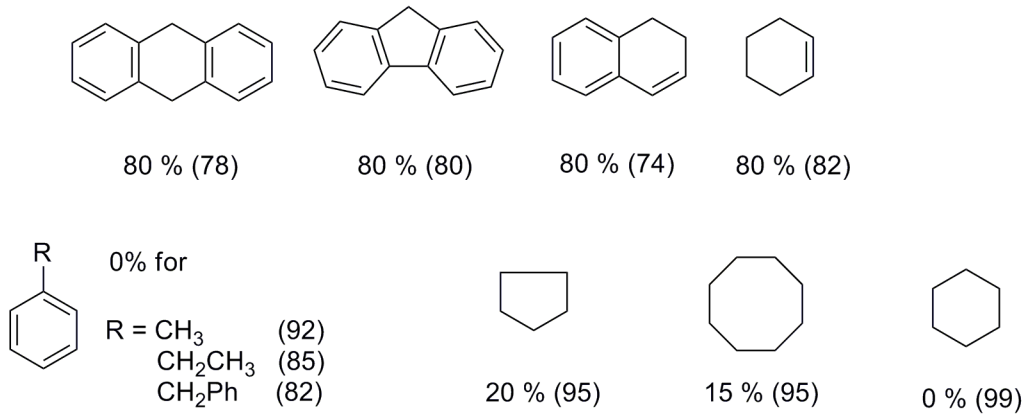

Table 2.2 summarizes all the substrates and their relative amounts of interception at different concentrations. It was apparent that substrates with strong C-H bonds intercept poorly or not at all at 0.1 M concentration. Interestingly, a higher amount of interception (65%) was noted when the cyclooctane concentration was increased to 1 M. Moreover, when oxygenation of **1** was carried out in the presence of 1 M cyclohexane, the residual absorbance at the 650 nm suggested that **2** was formed in about 50% yield, implying that under those conditions the oxidant responsible for ligand hydroxylation could be intercepted by 30%, by a substrate with C-H bond strength as high as 99.3 kcal/mol. [Figure 2.9, inset].

Our success with cyclohexane oxidation provoked us to investigate the oxygenation of **1** in the presence of 1 M *n*-alkanes, which have C-H bond strengths similar to cyclohexane. 1 M *n*-heptane or *n*-octane was even more effective than cyclohexane in the trapping of the oxidant, exhibiting 80% interception (Figure 2.9). There is a stark difference between cyclohexane and *n*-heptane. *n*-Heptane not only showed higher interception at 1 M concentration but also afforded ligand interception at lower concentration (0.2 M) but cyclohexane did not (Figure 2.9 inset). Product analysis of the *n*-heptane reaction solution at the end showed only 1-heptene as product with 40% yield. As observed for other hydrocarbons no evidence for the ketone products (i.e. 2-heptanone, 3-heptanone, 4-heptanone) or alcohol products (i.e. 1-heptanol, 2-heptanol) was obtained. But perhaps the most surprising observation was the absence of 2-heptene (or any other internal alkenes) as product, as it suggests that relatively weaker methylene C-H bonds of the *n*-alkane (methylene group) were not oxidized by the putative oxidant. Similar results were obtained with *n*-octane, desaturation of *n*-octane resulted in formation of 1-octene as the exclusive product in 38% yield.

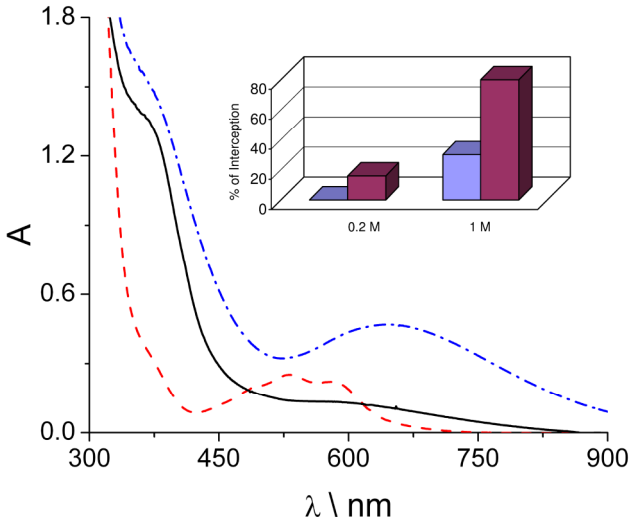

Figure 2.9 UV-vis spectral changes monitored when **1** (1mM) was oxygenated at room temperature in a 0.5-cm cell. **1** alone - dashed red line; **1**+O_2 - dashed-dotted-blue line; **1**+ 1M *n*-heptane + O_2 - black solid line. Inset: Concentration dependence of substrates to trap the nascent oxidant formed by the reaction of **1** and O_2. violet – cyclohexane; maroon – *n*-heptane

Table 2.1: Product analysis with various hydrocarbons

Hydrocarbon (concentration at which product analysis was performed)	Bond Dissociation Energy of attacked C-H bond (kcal/mol)	Product (Yield)	Maximum Percent of Interception
9,10-dihydroanthracene (0.1 M)	78	Anthracene (35%)	80
1,2-dihydronaphthalene (0.1 M)	74	Naphthalene (30%)	70
Cyclohexene (0.1 M)	82	1,3-cyclohexadiene (40%)	80
Fluorene (0.1 M)	80	Fluorenone (50%)	80
Toluene (1 M)	92	Benzaldehyde (35%)	25
Cyclooctane (1 M)	95	Cyclooctene (30%)	65
n-Heptane (1 M)	99	1-heptene (40%)	80
n-octane (1 M)	99	1-octene (38%)	80
Ethylbenzene (1 M)	85	Styrene*	60

* not quantified

Table 2.2. Substrate concentration dependence of the amount of interception

Substrate	Bond dissociation energy (C-H) (kcal/mol)	Concentration (M)	Interception [%]	$FeTp^{Ph2}$*OBz yield
		0.001	40	42
cyclohexene	82	0.002	45	30
		0.01	65	24
		0.05	68	22
		0.1	75	17
		1	80	14
		0.001	0	70
		0.01	0	70
9,10-DHA	78	0.05	70	21
		0.075	78	15
		0.1	80	14
		1	90	8
		0.05	55	32
THF	92	0.1	70	21
		0.2	80	16
		0.002	45	38
DHN	74	0.01	70	21

		0.05	75	17
		0.1	80	14
		0.2	80	14
		0.1	15	60
cyclooctane	95	0.2	41	41
		1	65	24
		0.1	0	70
cyclohexane	99	1	30	50
		0.2	15	60
n-Heptane	99	0.5	55	32
		1	80	14
n-Octane	99	0.5	55	30
		1	80	14
TMS	100	1	25	53
t-Butanol	99	1	60	27
t-Butanol-d_1		1	60	27
Methanol	96	0.2	75	18

cyclohexene-d_{10}		0.001	40	45
		0.1	65	
THF-d_8		0.2	45	38
n-Octane-d_6		1	0	70
		0.5	0	70
cyclohexane-d_{12}		1	0	70
MTBE	82	1	80	12

In order to explain the accumulated observations, a common mechanism could be invoked as shown in scheme 2.2, which is based upon the mechanism for α-ketoglutarate-dependent enzymes.[4,35,36,103] It is proposed that complex **1** is able to generate a high-valent iron-oxo intermediate in the presence of oxygen. In benzene, when no substrate is introduced to the reaction mixture, this iron-oxo intermediate hydroxylates the phenyl ring of the ligand to generate **2**.[84] But when oxygenation of **1** is carried out in the presence of the added substrates, this iron-oxo indermediate could have different fates. When thioethers are introduced as added substrates, the iron-oxo intermediate transfers its oxo group to thioethers to generate the corresponding sulfoxide and is reduced to the iron(II) state as indicated by the featureless spectrum (Figure 2.7 inset). The featureless spectrum of the thioanisole solution is consistent with formation of $[Fe^{II}(Tp^{Ph2})(OBz)(OSR_2)]$ described earlier. This is further corroborated by Mössbauer studies. But, in the case of hydrocarbon substrates, the solutions at the end are not colorless. The strong absorbance near 350 nm observed in the cyclohexene solution suggested formation of an iron(III) byproduct. The latter is confirmed by Mössbauer spectroscopy, which shows that 70% of the Fe in the sample belongs to antiferromagnetically coupled diiron(III) centers (Figure 2.10). This 350-nm band is observed in all our hydrocarbon oxidation studies except in the case of oxidation of 9,10-DHA, where it is obscured by the sharp peaks of the anthracene product. The consistent observation of the 350-nm band in all our hydrocarbon interception studies further suggests that they all follow the same route and give rise to the same diiron(III) product. We suggest that the diiron(III) complex arises from the comproportionation of the initial $[Fe^{II}(Tp^{Ph2})(OBz)]$ product with the Fe^{IV}=O oxidant as it is formed. Indeed the reaction of

1 with O_2 in the presence of an equimolar amount of $[Fe^{II}(Tp^{Ph2})(OBz)]$ shows no self-hydroxylation of the ligand phenyl ring and instead affords the diiron(III) byproduct. We attribute the different outcome in the thioanisole experiment to the likelihood that the product sulfoxide remains coordinated to the iron(II) center, inhibiting the comproportionation.

Scheme 2.2 Proposed mechanistic profile for oxygenation of **1** at room temperature

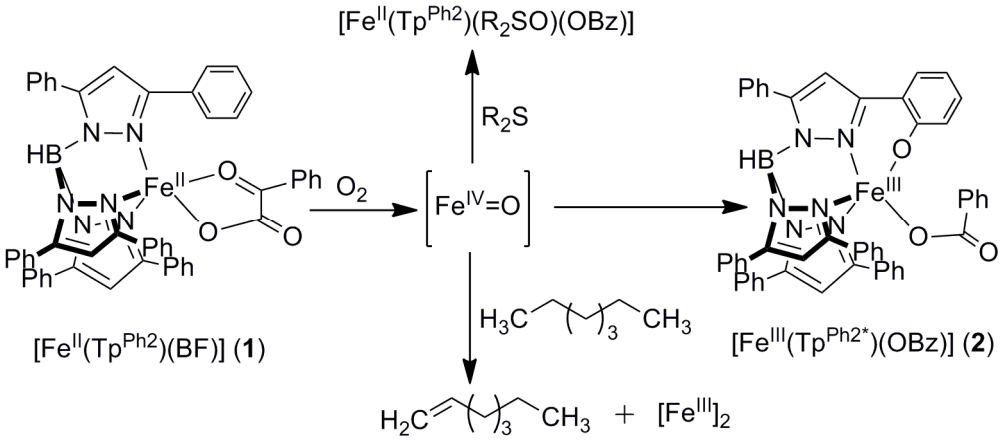

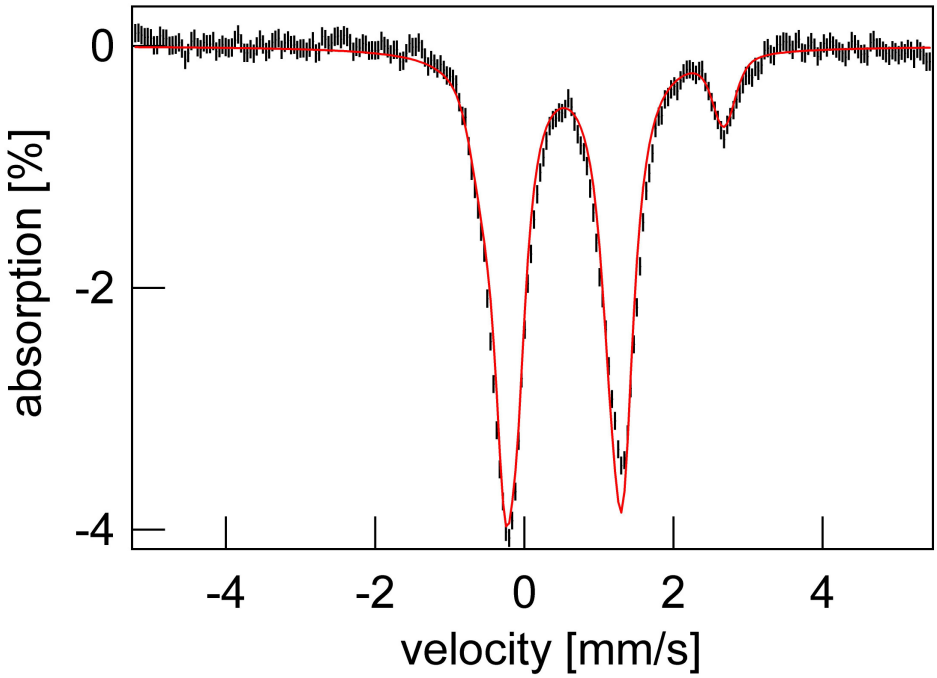

Figure 2.10. 4.2 K Mössbauer spectrum recorded in zero field of **1** + 0.1 M cyclohexene + O_2 in benzene. Isomeric shift of the major species was observed as 0.55 mm/s with ΔE_Q = 1.62 mm/s suggesting that this doublet belonged to the diamagnetic $[Fe^{III}]_2$ species. Sincere thanks to Prof. Münck and his group at Carnegie Mellon University for their help in Mössbauer measurements.

2.5. Effect of Concentrations on Oxidation of Hydrocarbons with Diverse Sizes

In order to establish the relation between percent of interception to the strength of the substrate C-H bond, a library of substrates was investigated. One unexpected observation was noted as shown in scheme 2.1. Not all substrates with similar bond dissociation energy resulted in a similar amount of interception. Interestingly, toluene,

ethylbenzene, and diphenylmethane did not intercept the oxidant at all at the 0.1 M concentrations used for these trapping experiments, despite the fact that their C-H bonds have bond strengths comparable to those of cyclohexene. The contrasting behavior of diphenylmethane and fluorene is particularly illustrative. These results suggest that trapping efficiency is modulated not just by the strength of the target C-H bond but also by the accessibility of the substrate to the nascent [Fe=O] oxidant.

Further corroboration of the above notion comes from the concentration dependences of oxidant trapping, as illustrated in Figure 2.11. PhSMe (blue bars) intercepted the oxidant even at a concentration equivalent to that of **1** (1 mM), but isosteric PhEt (indigo bars) required a 1000-fold higher concentration to have the same effect. This difference likely reflects the greater thermodynamic driving force for sulfoxidation than for H-atom abstraction. On the other hand, a similar concentration difference was found for the trapping of the oxidant by cyclohexene (red bars) and PhEt, despite the fact that the two have similar C-H bond strengths. Indeed a competitive oxidation of cyclohexene and PhEt, both at 0.1 M concentration, yielded only cyclohexadiene as the oxidation product. Also cyclohexene at 1 or 10 mM is able to trap the oxidant while DHA does not; at 0.1 M concentration however, both intercept the oxidant with comparable effectivity. These differences suggest that the allylic C-H bonds of cyclohexene have more facile access to the [Fe=O] 'active site' than the benzylic C-H bonds of either ethylbenzene or DHA.

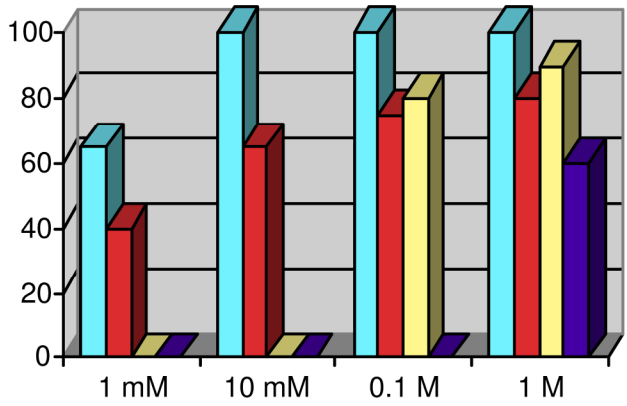

Figure 2.11. Substrate concentration dependence on the % trapping of the oxidant formed by the reaction of **1** and O_2 in benzene at 25 °C. Legend for each data cluster from left to right: thioanisole (blue), cyclohexene (red), DHA (yellow), ethylbenzene (indigo).

In the previous section it was depicted that the [Fe=O] active site selectively oxidizes hydrocarbons with relatively weak C-H bonds and obloid shapes. In this section, we are going to compare the different amounts of interception among substrates with higher C-H bond dissociation energies (BDEs). As mentioned previously, hydrocarbons with strong C-H bonds (95 - 99 kcal/mol)[104] required higher concentrations in order to obtain any measurable interception. While 1 M cyclooctane leads to 65% interception, 1 M cyclohexane affords only 30% interception. Tetramethylsilane (TMS) showed almost a similar amount of interception (25%) when used in 1 M concentration (Figure 2.12). The amount of interception mentioned above can be correlated to the C-H BDEs of the

substrates. Cyclooctane with C-H BDE of 95 kcal/mol was able to intercept the ligand hydroxylation better than cyclohexane or TMS, both of which has the C-H BDE of ~99 kcal/mol. But this argument could not explain the high amount of interception observed for *n*-heptane or *n*-octane (cyan and magenta bars in Figure 2.12). *n*-Alkanes have strong C-H bonds their BDEs range from 99 kcal/mol for the terminal methyl groups to 98 kcal/mol for the internal methylene groups. However, both *n*-heptane and *n*-octane showed 80% interception, quite high compared to cyclooctane or cyclohexane. Therefore it is clear that C-H BDE alone could not explain the observed amount of interception. One difference between cyclohexane (or TMS) and *n*-heptane is their flexibilities. Cyclohexane because of its cyclic structure has less flexibility than that of *n*-heptane and this might control the access of the substrates to the [Fe=O] 'active site'. From Figure 2.12 it is apparent that, despite similar propensity toward oxidation, linear hydrocarbons were more efficient at interception because of their facile access of the [Fe=O] 'active site' compared to cyclohexane or tetramethylsilane (see Table 2.2 for a tabulated comparison on substrate concentration and amount of interception).

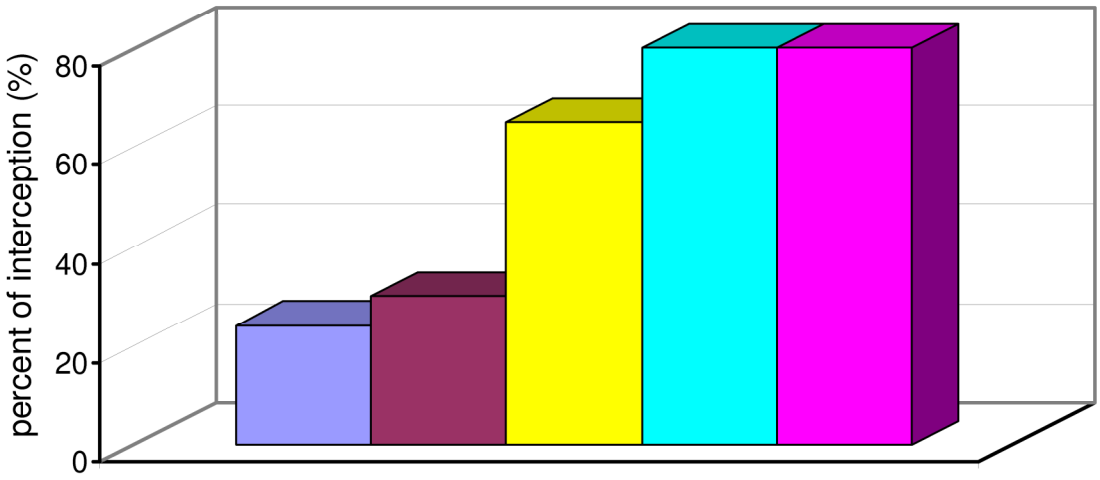

Figure 2. 12. Substrate dependence on the % trapping of the oxidant formed by the reaction of **1** and O_2 in benzene at 25 °C. Legend from left to right: tetramethylsilane (blue), cyclohexane (maroon), cyclooctane (yellow), n-heptane (cyan), and n-octane (magenta).

2.6. Effect of Substrate Deuteration on the Amount of Interception

We noted that addition of thioethers or hydrocarbons did not significantly affect the one hour reaction time between complex **1** and oxygen, suggesting that the rate of ligand hydroxylation was not perturbed in the presence of substrates. This observation is consistent with the rate determining step for the oxygenation occurring prior to the interception step, as demonstrated by earlier kinetic studies that showed first order dependence on both iron complex and oxygen.[84] Even though the rate of ligand hydroxylation was not perturbed in the presence of cyclohexene or cyclohexene-d_{10}, experiments with cyclohexene-d_{10} showed that C-H bond cleavage is a key step in substrate oxidation. While the oxidation rate of **1** was not affected by the presence of either 0.1 M of cyclohexene or cyclohexene-d_{10}, a product isotope effect of 10 was manifested in a competitive oxidation of cyclohexene and cyclohexene-d_{10}. It was also noted that the amount of interception of the ligand hydroxylation, in the presence of cyclohexene (1 mM) or cyclohexene-d_{10} (1 mM) was not changed. Interestingly, this is only true for a substrate like cyclohexene. For example, when a reaction was performed in the presence of tetrahydrofuran, 0.2 M with respect to 1 mM of **1,** we observed 80% of interception. But the amount of interception was significantly reduced (45%), when the reaction was performed in the presence of tetrahydrofuran-d_8, under the same conditions. A similar effect was demonstrated, when cyclohexane was used as a substrate. As mentioned in the previous section, cyclohexane can only exert a significant amount of interception (30%), when it was used in high excess, 1 M. When oxygenation of **1** was performed in the presence of 1 M of cyclohexane-d_{12} in benzene, complete formation of **2** was monitored. More interestingly, a similar effect was noted when the oxygenation

reactions of *n*-octane and *n*-octane-d_6 were compared. Even though *n*-octane was able to intercept 80% percent of ligand hydroxylation, when the reaction was performed in the presence of 1,1,1,8,8,8-octane-d_6, we also observed no interception as in the case of cyclohexane-d_{12}. (Figure 2.13) This observation was quite unique, as it clearly suggested that the terminal methyl group (-CH_3), not the weaker methylene (-CH_2-) group, of the n-octane was involved in the key C-H bond cleavage step. (see Table 2.2 for a tabulated comparison on substrate concentration and amount of interception)

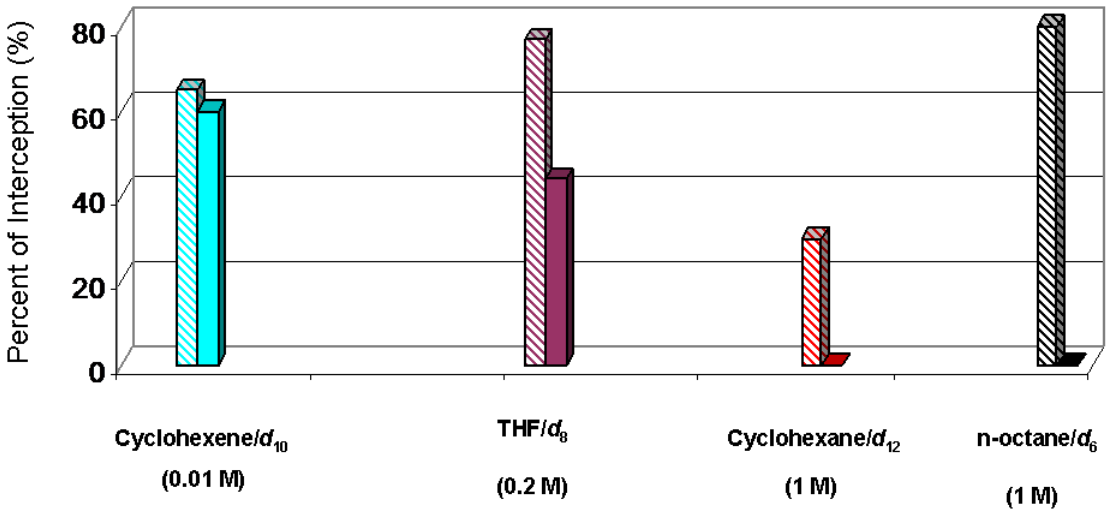

Figure 2.13. Substrate dependence on the % trapping of the oxidant formed by the reaction of **1** and O_2 in benzene at 25 °C. Legend for each data cluster from left to right: cyclohexene (cyan), THF (maroon), cyclohexane (red), *n*-octane (black); shaded bars represent the substrates and solid bar represent their deuterated analogues.

In all the cases, deuterated substrates did not change the time course of the ligand hydroxylation, but they led to different amounts of interception. A substrate that has the easy access to the [Fe=O] behaved similarly despite the bond strength difference between a C-H bond or a C-D bond, whether the reaction was performed under stoichiometric condition (1 mM) or in excess of a substrate (10 mM). But for substrates with stronger C-H bonds, deuteration had a drastic effect, leading to zero interception (see appendix for an explanation).

2.7. Oxidation of Alcohols by Complex 1

When the reaction of complex **1** (1 mM) was performed in the presence of alcohols, we observed interception of the ligand hydroxylation. Alcohol substrates with different C-H bond strengths, namely methanol, benzyl alcohol and *t*-butanol, were chosen for the study. As observed for hydrocarbons, the alcohol with strong C-H bonds, *t*-butanol (cyan), was only able to intercept the oxidant at 1 M concentration. On the other hand, methanol (violet) and benzyl alcohol (maroon) were able to intercept the oxidant at 0.2 M concentration. In all the cases, we observed a high level of interception, as **2** was only formed in ~ 15% yield for methanol and benzyl alcohol and 25 % yield for *t*-butanol.

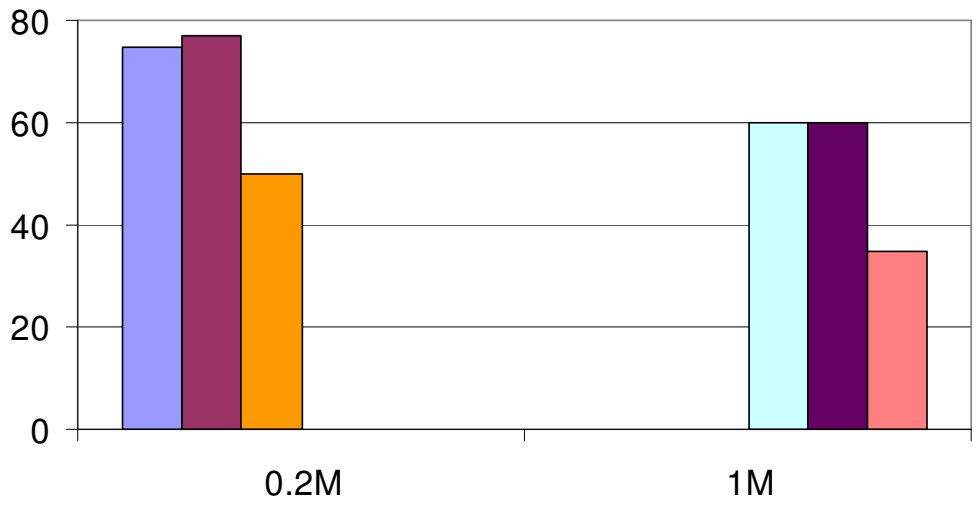

Figure 2.14. Substrate dependence on the % trapping of the oxidant formed by the reaction of **1** and O_2 in benzene at 25 °C. Legend for each data cluster from left to right: methanol (blue), benzyl alcohol (maroon), methanol-d_4 (orange), *t*-Butanol (cyan), *t*-Butanol-*d* (deep-purple), *t*-Butanol-d_9 (salmon-red).

Unlike hydrocarbons, alcohols have two positions that can possibly react with the active [Fe=O], the weaker C-H bond or the stronger O-H bond. When oxygenation of **1** was performed in the presence of CD_3OD, we observed a significant decrease in the amount of interception (orange bar) compared to methanol. Similarly, -$(CD_3)_3$C-OH resulted in 35% interception, but the amount of interception remained the same (60%), when $(CH_3)_3$C-OD was used as a substrate (deep purple). This data series indicated that even with alcohol, the putative [Fe=O] reacted with the C-H bond of the alcohol, not with the O-H bond. This observation was in contrast to the recently reported behavior of a

strongly oxidizing high-valent diiron-oxo intermediate, where the oxidant preferentially attacks the stronger O-H bond of alcohols.[98]

2.8. Oxidation of Hydrocarbons by Complex 3 and 4 at Room Temperature

From the previous discussion it is clear that the oxidant generated from the reaction of **1** and O_2 performed substrate oxidation with unique selectivity. Results described herein also suggested that this selectivity is intrinsic to the [Fe(O)(Tp^{Ph2})(OBz)] oxidant and hydrocarbons with easy access to the [Fe=O] have high propensity for oxidation. The oxo-transfer reactions to thioethers along with oxidation of hydrocarbons with strong C-H bonds implied that the active oxidant must be a high-valent oxoiron species. The inherent nature of the selectivity arising from the oxoiron intermediate suggested that the phenyl group of the Tp ligand might play a role in controlling the selectivity. In order to test this hypothesis a series of iron complexes with different alkyl substituents on the Tp framework was synthesized ([Fe(Tp^{Me2})(BF)], **3**; [Fe(Tp^{iPr2})(BF)], [Fe(Tp^{tBu})(BF)], **4**) and their reactions toward a common hydrocarbon (9,10-dihydroanthracene, DHA) were investigated. As depicted in Figure 2.11, the oxoiron ([Fe=O]) intermediate derived from complex **1** could only be intercepted by 9,10-dihydroanthracene (DHA) at high concentration (0.1 M). When the concentration of DHA was lowered to 0.01 M, it led to complete formation of **2**, i. e. zero interception, suggesting that the substrates had a restricted access toward the [Fe=O] species. Therefore, DHA could only access it in higher concentration and intercept the ligand hydroxylation, and gave anthracene as product (characterized by growth of sharp UV-vis peaks). If the DHA oxidation could be achieved at lower concentration by the putative

[Fe=O] derived from **3** or **4**, it would suggest that the substituents on the Tp framework might control the accessibility of the substrates toward the [Fe=O] unit.

In 1995, Valentine and co-workers reported that [Fe(Tp^{Me2})(BF)] (**3**) was able to perform epoxidation of olefins by activating oxygen at room temperature.[81] But reactivity toward a C-H bond was not explored. We thus investigated oxygenation of **3** in the presence of DHA at room temperature. Due to insolubility of **3** in benzene these reactions were performed in acetonitrile. Upon oxygenation, complex **3** was able to oxidize 9,10-dihydroanthracene at room temperature in acetonitrile. Complex **1** was able to oxidize DHA only at 0.1 M, but **3** was able to perform DHA oxidation at both 0.01 M and 0.1 M concentration. Not surprisingly, the yield of anthracene was very low (~ 2%, whereas 16% yield was obtained when DHA concentration was raised to 0.1 M) at 0.01 M concentration. Observation of anthracene even with a lower amount of DHA suggested that replacing the Ph group with the Me group enhanced the accessibility of the DHA toward the [Fe=O] oxidant.

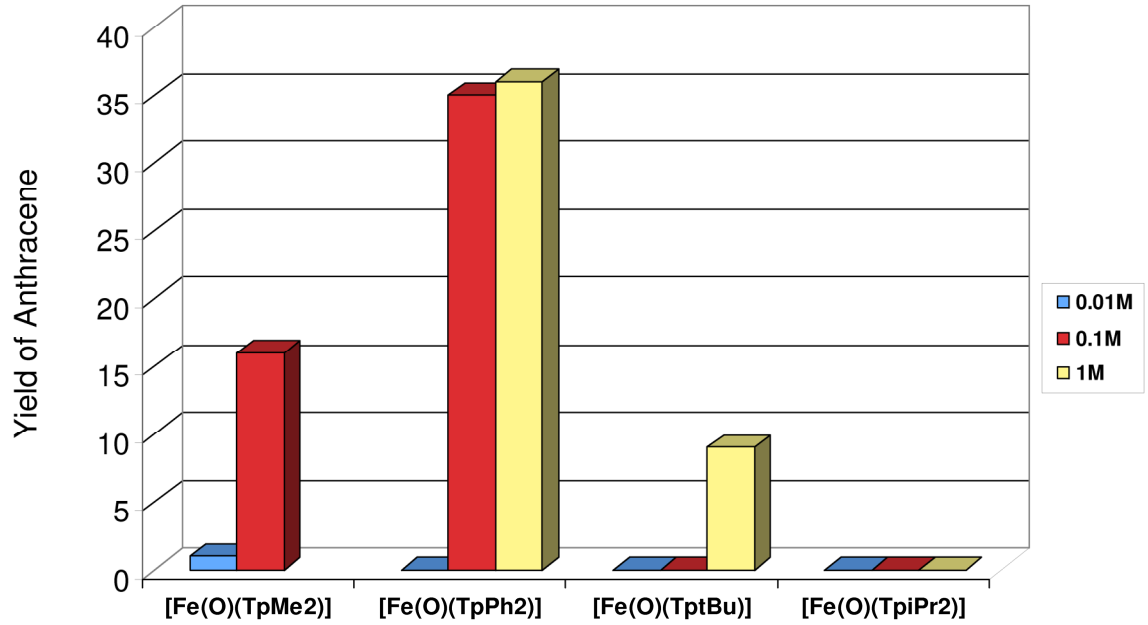

Figure 2.15. DHA oxidation with the putative oxidant generated from the reaction of iron-complexes and oxygen. Y-axis represents the yields of anthracene. Each legends of a data cluster corresponded to a different concentration of DHA used for the oxygenation reaction of [Fe(Tp^{R2})(BF)] complexes: blue: 0.01 M; red: 0.1 M, yellow: 1 M.

When oxygenation of **4** was performed in the presence of DHA, DHA concentration had to be raised to 1 M, in order to obtain any anthracene. The initial bluish-purple chromophore associated with complex **4** disappeared upon oxygenation in benzene at room temperature to generate a yellow colored solution in an hour. This observation remained the same when oxygenation of **4** was performed in the presence of 0.01 M or 0.1 M DHA in benzene. When oxygenation of **4** was performed in the presence of 1 M DHA, three sharp features in the near UV-region associated with anthracene grew over the course of 1 hr. For comparison, the $FeTp^{iPr2}$BF complex was also studied for DHA

oxidation, but it was not able to oxidize DHA at all in benzene, even when the concentration of DHA was raised to 1 M. In all the cases, hydroxylation of the Tp^{iPr2} ligand was observed upon oxygenation (please see next chapter for details). From this series of experiments it was very clear that making the pyrazoles of the Tp ligand bulky made the [Fe=O] oxidant less accessible for substrates and as a result the highest concentration of DHA was required to intercept the [(Tp^{tBu})Fe(O)(OBz)] oxidant whereas a lower concentration of DHA sufficed for the [(Tp^{Me2})Fe(O)(OBz)] oxidant.

2.9. Discussion

From our reactivity studies of complex **1** with oxygen, it was observed that **1** generates an oxidant that can oxidize added substrates. The putative oxidant can transfer its oxo to thioethers and can dehydrogenate hydrocarbon substrates. Based on the accumulated data, the nature of the active oxidant is proposed to be an oxoiron(IV) species. It was also noted that the putative oxoiron(IV) species prefers oxidizing cyclic alkanes with weak C-H bonds or linear alkanes at the terminal position. The extent to which a hydrocarbon is able to intercept ligand hydroxylation does not follow a direct trend with the C-H bond dissociation energies of the substrates. In order to explain the observed data, our collaborators have carried out DFT calculations on the $[Fe^{IV}(O)(Tp^{Ph2})(OBz)]$ intermediate proposed to carry out the oxidations.[101] Figure 2.16 shows a representation of the hypothetical Fe^{IV}=O oxidant where two of the three 3-phenyl groups of the Tp^{Ph2} ligand form a rudimentary cleft that may serve to discriminate among various hydrocarbons on the basis of shape. The computations show that the energy for the $S = 2$ isomer is lower than for the $S = 1$ isomer by 6.2 kcal/mol. Although this energy difference is usually deemed to be greater than the inherent uncertainty of current DFT calculations, its interpretation is complicated by the fact that the two geometry-optimized structures differ in iron coordination number. The S = 1 isomer is found to be six-coordinate and the S = 2 isomer is found to be five-coordinate due to a change in the coordination mode of the carboxylate ligand from bidentate to monodentate. Thus the calculated energy difference reflects not only the change in the spin state but also the change in carboxylate binding mode.[101] This geometry difference was postulated to derive from steric crowding of the phenyl groups around the [Fe=O]

unit to afford the lower coordination number for the S = 2 isomer. In support, calculations for a truncated model, containing only one phenyl group showed that both S = 2 and S = 1 structures have six-coordinate Fe(IV) centers, in agreement with the results reported by Borowski *et al.*[105] Notably, our computed *S* = 2 structure resembles that calculated for the high-spin Fe^{IV}=O intermediate of the enzyme TauD.[57] Whichever the spin state of the [Fe=O] species, it is clear from the experimental data that it must be an oxidant powerful enough to cleave the very strong C-H bonds of *n*-heptane, cyclohexane and tetramethylsilane, within the 1-hr time frame of the reaction of **1** and O_2.

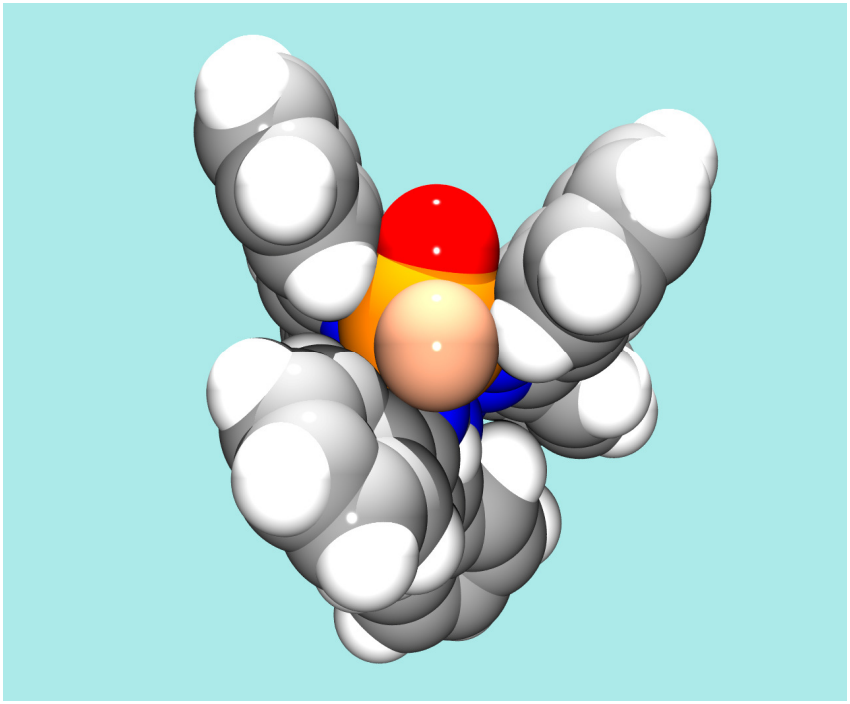

Figure 2.16. A DFT generated model of the rudimentary pocket. Sincere thanks to Prof. Münck and his group at Carnegie Mellon University for performing the DFT calculations.

A separate calculation from Shaik and co-workers also reported the spin state of the iron-oxo intermediate to be high-spin.[106] In a recent communication, Shaik and co-workers also addressed why we observed exclusive desaturation by the [Fe=O] derived from **1**, a model of TauD, which performs C-H bond hydroxylation.[64] The key step in the reaction of [Fe=O] with a hydrocarbon is the H-atom abstraction by the ferryl intermediate. The substrate-derived radical can have two fates; it can either undergo rebound to yield an alcohol or produce an olefin by a second H-atom abstraction.[63,64] The calculations on the [Fe(O)(Tp^{Ph2})(OBz)] intermediate suggested that the outcome of the hydroxylation or desaturation of a hydrocarbon will be controlled by some intrinsic factors. Some of these factors could be C-H bond strength, its steric bulk, and delocalization of the substrate based radical. The other factor that controls the outcome is the spin state of the ferryl intermediate and also its orbital structure.[64] Hence substrates like 1,4-cyclohexadiene will always prefer to desaturate because of extra stabilization of the aromatic product. On the other hand, a substrate like ethane will be hydroxylated to give ethanol, as the subsequent H-atom abstraction from the ethyl radical does not have any extra stabilization. Although it may appear in this context that our experimental result of obtaining 1-heptene product exclusively, is contradictory, there have been other examples where desaturation of relatively unreactive alkanes have been implied.[107]

A few other points deserved further discussion. Substrates that are sterically less hindered can more easily access the ferryl intermediate derived from **1** and oxygen.[101] It has been previously established in this system that the rate determining step was the generation of the ferryl intermediate, not the decay of the ferryl intermediate. But substrates with different C-H bond strength behaved differently upon deuteration (*vide supra*).

Cyclohexene and its deuterated analog did not show any difference in the amount of interception. But substrates with strong C-H bonds exhibit a dramatic effect upon deuteration. Cyclohexane intercept ligand hydroxylation less efficiently than n-octane. But perdeuterated cyclohexane and 1,1,1,8,8,8-d_6-*n*-octane both allowed full formation of **2,** the ligand hydroxylated product. This data fits well with our initial hypothesis: hydrocarbon oxidation is controlled by its access. Two independent experiments corroborated this hypothesis. First, a straight chain alkane can have easy access to the [Fe=O] than a cyclic hydrocarbon. Hence we observed a higher amount of interception with *n*-octane and *n*-heptane compared to cyclohexane. Product analysis from the *n*-heptane reaction showed 1-heptene as the exclusive product, suggesting that the putative [Fe=O] indeed oxidizes the C-H bond that have the easiest access in the long chain, *i.e.* the terminal methyl group. Moreover, when terminal positions in *n*-octane were deuterated, the methyl groups were replaced with more difficult to oxidize -CD_3 groups, the inner methylene groups, although easier to oxidize, could not intercept the [Fe=O] due to the restricted access. These observations further establish that the oxidation of substrates is controlled by its access to the putative [Fe=O], not just by the C-H bond strength.

Different substituted Tp ligand-supported iron complexes further confirmed that this selectivity arises from the [Fe(O)(Tp^{Ph2})(OBz)] oxidant. Toward the same substrate, DHA, complexes **1, 3,** and **4** behaved differently. Even though DHA was oxidized in all cases, the substrate concentration requirement varied widely. The putative oxidant generated from **3** was able to oxidize DHA at the lowest concentration and **4** was able to oxidize DHA only at the highest concentration. These observations are in accord with the

DFT-generated model of [Fe=O] derived from **1**. From DFT calculations it was shown that the [Fe=O] unit resides in a rudimentary cleft made by the phenyl group of the ligand. Upon substitution of the phenyl groups by methyl groups, the cleft size widens, increasing the access of DHA toward the [Fe=O] unit. But substitution of the phenyl groups by *t*-butyl groups narrowed the cleft size, restricting the access of DHA toward [Fe=O] unit. This trend is in accord with the effective steric bulk of the Tp ligands.[108]

Oxidation of an unactivated C-H bond by a synthetic complex has stymied chemists for a long time. The major challenge is to attain the selectivity depicted by the enzyme active site, which is accomplished often using molecular recognition by means of non-covalent interaction.[109] For example, the enzyme alkane ω-hydroxylase *alk*B specifically oxidizes ω-position of an alkane.[110] In order to replicate that reactivity in a model complex, synthetically challenging metal-porphyrin complexes were designed.[93] These complexes were able to oxidize hydrocarbons, but mostly secondary positions of a hydrocarbon were oxidized over the primary.[93-95,111] Suslick and co-workers successfully designed a very sterically crowded metal-porphyrin complex that oxidized an *n*-alkane and obtained primary alcohol as major product.[88] Even with this complex, specific oxidation of primary position, as observed in the enzymes was not attainable. Recent efforts from Brudwig and Crabtree group led to design of a dimanganese catalyst, based on terpyridine ligand equipped with phenylene linker and Kemp's triacid that gave selective products based on the molecular recognition of the substrate ibuprofen by the catalyst.[109,112] In that context, **1** is an easy-to-synthesize bio-inspired iron complex that can oxidize various substrates at room temperature in the presence of oxygen. Moreover, to our knowledge, the oxidant generated from complex **1** is the only known bio-mimetic

complex that performs specific ω-oxidation of an *n*-alkane. Our exploration of the system revealed the origin of this selectivity and our experimental results taken together with the theoretical calculations allowed us to hypothesize that this selectivity arises from a rudimentary cleft made by the phenyl groups of the ligand that flank the [Fe=O] unit and restrict the access of the substrates.

Chapter 3

Oxygen Activation by [Fe(Tp^{iPr2})(X)]Complexes: Effects of Different Ancillary Ligands

A part of the content of this chapter was published in: Anusree Mukherjee, Matthew A. Cranswick, Mrinmoy Chakrabarti, T. K. paine, Kiyoshi Fujisawa, Eckard Münck, Lawrence Que, Jr. *Inorg. Chem.* **2010**, *49*, 3618-28.

Compound Abbreviations

1 = [Fe(Tp^{iPr2})(PRV)]

2 = [Fe(Tp^{iPr2})(BF)]

3 = [Fe(Tp^{iPr2})(OBz)]

4 = [Fe(Tp^{Ph2})(PRV)]

5 = [Fe(Tp^{Ph2})(BF)]

6 = [Fe(Tp^{tBu,iPr})(BF)]

3.1 Introduction

Oxygen activation performed by diverse non-heme iron enzymes all involve a common intermediate at the very early stage of the catalytic cycle that is formed through the binding of oxygen to an active site iron to generate an iron-oxygen adduct.[113] Oxygen is then activated by the reduced iron(II) cofactor and a sacrificial co-substrate (α-ketoglutarate, tetrahydrobiopterin, or reduced nicotinamide), resulting in O-O bond cleavage and generating an iron(IV)-oxo (ferryl) intermediate.[7,114] This ferryl intermediate then performs substrate oxidation by abstracting a hydrogen atom.[34,54,58] In the last decade, continuing efforts from Bollinger and Krebs revealed the nature of the ferryl species and its role in the mechanism of substrate oxidation in many different non-heme iron enzymes.[58] In contrast, much less is known about the nature of the Fe–O_2 adducts ('pre-ferryl') that must initially form in the course of dioxygen activation.[113] Often these species are considered merely as pass-through points en route to the high-valent intermediates that have been the focus of current efforts. However recent developments suggest that more attention should be paid to some of these adducts, as

they may perform more important roles than earlier considered.[115] Interestingly, a number of possible functions has been proposed for the bound O_2 in the mechanisms of these nonheme iron enzymes.[7] The initial iron-superoxo species can be further reduced by another iron center to an iron-peroxo species, an intermediate commonly observed in the diiron enzyme family.[2,116] For α-ketoglutarate dependent enzymes, this mononuclear iron-superoxo species is trapped by the co-substrate α-ketoglutarate, to generate a high-valent iron-oxo intermediate responsible for substrate oxidation.[6,36] For isopenicillin N synthase (IPNS),[115] hydroxyethylphosphonate dioxygenase (HEPD),[117], and CloR[118] the bound O_2 is proposed to initiate the four-electron oxidation of substrate by abstracting an H-atom from the substrate. How an Fe–O_2 adduct can be tuned to perform such a variety of functions is a fascinating question for further investigation.

Scheme 3.1 Diverse reactions executed by iron-superoxo intermediates

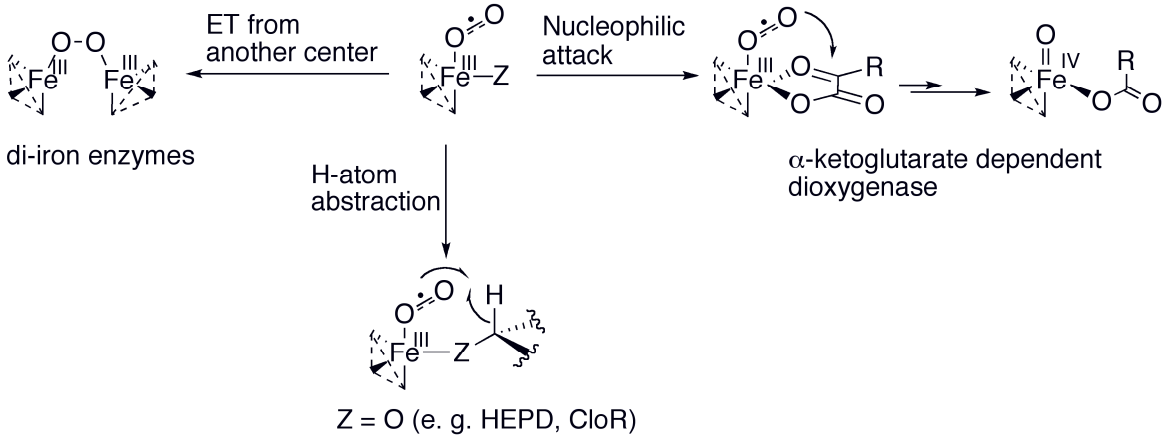

To date spectroscopic evidence is available for only two superoxo intermediates among iron enzymes. The first evidence of a mononuclear iron-superoxo intermediate

was detected for the enzyme homoprotocatechuate 2,3-dioxygenase (2,3-HPCD) by X-ray crystallography[119] using a non-native substrate 4-nitrocatechol (4NC). Spectroscopic evidence of this iron-superoxo species came last year. When the oxygenation reaction of the H200N mutant of 2,3-HPCD was performed in the presence of 4NC as a substrate, a blue intermediate (λ_{max} = 610 nm) was initially detected. This intermediate is characterized by EPR and Mössbauer spectroscopies. The blue intermediate exhibits a parallel mode EPR signal at g = 8.17, 8.8, 11.6 that was significantly broadened by $^{17}O_2$ hyperfine interactions. Mössbauer measurements further established that this intermediate has a high spin iron(III) signal antiferromagnetically coupled to an S = ½ radical signal.[120] The other superoxo intermediate was observed for *myo*-inositol oxygenase (MIOX), the mammalian enzyme that carries out the four electron oxidation of *myo*-inositol to D-glucoronate by cleaving the C1–C6 bond.[121] X-ray crystallography revealed MIOX to have a carboxylate-bridged diiron active site,[122] which was shown to be in the Fe(II)Fe(III) state by EPR and Mössbauer measurements.[123] In the crystal structure of the enzyme-substrate complex,[122] *myo*-inositol binds as a bidentate ligand to one iron, presumably the iron(III) site to activate the substrate. O_2 is then proposed to bind at the other iron, presumably the iron(II) site. Indeed a reversible O_2 adduct can be trapped and it exhibited an S = ½ EPR signal that was proposed to arise from a diiron(III)-superoxo species.[124] Because the decay of this species could be retarded with the use of deuterated substrate, it was surmised that the superoxo intermediate must be involved in the cleavage of the labeled C–H bond, which likely represents the first step in substrate oxidation.[124] This proposed H-atom abstraction by the iron-bound O_2 is in fact analogous

to the initial steps postulated in the mechanisms of IPNS and HEPD briefly mentioned above.[114,115]

To date there are only two well characterized synthetic Fe-O_2 adducts with nonheme ligand environments. In both cases, the iron-oxygen adduct were derived from a binuclear iron center. Oxygenation of the diiron(II) precursor $[Fe^{II}_2(\mu\text{-}OH)_2(6\text{-}Me_3\text{-}TPA)_2]^{2+}$ performed at – 80 °C afforded an intermediate that converts to the well characterized 1,2-peroxo-bridged intermediate $[Fe^{III}_2(\mu\text{-}O)(\mu\text{-}1,2\text{-}O_2)(6\text{-}Me_3\text{-}TPA)_2]^{2+}$ upon warming to – 60 °C.[125] The new intermediate was characterized by a ν(O–O) Raman mode found at 1310 cm^{-1} that downshifts 71 cm^{-1} with $^{18}O_2$. A doublet pattern was observed for the ν(O–O) mode associated with the $^{16}O^{18}O$ isotopomer in the mixed isotope Raman experiment, and the vibrational frequency along with the doublet pattern of the ν(^{16}O–^{18}O) mode established the nature of the new intermediate as an end-on iron-superoxo species. The ν(O–O) mode of 1310 cm^{-1} represents the highest frequency yet observed for a metal-bound superoxo species. Like their copper-superoxo counterparts,[126-129] this intermediate was reactive even at – 80 °C and can abstract an H-atom from 2,4-di-*tert*-butylphenol,[125] a reactivity that stands in stark contrast to the inability of the corresponding peroxo intermediate to react with the same phenol at – 60 °C.

Scheme 3.2 Evidence of 'pre-ferryl' species in diiron complexes.

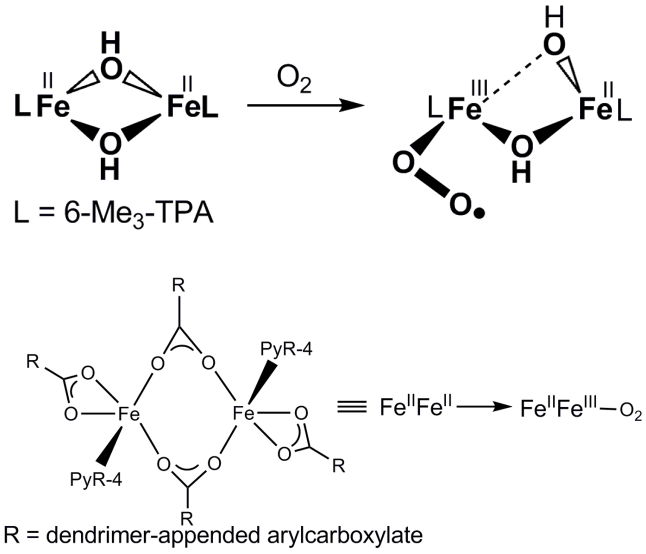

Related chemistry has been reported for diiron(II) complexes of carboxylates that are appended to dendrimers, which provide a hydrophobic environment to surround and protect the diiron center.[130] For these complexes, O_2 binding results in the formation of an EPR-silent intermediate that exhibits two Mössbauer doublets corresponding to an antiferromagnetically coupled iron(II)iron(III) center. Unfortunately in this case, no resonance Raman data could be obtained.

In this chapter, we discuss oxygen activation by iron complexes supported by the hydrotris-(3,5-diisopropylpyrazol-1-yl)-borate ligand and how the fate of the pre-ferryl species is controlled by the ancillary ligand. Our results indicate the first evidence of an 1:1 iron-oxygen adduct that could be chemically trapped by adjusting reaction conditions and tuning ligand electronics. We also discuss how the incipient iron-oxygen species decays in different pathways to give similar products.

3.2 Experimental Section

Materials and General Procedures. All reagents and solvents were purchased from commercial sources and were used without further purification unless otherwise noted. Methanol was rigorously dried by distilling from $Mg(OMe)_2$ and degassed under N_2 prior to use. Anhydrous dichloromethane and acetonitrile were purchased from Aldrich. Ligand Tp^{iPr2} was prepared by following a published procedure in collaboration with Prof. Kiyoshi Fujisawa. Preparation and handling of air-sensitive materials were carried out under an inert atmosphere (N_2) in a glovebox. ***Caution!*** *Perchlorate salts are potentally explosive and should be handled with care.*

Synthesis of [Fe(Tp^{iPr2})(PRV)] (1). To a mixture of KTp^{iPr2} (0.126 g, 0.25 mmol) and $Fe(ClO_4)_2$ (0.10 g, 0.25 mmol) in methanol (3 mL), sodium pyruvate (0.029 g 0.25 mmol) was added resulting in an immediate color change of the solution from colorless to red. This cloudy solution was stirred for an hour at room temperature. The solid was then filtered and dried in vacuo. X-ray quality crystals were grown via slow evaporation of a saturated CH_2Cl_2 solution at -20°C. Anal. Calcd for 1, $C_{31}H_{53}BFeN_6O_4 \bullet 3CH_2Cl_2$ (895.3 g/mol): C, 45.61; H, 6.64; N, 9.39. Found: C, 45.54; H, 6.70; N, 9.30. UV- vis [λ_{max}, nm (ε, $M^{-1}cm^{-1}$) in MeCN]: 458 (sh, 460), 500 (510), 540 (sh, 390). ^{1}H-NMR (benzene-d6, 300 MHz, 25 °C): –7.8 (s, B*H*), -2.8 (s, C*H*Me_2) 3.7 (s, CH*Me_2*), 14.4 (s, C*H*Me_2), 8.04 (s, C*H*Me_2), 63.7 (s, pz-4-*H*), 114.8 (s, $O_2CC(O)CH_3$).

Synthesis of [Fe(Tp^{iPr2})(BF)] (2). To a mixture of KTp^{iPr2} (0.126 g, 0.25 mmol) and $Fe(OTf)_2 \cdot 2MeCN$ (0.10 g, 0.25 mmol) in methylene chloride (3 mL), solid sodium benzoylformate (0.043 g 0.25 mmol) was added. The solution turned blue immediately

and was stirred for an hour at room temperature. The solid was filtered and dried in vacuo. X-ray quality crystals were grown via slow evaporation of a saturated pentane solution at -20° C. Anal. Calcd for 2, $C_{35}H_{51}BFeN_6O_3$ (670.47 g/mol): C, 62.70; H, 7.67; N, 12.53. Found: C, 62.92; H, 7.83; N, 12.47. UV- vis [λ_{max}, nm (ε, $M^{-1}cm^{-1}$) in MeCN]: 553 (sh, 510), 610 (610). ^{1}H-NMR (benzene-d_6, 300 MHz, 25 °C): -8.1 (s, B*H*), -1.78 (s, C*H*Me$_2$) 3.8 (s, CH*Me*$_2$), 13.2 (s, C*H*Me$_2$), 20.3 (*o*-BF), 16.7 (*m*-BF), 63.8 (s, pz-4-*H*).

Synthesis of [Fe(Tp^{iPr2})(OBz)] (3). Complex **3** was prepared by slightly modifying a published procedure.[131] To a mixture of KTp^{iPr2} (0.126 g, 0.25 mmol) and Fe(OTf)$_2$·2MeCN (0.10 g, 0.25 mmol) in toluene (3 mL), solid sodium benzoate (0.035 g, 0.25 mmol) was added. The solution was stirred for two hours at room temperature. It was filtered to remove any insoluble impurities and dried in vacuo. The solid is then redissolved in minimum amount of pentane and crystals were grown via slow evaporation of a saturated pentane solution at – 20 °C.

Identification of ligand hydroxylation product by ^{1}H-NMR spectroscopy. A 5 mM solution of **1** in 2 mL MeCN was bubbled with O_2 using a balloon and the solution was stirred vigorously for 15 minutes. To this solution was added *ca.* 2 mL of 1 M HCl with vigorous stirring. To the above solution excess NH_3 (aq) was added and organic products were extracted with diethyl ether. The extract was dried over $MgSO_4$ and to this solution 1,4-dimethoxybenzene was added as an internal standard. Evaporation of solvent resulted in colorless residue soluble in $CDCl_3$ that was analyzed by ^{1}H-NMR spectroscopy.

Identification of the acid decarboxylation product by ^{1}H-NMR spectroscopy. A 5 mM solution of **2** in 2 mL MeCN was bubbled with O_2 using a balloon and the solution

was stirred vigorously for 15 minutes. To this solution was added *ca* 2 mL 3 M HCl with vigorous stirring. The organic layer was extracted with diethyl ether and washed with distilled water. The extract was then dried over $MgSO_4$ and to this solution 1,4-dimethoxybenzene was added as an internal standard. Evaporation of solvent resulted in a faintly colored residue soluble in $CDCl_3$ that was analyzed by ^{1}H-NMR spectroscopy.

Crystallography of 1 and 2. For both complexes a crystal (approximate dimensions 0.40 x 0.35 x 0.30 mm^3) was placed onto the tip of a 0.1 mm diameter glass capillary and mounted on a CCD area detector diffractometer for data collection at 173(2) K. A preliminary set of cell constants was calculated from reflections harvested from three sets of 20 frames for **1** and four sets of 30 frames for **2**. These initial sets of frames were oriented such that orthogonal wedges of reciprocal space were surveyed. This produced initial orientation matrices determined from 101 reflections for **1** and 324 reflections for **2**. The data collection was carried out using MoKa radiation (graphite monochromator) with a frame time of 20 seconds for **1** and 45 seconds for **2** and a detector distance of 4.9 cm. A randomly oriented region of reciprocal space was surveyed to the extent of one sphere and to a resolution of 0.82 Å for **1** (0.80 Å for **2**). Four major sections of frames were collected with 0.30º steps in w at four different f settings and a detector position of -28º in 2q. The intensity data were corrected for absorption and decay (SADABS).[132] Final cell constants were calculated from 2801 (for **1**) and 2982 (for **2**) strong reflections from the actual data collection after integration (SAINT).[133] Please refer to Table 3.1 for additional crystal and refinement information.

The structures were solved and refined using SHELXTL.[134] The space groups of P-1 (for **1**) and P2/c (for **2**) were determined based on systematic absences and intensity

statistics. A direct-methods solution was calculated, which provided most non-hydrogen atoms from the E-map. Full-matrix least squares / difference Fourier cycles were performed which located the remaining non-hydrogen atoms. All non-hydrogen atoms were refined with anisotropic displacement parameters. All hydrogen atoms were placed in ideal positions and refined as riding atoms with relative isotropic displacement parameters. The final full matrix least squares refinement converged to $R1 = 0.0473$ for **1** and 0.0416 for **2** and $wR2 = 0.1358$ for **1** and 0.1100 for **2** (F^2, all data).

Physical Methods. Elemental analyses were performed by Atlantic Microlab, Inc. UV/vis spectra were recorded on a HP 8452A diode-array spectrometer with samples maintained at low temperature using a cryostat from Unisoku Scientific Instruments, Osaka, Japan. ESI-MS studies were performed by using Bruker BioTOF mass spectrometer and the data processing was done by using Bruker Daltonics software. NMR spectra were recorded on a Varian VXR-300 spectrometer at room temperature. Product analysis was performed on a Perkin Elmer sigma 3 gas chromatogram (AT-1701 column, 30m) with flame ionization detector. Resonance Raman spectra were collected using an excitation wavelength of 647.1 nm from a Spectra-Physics Model 2060 krypton ion laser and an ACTON AM-506 monochromator equipped with a Princeton LN/CCD data collection system. Low temperature spectra in CH_3CN were obtained at 77 K using a 135° backscattering geometry. Samples were frozen onto a gold-plated copper cold finger in thermal contact with a Dewar flask containing liquid nitrogen. Raman frequencies were calibrated to indene prior to data collection. The monochromator slit width was set for a band-pass of 4 cm^{-1} for all spectra. rR spectra were intensity corrected to the 773 cm^{-1} solvent peak. Mössbauer spectra were recorded with two spectrometers, using Janis

Research Super-Varitemp dewars that allowed studies in applied magnetic fields up to 8.0 T in the temperature range from 1.5 to 200 K. Mössbauer spectral simulations were performed using the WMOSS software package (WEB Research, Edina, MN). Isomer shifts are quoted relative to Fe metal at 298 K.

Table 3.1. Summary of crystallographic data for [Fe(Tp^{iPr2})(PRV)] (**1**) and [Fe(Tp^{iPr2})(BF)] (**2**).

	1.3CH_2Cl_2	**2**.C_5H_{12}
Empirical formula	C_{34} H_{59} B Cl_6 Fe N_6 O_4	C_{75} H_{114} B_2 Fe_2 N_{12} O_6
Formula weight	895.23	1413.10
T (K)	173(2)	173(2)
Mo Kα λ, Å	0.71073	0.71073
space group	P-1	P2/c
a (Å)	12.549(3)	11.3474(10)
b (Å)	13.537(3)	13.0436(11)
c (Å)	13.733(3)	26.760(2)
α (deg)	88.421(3)	90°
β (deg)	89.132(3)	97.690(1)°
γ (deg)	80.386(3)	90°
V (Å ^{3})	2299.2(10) Å3	3925.1(6)
Z	2	2
R1[a]	0.0473	0.0416
wR2[b]	0.1358	0.1100

[a]$R_1 = \Sigma||F_o|-|F_c|| / \Sigma|F_o|$; [b]$wR2 = [\Sigma[w(F_o^2-F_c^2)^2] / \Sigma [w(F_o^2)^2]]^{1/2}$

3.3 Synthesis and Characterization of Iron(II) complexes ($FeTp^{iPr2}PRV$ and $FeTp^{iPr2}BF$)

The two complexes, $[Fe^{II}(Tp^{iPr2})(O_2CC(O)CH_3)]$ (**1**) and $[Fe^{II}(Tp^{iPr2})(O_2CC(O)Ph)]$ (**2**), were synthesized by mixing equimolar portions of the iron(II) salt with KTp^{iPr2}, followed by addition of sodium pyruvate (NaPRV) or sodium benzoylformate (NaBF) (see Scheme 3.3 for ligand structures). Diffraction quality crystals could be obtained for both **1** and **2**, and their crystal structures are shown in Figure 3.1.

Scheme 3.3 Tridentate **Tp** ligand and co-substrate α-ketoacid anions

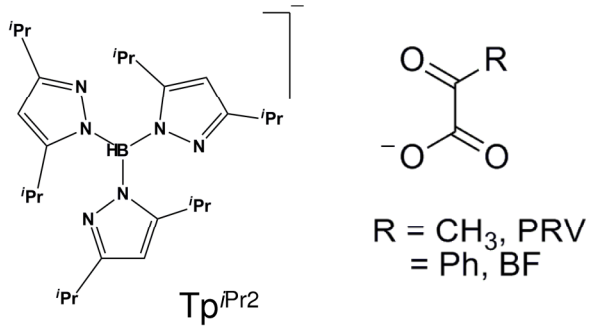

The structure of **1** shows a six-coordinate iron center with a face-capping tridentate Tp^{iPr2}, a bidentate PRV, and a methanol solvate. The structure of **2** exhibits a similar iron coordination environment but features a centrosymmetric dinuclear complex where the methanol solvate in the sixth coordination site of **1** is replaced by the carbonyl oxygen atom of the carboxylate of the BF ligand of the adjacent iron unit in **2**. Complex **2** represents in fact the first example of a complex with a κ^3-bridging mode of BF. The only

other example of a κ^3-bridging mode for an α-ketoacid is found in the structure of the $[Fe^{II}_2(6\text{-}Me_3\text{-}TPA)_2(phenylpyruvate)]^{2+}$ complex.[135] In this latter case, the keto group of the phenylpyruvate has become enolized and the ligand is bound as a dianion, as indicated by a C2–C3 bond length corresponding to a double bond. In contrast, the C2–C3 bond of the BF ligand of **2** has a C–C bond length consistent with a C–C single bond (1.475(3) Å) and the BF binds as the monoanionic keto tautomer.

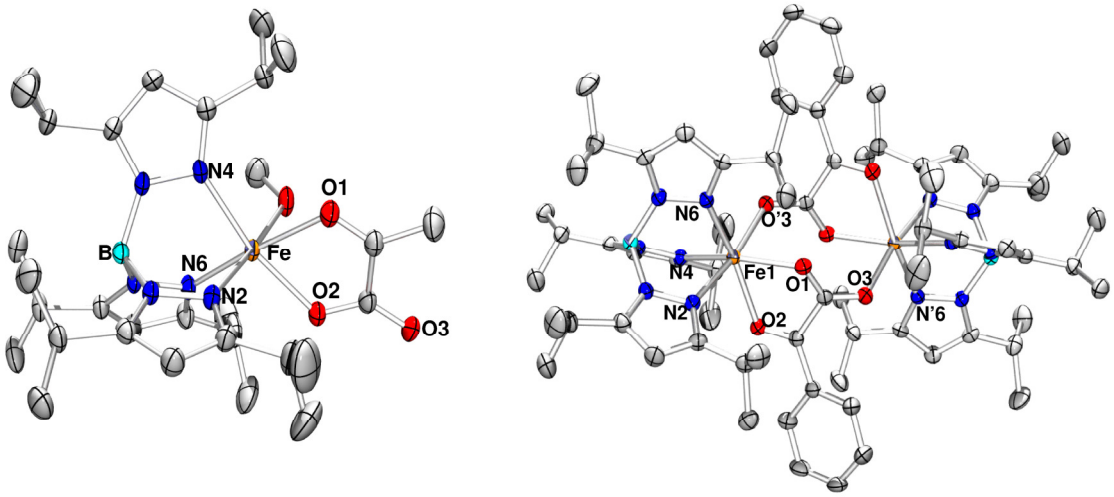

Figure 3.1: X-ray crystal structures of [Fe(Tp^{iPr2})(PRV)(MeOH)] (**1**) and [Fe(Tp^{iPr2})(BF)] (**2**). ORTEP (Oak Ridge thermal ellipsoid plot) drawings with atoms at 50% probability, hydrogen atoms are omitted for clarity.

Selected bond lengths are listed in Table 3.2 and compared with those from related structures. The Fe–$N_{pyrazole}$ bond lengths of **1** and **2** are typical of Tp$^{R,R'}$

complexes with high-spin iron(II) centers.[82,84,136] ^{1}H-NMR spectra of **1** and **2** support this conclusion as well (see Experimental Section). Both α-ketoacids bind as monoanions, as indicated by the absence of counterions in **1** and **2**. While the observed Fe–O_{keto} bond lengths are comparable to those found for related [Fe($Tp^{R,R'}$)(α-ketocarboxylate)] complexes, the Fe–$O_{carboxylato}$ bonds are at least 0.14 Å longer than those found for five-coordinate complexes.

Table 3.2: Comparison of selected bond lengths of **1** and **2** with those of related structures.

	1	**2**	**4**[a]	**5**[a]	**6**[b]
Fe–$O_{carboxylato}$	2.1180(18)	2.1691(15) 2.1832(15)[c]	1.967(5)	1.968(4)	1.975(7)
Fe–O_{keto}	2.2294(18)	2.2514(15)	2.242(6)	2.206(5)	2.261(7)
Fe–N2	2.181(2)	2.1954(17)	2.163(6)	2.188(5)	2.116(9)
Fe–N4	2.138(2)	2.1041(17)	2.088(8)	2.068(5)	2.173(9)
Fe–N6	2.139(2)	2.0919(17)	2.106(8)	2.086(5)	2.112(9)
C2–C3$_{α\text{-ketoacid}}$	1.483(4)	1.475(3)	1.498(9)		

a # [84]; b # [82], [c] Corresponding to *r*(Fe1-O3′)

The observed nuclearities of **1** and **2** derive from a difference in solvents used for the preparation of the complexes and their recrystallization, MeOH/CH_2Cl_2 for **1** and CH_2Cl_2/pentane for **2**. These results are consistent with those reported by Kitajima for [Fe^{II}(Tp^{iPr2})(O_2CPh)] (**3**) where **3** crystallized as the five-coordinate complex in pentane and as the six-coordinate solvate in MeCN.[136] Indeed FeTp complexes are often found to

crystallize as six-coordinate MeCN or pyrazole adducts.[82,84,131,136] It would thus appear likely that **2** is mononuclear in MeCN solution. In support, the λ_{max} for **2** in toluene is observed at 627 nm, somewhat red-shifted relative to that in MeCN (610 nm), whereas the λ_{max} for **1** remains unchanged in both of these solvents. The latter observation suggests that a change in solvent polarity does not affect the position of the MLCT band in **1**. The blue shift observed for **2** in MeCN must have a different rationale and can be understood by considering that **2** retains its dimeric structure in the nonpolar toluene solvent but becomes monomeric in the coordinating MeCN solvent. Thus the displacement of the carboxylate oxygen from the other iron unit of dimeric **2** by a stronger-field MeCN ligand to the iron(II) center would be expected to lower the energy of the iron(II) d_π orbitals and increase the energy gap for the iron(II)-to-α-ketocarboxylate MLCT transition.

3.4. Reactions of FeTp^{iPr2}PRV(1) and FeTp^{iPr2}BF(2) with Dioxygen at Room Temperature

Complex **1** exhibits a distinct red color in solution corresponding to a visible band with an absorption maximum at 500 nm along with two shoulders at 540 and 458 nm (Figure 2). The corresponding transitions in **2** are red-shifted with a maximum at 610 nm, giving rise to a blue solution (Figure 2). These bands in the visible region are assigned to metal-to-ligand charge transfer (MLCT) transitions of an iron(II)-(κ^2-α-ketocarboxylate) unit by analogy to previous work.[80,84] The MLCT assignment is consistent with the observed red shift upon replacement of the methyl group with a more electron withdrawing phenyl group on the α-ketocarboxylate.[84]

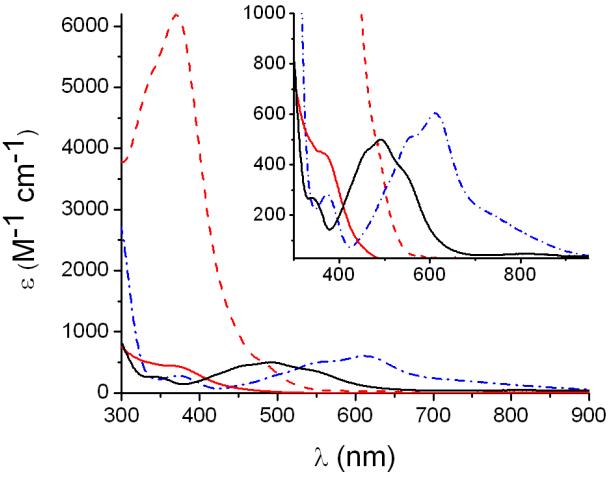

Figure 3.2. UV-Vis spectra in MeCN of **1** (black solid line), **2** (blue dashed-dotted line), the yellow solution obtained upon oxygenation (red dashed line) and the solution obtained upon oxygenation in the presence of THT (red solid line). Inset shows the corresponding magnified spectra in the visible region.

Bubbling O_2 through the red solution of **1** in MeCN at 25 °C resulted in the onset of immediate spectral changes consisting of the loss of the MLCT band at 500 nm and its replacement by an intense near-UV feature with an absorption maximum at 370 nm (ε = 6000 $M^{-1}cm^{-1}$) over the course of 15 min (Figure 2). ESI-MS analysis suggested the formation of an alkoxoiron(III) product, as manifested by peaks at *m/z* = 536 and 688 that were observed along with peaks at *m/z* = 521 and 673. The peak at *m/z* = 521 together with its isotope distribution pattern can be assigned to the $[Fe^{II}(Tp^{iPr2})]^+$ ion. On the other hand, the peak at *m/z* = 536 has a mass and an isotope distribution pattern that correspond to an ion with the composition of $[[(Tp^{iPr2})Fe^{III}] + O - H]^+$(see Figure 3.3); that is, one hydrogen atom has been replaced by an oxygen atom, suggesting that the hydroxylation of the Tp^{iPr2} ligand in the course of the reaction to form the oxidation product **4**. The most likely place for ligand hydroxylation is at one of the 3-isopropyl methine carbons, as methine groups have the weakest C–H bonds present in the ligand and is also in the close vicinity of the iron center. Hydroxylation of a 3-isopropyl group of the Tp^{iPr2} ligand would introduce a tertiary alcohol functionality near the iron center and lead to the formation of a metal-alkoxide bond. We thus assign the *m/z* = 536 peak as $[Fe(Tp^{iPr2*})]^+$ where Tp^{iPr2*} represents the Tp^{iPr2} ligand in which the 3° C–H bond of one 3-isopropyl group on the Tp^{iPr2} ligand has been hydroxylated. The peaks at *m/z* = 673 and 688 correspond respectively to the 3,5-diisopropylpyrazole adducts of the ions with *m/z* = 521 and 536. Analogous attack of a 3-isopropyl C–H bond has previously been demonstrated in the reactions of $[Mn^{II}_2(Tp^{iPr2})_2(OH)_2]$ and $[Co^{I}(Tp^{iPr,Me})]$ with O_2, with a crystal structure reported for the alkoxomanganese product complex.[137,138] The yellow chromophore **4** thus arises from an alkoxo-to-iron(III) charge transfer transition, as

observed for $[Fe^{III}(Py5)(OMe)]^{2+}$ (λ_{max}, 337 nm; ε, 3600 $M^{-1}cm^{-1}$; Py5 = 2,6-bis(bis(2-pyridyl)methoxymethane)pyridine)[139] and $[Fe^{III}(N4Py)(OMe)]^{2+}$ (λ_{max}, 360 nm; ε, 4000 $M^{-1}cm^{-1}$; N4Py = *N,N*-bis(2-pyridylmethyl)bis(2-pyridyl)methylamine)).[140]

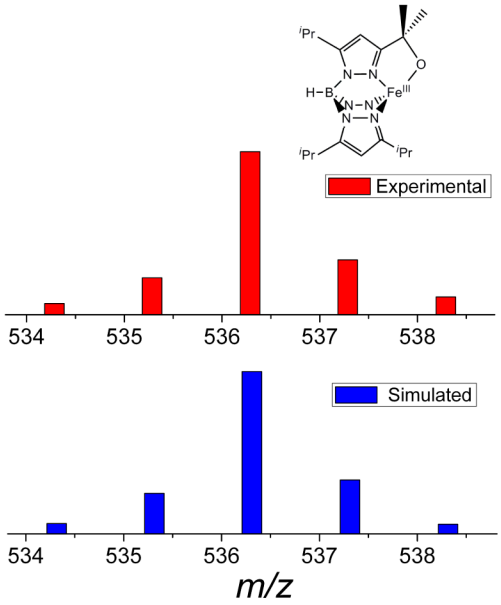

Figure 3.3 ESI-MS spectrum when MeCN solution of **1** or **2** (1 mM) is exposed to oxygen at room temperature. The peak at m/z = 536, matches with the formula $[Fe(Tp^{iPr2}*)]^{+}$ as schematically described at right.

Additional corroboration for the ESI-MS results was obtained from ^{1}H-NMR analysis of the organic components of the yellow solutions derived from the oxygenation of **1** and **2**, extracted after treatment of the yellow solutions with strong acid. In the case of **2**, quantitative conversion of benzoylformate to benzoate was indicated by the disappearance of peaks characteristic of the *ortho* protons of the benzoylformate at 8.36 ppm and the appearance of corresponding benzoate features at 8.14 ppm (Figure 3.4).

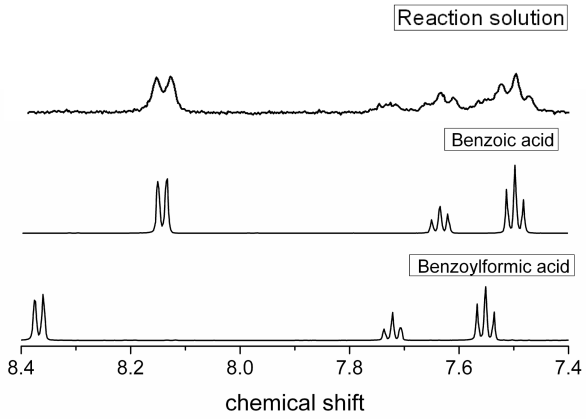

Figure 3.4. ^{1}H-NMR spectrum (300MHz, $CDCl_3$ at 25°C) of the organic product after reaction of **2** with O_2.

More importantly for both **1** and **2**, NMR features were observed for two pyrazoles, namely 3,5-diisopropylpyrazole (5.90 ppm for the pyrazole-4-H) and 3-isopropenyl-5-isopropylpyrazole (5.84 ppm for the pyrazole-4-H and 5.3 ppm for one of the vinyl C–H protons). These features were found to be in a ratio of 2:1 (Figure 3.5), showing that one of the three pyrazoles in the Tp^{iPr2} ligand had been modified. Both 3,5-diisopropylpyrazole and 3-isopropenyl-5-isopropylpyrazole were formed upon acid decomposition of the Tp^{iPr2*} ligand. The 3-isopropenyl-5-isopropylprazole most likely derived from dehydration of hydroxylated 3,5-diisopropylpyrazole, as tertiary alcohols are well known to lose water easily upon reaction with acid to generate alkenes. Notably, ESI-MS analysis of the yellow product solution prior to acid decomposition (Figure 3.5) did not show a prominent peak at m/z = 519 corresponding to the $[(Tp^{iPr2})Fe^{II} - 2H]$ ion, indicating that 3-isopropenyl-5-isopropylpyrazole was not formed during the initial oxygenation. These NMR results demonstrate the quantitative oxidative decarboxylation

of the bound α-keto acid and concomitant formation of an oxidant that carries out the ligand oxidation, as precedented in the oxygenation of [$Fe^{II}(Tp^{Ph2})$(α-ketocarboxylate)] complexes.[83,84,135]

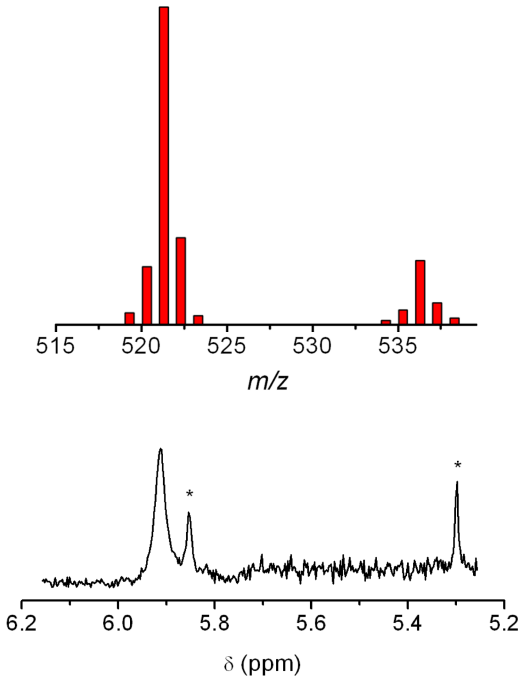

Figure 3.5. Top: ESI-MS spectrum of **1** after oxygenation but prior to acid treatment. Bottom: ^{1}H-NMR spectrum in the 5.2-6.2-ppm region of the pyrazoles in $CDCl_3$ obtained from the reaction of **1** with O_2 after acid treatment to decompose the Tp^{iPr2} ligand (*-marked peaks are from 3-isopropenyl-5-isopropylpyrazole; the peak at 5.90 ppm is the 4-*H* of the 3,5-diisopropylpyrazole).

To further characterize the oxidant responsible for ligand hydroxylation, experiments were carried out in the presence of potential substrates in an attempt to intercept this oxidant intermolecularly. Such interceptions by either dialkyl sulfides or hydrocarbons have been documented in the oxygenation of [$Fe^{II}(Tp^{Ph2})$(BF)].[101] When

the oxygenation of **1** or **2** was performed in the presence of 100 mM tetrahydrothiophene (THT), the intense yellow chromophore associated with $[Fe(Tp^{iPr2*})]^+$ did not form. ESI-MS analysis of this solution revealed only one major peak at m/z = 625, whose mass and isotope distribution pattern matched those for $[Fe^{II}(Tp^{iPr2})[(OS(CH_2)_4]]^+$ (Figure 3.6). Tetramethylenesulfoxide was confirmed to be the oxidation product by GC and GC-MS analysis (80% yield with naphthalene as an internal standard). Interestingly, neither thioanisole nor diphenyl sulfide was capable of intercepting the oxidant, in contrast to what was reported in the oxygenation of $[Fe(Tp^{Ph2})(BF)]$;[101] instead the 370-nm chromophore obtained in the absence of any substrate was observed. Thus **1** and **2** are only able to carry out oxo-transfer to THT. Both steric and electronic factors can be used to rationalize the lack of reactivity towards thioanisole and diphenyl sulfide. Clearly the rates of oxo-transfer to these potential substrates are smaller than the rate of intramolecular C–H bond cleavage by the incipient oxidant.

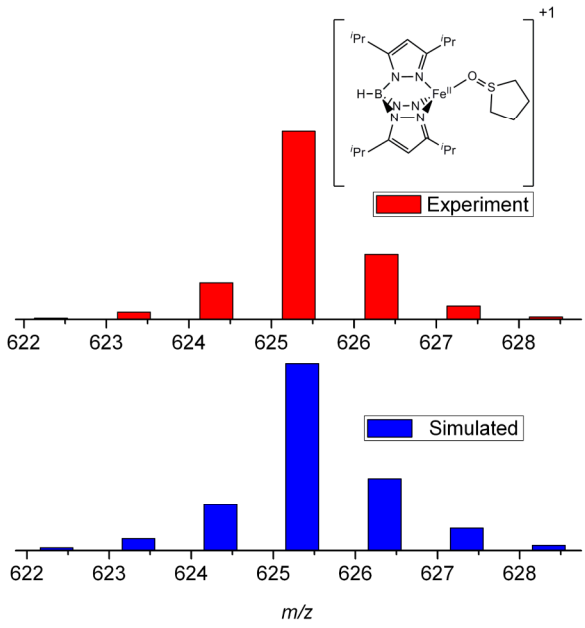

Figure 3.6. ESI-MS spectrum, when MeCN solution of **1** or **2** (1 mM) is exposed to oxygen at room temperature in the presence of tetrahydrothiophene (100 mM). The peak at m/z = 625, matches with the formula $[Fe(Tp^{iPr2})(OS(CH_2)_4)]^+$ as schematically described at right.

3.5. Oxygen Activation at Low Temperature

3.5.1 Reactions of $FeTp^{iPr2}PRV$ and $FeTp^{iPr2}BF$ with Dioxygen at - 40 °C

The reactivities of **1** and **2** with O_2 diverge at – 40 °C. While the reactivity of **2** with O_2 at – 40 °C mirrored that at 25 °C, i.e. intramolecular ligand hydroxylation and intermolecular sulfoxidation, this behavior did not apply to **1**. Oxygenation of **1** at – 40 °C in MeCN afforded a distinct chromophore with λ_{max} at 680 nm ($\varepsilon \sim 1600\ M^{-1}cm^{-1}$/Fe) that was stable for days at this temperature (Figure 3.7). This green chromophore was very similar to those observed in the oxygenation of $[Fe^{II}(Tp^{iPr2})(O_2CPh)]$ (**3**) (λ_{max} 682 nm; $\varepsilon = 1700\ M^{-1}cm^{-1}$/Fe) and $[Fe^{II}(Tp^{iPr2})(O_2CCH_2Ph)]$ (λ_{max} 694 nm; $\varepsilon = 1300\ M^{-1}cm^{-1}$/Fe) in toluene, which was shown by spectroscopy and crystallography to be $[Fe_2(O_2)(Tp^{iPr2})_2(O_2CR)_2]$, a complex with a (μ-1,2-peroxo)diiron(III) core supported by two carboxylate bridges.[136,141]

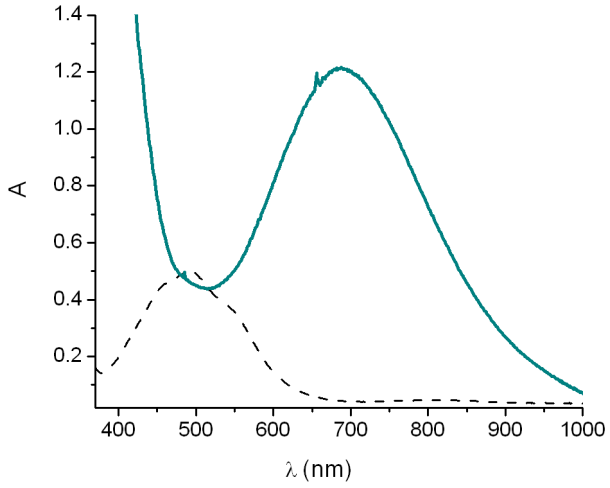

Figure 3.7. Oxygenation of 1 mM [$Fe^{II}(Tp^{iPr2})$(PRV)] (**1**) (dashed line) at -40°C in MeCN resulting in the formation of a green chromophore (solid line), that is assigned to a (μ-1,2-peroxo)diiron(III) complex.

The resonance Raman (rR) spectrum of the green chromophore was thus obtained to determine its similarity to the O_2 adduct described by Kitajima.[136] Excitation at 647.1 nm elicited two resonance enhanced vibrations at 889 and 424 cm^{-1} (Figure 3.8); these were respectively assigned to ν(O–O) and ν(Fe–O) modes of the (μ-1,2-peroxo)diiron(III) unit by their frequencies and ^{18}O isotopic shifts, which closely matched those reported for the Kitajima O_2 adducts (Table 3.3). The isotopic shifts observed for these vibrations, from 889 cm^{-1} to 842 cm^{-1} and 424 cm^{-1} to 408 cm^{-1}, are in accord with the isotopic shifts predicted for a diatomic oscillator (838 and 405 cm^{-1}, respectively), supporting the assignment of the visible absorption band as a peroxo-to-Fe^{III} charge transfer transition (Figure 3.7). While there are many examples of (μ-η^1:η^1-

peroxo)diiron(III) complexes in the literature,[6,142,143] only a handful derive from dioxygen binding to a mononuclear iron complex.

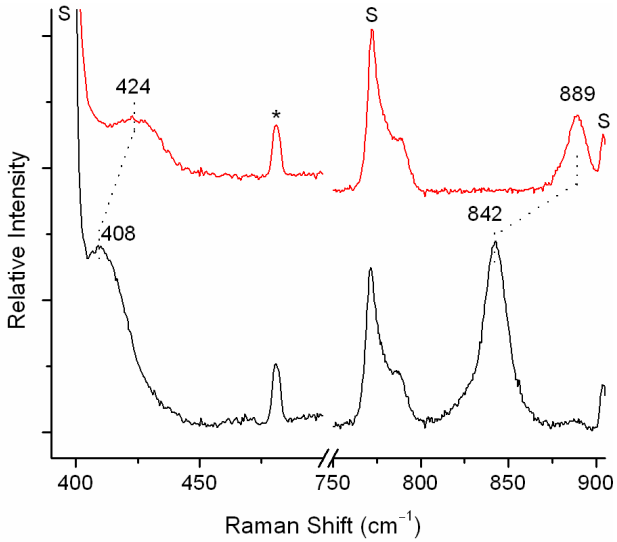

Figure 3.8. Resonance Raman spectra using λ_{ex} = 647.1 nm of the green chromophore in MeCN with $^{16}O_2$ (top) and $^{18}O_2$ (bottom). Solvent peaks are denoted as "S" and the asterisk denotes a laser plasma line.

In order to further corroborate the nature of the O_2 adduct, the frozen MeCN solution of the green chromophore was studied with Mössbauer spectroscopy. The zero field spectrum of Figure 3.9A exhibits two doublets. One doublet (ΔE_Q = 3.42(4) mm/s, δ = 1.21(2) mm/s, 40% of Fe) is attributable to a high-spin iron(II) complex and very likely represents the starting material **1**. The second doublet (45% of Fe), outlined by the solid line, has parameters (ΔE_Q = 1.32(3) mm/s and δ = 0.65(2) mm/s) that are very similar to those of the O_2 adduct of [$Fe^{II}(Tp^{iPr2})(O_2CCH_2Ph)$] characterized by Kim and Lippard.[141]

Studies in strong applied magnetic fields revealed that the sample contained also a mononuclear $S = 5/2$ Fe^{III} species (10%). The spectra of Figure 3.9B and C, representing the green chromophore, were obtained by subtracting from the raw data the contributions of the Fe^{II} and $S = 5/2$ Fe^{III} species. The solid line in Figure 3.9B is a spectral simulation based on the assumption that the peroxo intermediate has a diamagnetic ground state. The magnetic splitting at 100 K (Figure 3.9C) is smaller than at 4.2 K, a feature observed for antiferromagnetically coupled dinuclear Fe^{III} peroxo complexes with *J*-values around 70 cm^{-1} (in the $H = J\ \mathbf{S_1 \bullet S_2}$ convention; $S_1 = S_2 = 5/2$). The observed diamagnetism in conjunction with the observed exchange interactions demonstrates that the green chromophore is a diiron(III) complex. Our spectral simulation, performed with the 2Spin option of WMOSS, yielded $J = 70 \pm 10$ cm^{-1}. This J value is in good agreement with the value of 66 cm^{-1} determined from variable temperature magnetic susceptibility measurements on the O_2 adduct of $[Fe^{II}(Tp^{iPr2})(O_2CPh)]$.[136] Our studies thus formulate the green solution as having an antiferromagnetically coupled high-spin (μ-1,2-peroxo)diiron(III) unit, as found for other O_2 adducts of $[Fe^{II}(Tp^{iPr2})(O_2CR)]$ (Table 3.3).

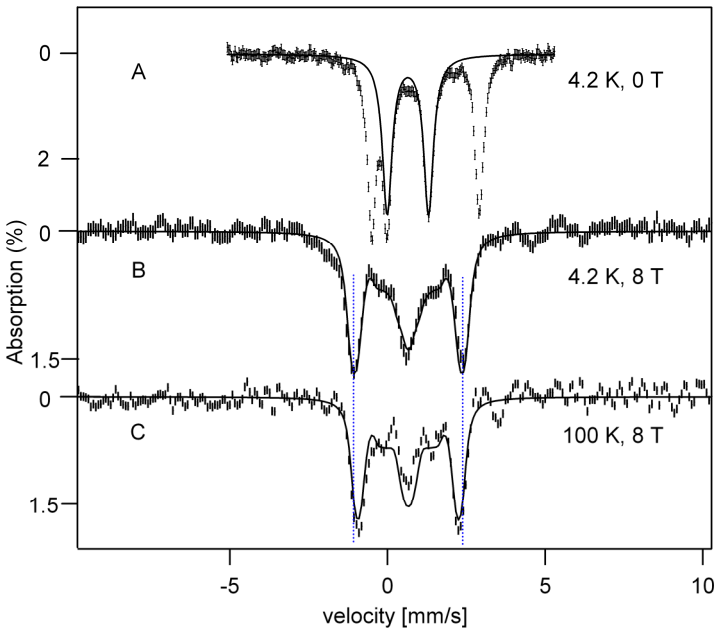

Figure 3.9. Mössbauer spectra of the green solution obtained from the oxygenation of **1** in MeCN at -40 °C. (A) Spectrum recorded for B = 0. The solid line outlines the contribution of the peroxo intermediate (45% of Fe). (B) and (C) Spectra of the peroxo intermediate recorded in a parallel field of B = 8.0 T at the temperatures indicated; features arising from the Fe^{II} and mononuclear Fe^{III} species were removed as described in Supporting Information. Solid lines in (B) and (C) are spectral simulations for $J = 70$ cm^{-1}. Hyperfine parameters are: $A_0/g_n b_n = -21$ T, $\Delta E_Q = +1.32$ mm/s, h = 1, and $\delta = 0.65$ mm/s for both sites; the Hamiltonian is given in SI. Sincere thanks to our collaborators, Prof. Münck and his students, for their help in Mössbauer analysis.

Table 3.3: Comparison of spectroscopic properties of the peroxo intermediate derived from **1** with similar complexes (^{18}O isotope shifts indicated in parentheses).

	δ ΔE_Q mm/s (mm/s)	λ_{max} (ε) nm (M^{-1} cm^{-1})	ν(O–O) cm^{-1}	ν(Fe–O) cm^{-1}
Peroxo intermediate (obtained from **1**+ O_2)	0.65 (1.32)	680 (2500)	889 (-47)	424 (-16)
$[Fe^{III}_2(\mu\text{-}1,2\text{-}O_2)(\mu\text{-}O_2CPh)_2(Tp^{iPr2})_2]$ [a]	--	682 (3450)	876 (-48)	421 (-12)
$[Fe^{III}_2(\mu\text{-}1,2\text{-}O_2)(\mu\text{-}O_2CCH_2Ph)_2(Tp^{iPr2})_2]$ [b]	0.66 (1.40)	694 (2650)	888 (-46)	415 (-11)
$[Fe^{III}_2(\mu\text{-}O)(\mu\text{-}1,2\text{-}O_2)(6\text{-}Me_2BPP)]^{2+}$ [c]	0.50 (1.31)	644 (3000)	847 (-33)	465 (-19)
$[Fe^{III}_2(\mu\text{-}1,2\text{-}O_2)(N\text{-Et-HPTB})(OPPh_3)_2]^{2+}$ [d]	0.51 (0.80)	588 (1500)	900 (-50)	471 (-16)
$[Fe^{III}_2(\mu\text{-}O)(\mu\text{-}1,2\text{-}O_2)(6\text{-Me-BQPA})]^{2+}$ [d]	--	not reported	853 (-45)	463 (-15)
$[Fe^{III}_2(\mu\text{-}O)(\mu\text{-}1,2\text{-}O_2)(BQPA)]^{2+}$ [d]	--	620 (1000)	844 (-44)	464 (-17)

[a] Ref #[136]. [b] Ref #[141]. [c] Ref #[144]; 6-Me_2BPP = *N*,*N*-bis(6-methyl-2-pyridylmethyl)-3-aminopropionate. [d]Ref #[143]; *N*-Et-HPTB = anion of *N,N,N′,N′*–tetrakis(2-benzimidazolylmethyl)-2-hydroxy-1,3-diaminopropane; BQPA = bis(2-quinolylmethyl)-2-pyridylmethylamine.

However the formation of the peroxo intermediate was prevented by the presence of 2,4,6-tri-*tert*-butylphenol (TBP-H). When the oxygenation of **1** (1 mM) was performed at – 40 °C in the presence of even only one equivalent of TBP-H, the green chromophore associated with the peroxo intermediate did not form at all. Instead, sharp peaks characteristic of TBP• were observed at 373 and 400 nm along with a weak broad band at

620 nm, (Figure 3.10) with intensities corresponding to an 80% yield of the phenoxyl radical. Under these conditions, phenoxyl radical formation occurred within 3 min, with an estimated first order rate constant of 2.1(4) x 10^{-2} s^{-1}. This value did not change significantly with the use of more equivalents of TBP-H, suggesting that the phenoxyl radical formation occurs after the rate determining step that generates the oxidant.

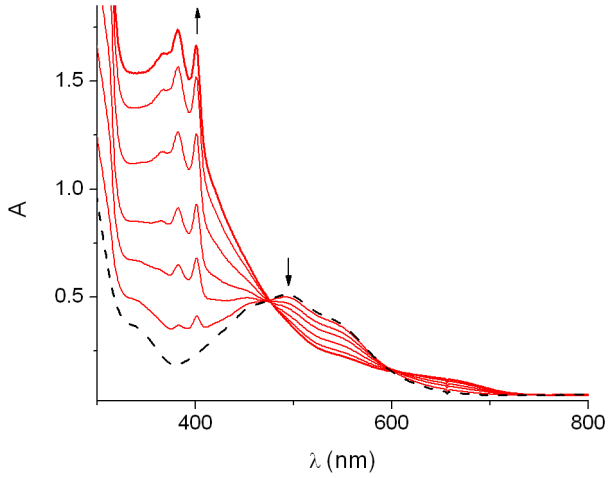

Figure 3.10. Oxygenation of 1 mM [Fe(Tp^{iPr2})PRV](black line) at -40°C in MeCN in the presence of 1 equiv TBP-H in a 1-cm cuvette. Red lines show the growth of TBP• features.

Control experiments showed that the pre-formed (μ-peroxo)diiron(III) species (1 mM in Fe) also decayed in the presence of TBP-H at – 40 °C but with complex kinetic behavior. Furthermore the time scale for decay was nearly two orders of magnitude longer (~70-fold). This much slower reaction cannot rationalize the effect of TBP-H in completely preventing peroxo intermediate formation. Instead, TBP-H must react more rapidly with a precursor of the peroxo intermediate to prevent its accumulation. We propose that this more reactive intermediate is the initial O_2 adduct of **1**, the formation of

which represents the rate-determining step. Following heme precedents, the **1**•O_2 adduct can be formulated as an iron(III)-superoxo species, which can abstract a hydrogen atom from phenol. Such H-atom abstractions have been observed for other metal-superoxo species. [125,127,128]

Interestingly, the oxygenation of [$Fe^{II}(Tp^{iPr2})(O_2CPh)$] at – 50 °C in the presence of as much as 100-fold excess of TBP-H did not prevent formation of the corresponding peroxo intermediate, which suggests that TBP-H is unable to intercept the corresponding iron(III)-superoxo species in this case before it reacts with residual iron(II) precursor. However there are some differences in the conditions under which the respective peroxo intermediates of **1** and **3** can be observed. In the latter case, formation of the peroxo intermediate was observed upon oxygenation of the iron(II) precursor in toluene but not in MeCN.[136] Kitajima conjectured that the likely coordination of MeCN to the metal may inhibit O_2 binding to the coordinately saturated iron(II) center. Clearly the solvent MeCN does not play such an inhibitory role in the case of **1**, as a good yield of the peroxo intermediate was observed in MeCN. In fact, only a 10% yield of the peroxo intermediate was obtained for the oxygenation of **1** at – 40 °C in toluene. The fact that TBP-H fails to inhibit peroxo intermediate formation in the case of **3** suggests that the lifetime of the putative iron(III)-superoxo intermediate is too short to allow its interception by TBP-H. The subsequent reaction with residual iron(II) precursor must be strongly favored over the reaction with TBP-H. Clearly, further investigation of the reaction of **3** with O_2 and its differences with **1** is warranted.

3.5.2 Effect of Substituted Phenols in the Iron-oxygen Adduct Derived from $FeTp^{iPr2}PRV$

Further investigation of the reaction of **1** with dioxygen in the presence of different H-atom donor leads to a unique observation. When oxygenation reaction of **1** (0.75mM) in MeCN was performed in the presence of different phenols (1 equivalent with respect to **1**), 4-methoxy-2,6-di-*tert*-butylphenol and 2,4,6-tri-*tert*-butylphenol were able to prevent the formation of the peroxo intermediate, but 4-methyl-2,6-di-*tert*-butylphenol lead to incomplete prevention. In the case of 4-methoxy-2,6-di-*tert*-butylphenol, sharp features at 380 and 406 nm along with weak absorbance near 600 nm region confirmed the formation of the corresponding phenoxyl radical. But no phenoxyl radical feature was observed in the case of 4-methyl-2,6-di-*tert*-butylphenol (Figure 3.11).[145]

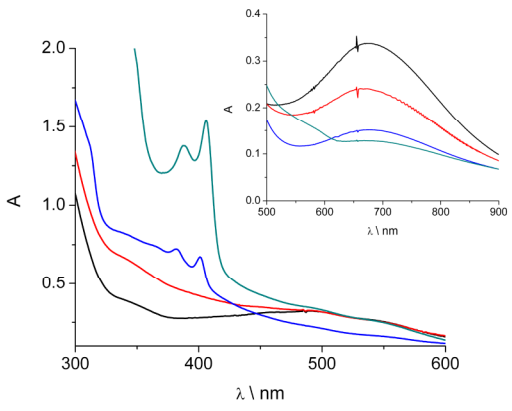

Figure 3.11 Initial oxygenation of **1** (0.75 mM) at -40 °C in MeCN in the presence of 1 equiv phenols in a 1-cm cuvette. Each spectrum correspond to a different experiment collected 45 second after bubbling of oxygen: black line **1** + O_2 + no phenol; red line **1** +

4-methyl-2,6-ditertbutylphenol + O_2; blue line **1** + 2,4,6-tri-*tert*-butylphenol(TBP-H) + O_2; green line **1** + 4-methoxy-2,6-di-*tert*-butylphenol + O_2. Inset: Show the growth of the peroxo features after 500 seconds in the same reactions. Low absorbance observed in the blue and green spectrum is associated with the phenoxyl radical feature.

Interestingly, when the oxygenation reaction of **1** was performed in the presence of 1 equivalent Bn-TEMPOH at – 40 °C in MeCN, incomplete prevention of the peroxo intermediate was observed (Figure 3.12). Raising the concentration of Bn-TEMPOH did reduce the formation of the peroxo, but it was not completely prevented even though the concentration of substrate was raised 5 times (because of the low solubility of Bn-TEMPOH, higher concentration experiments were difficult to carry out).

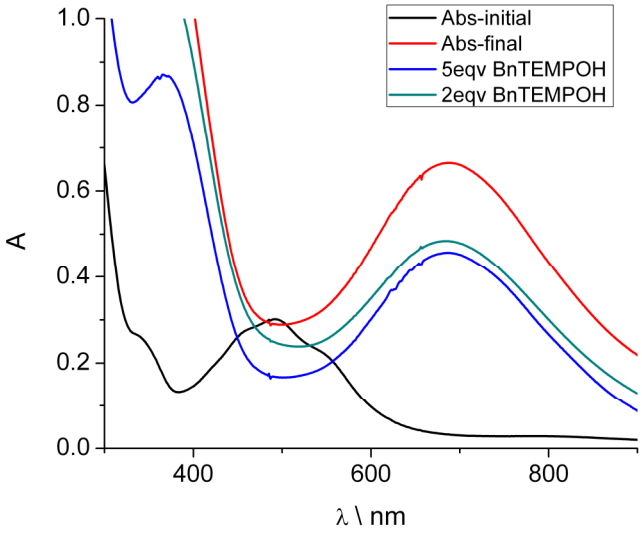

Figure 3. 12. Oxygenation of **1** in the presence of Bn-TEMPOH in MeCN at -40 °C. Black line: **1** alone; red line: **1** + O_2; blue and green line: **1** + Bn-TEMPOH + O_2.

3.6 Discussion

We have considered the accumulated observations described above and postulate the mechanistic framework illustrated in Scheme 3.4 to rationalize the different outcomes from **1** and **2**. We propose an iron(III)-superoxo species as the common intermediate that is formed initially in the oxygenation of **1** and **2**. This species has a number of possible fates (Scheme 3.4). The bound superoxide can act as a nucleophile and attack the electrophilic keto carbon of the bidentate α-keto acid to initiate oxidative decarboxylation, according to the generally accepted mechanism for 2-OG-dependent iron enzymes. [36] Alternatively, the bound superoxide can accept an electron from residual iron(II) precursor to form the diiron(III)-peroxo intermediate. Thirdly, the bound superoxide can abstract a hydrogen atom from added phenol. All three outcomes have been observed in the case of **1** depending on the reaction conditions.

Scheme 3.4. Reactions of [$Fe^{II}(Tp^{iPr2})X$] complexes with dioxygen

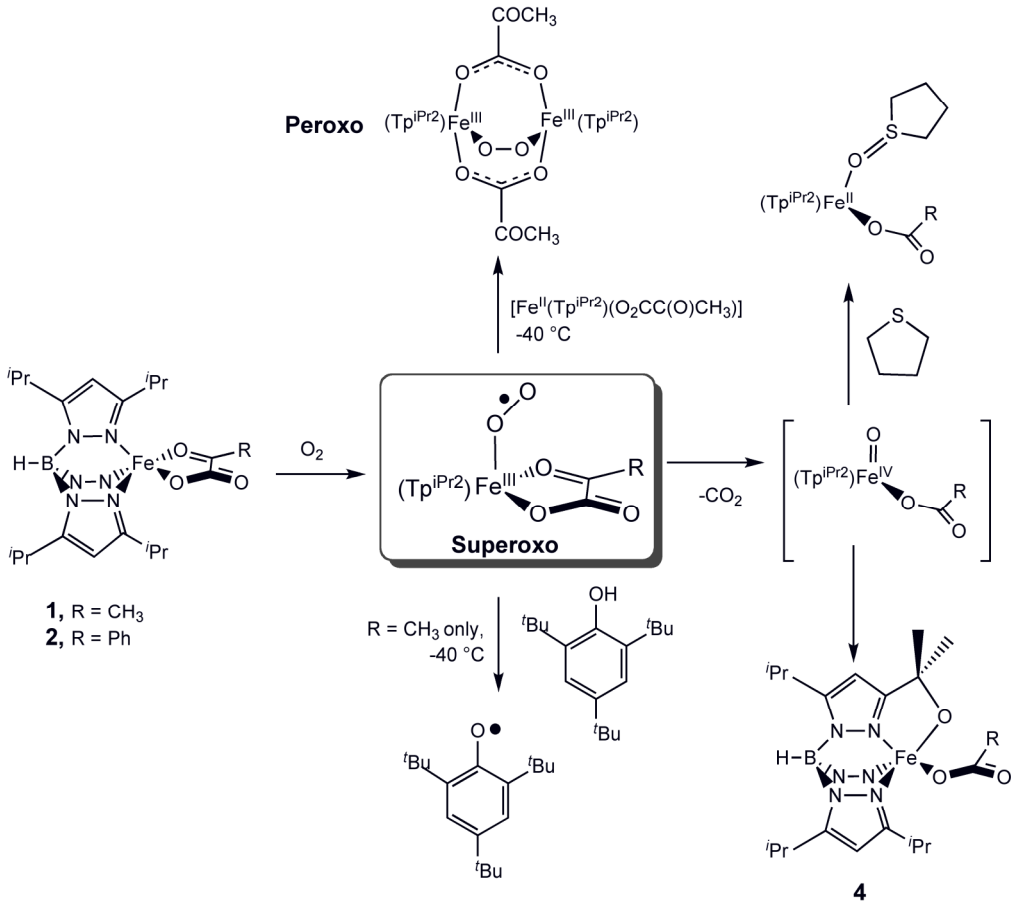

These three distinct reactions presumably have different activation barriers. For **1**, oxidative decarboxylation is strongly favored at 25 °C, and the putative iron(IV)-oxo oxidant produced therefrom is able to carry out intramolecular attack of an isopropyl C–H bond on the Tp ligand or intermolecular oxo-atom transfer to THT. In contrast, oxidative decarboxylation does not readily occur at – 40 °C; instead a green chromophore identified to be a diiron(III)-peroxo intermediate forms, analogous to that previously reported in the oxygenation of **3**. However, peroxo formation can be prevented by the presence of the phenol TBP–H, which is oxidized to TBP•. This interception suggests

involvement of a superoxo species that is a precursor of the peroxo intermediate but can also abstract a hydrogen atom from TBP–H.

Further investigation on the reactivities of this superoxo species lead to a unique observation. Complete prevention of the green peroxo intermediate is only observed in the presence of TBP-H and 4-methoxy-2,6-di-*tert*-butylphenol but not with 4-methyl-2,6-ditertbutylphenol or Bn-TEMPOH (4-benzyloxy-2,2-6,6-teramethylpiperidin-1-ol). The O-H bond energies of these phenols increases in the order 4-methoxy-2,6-di-*tert*-butylphenol (79.6 kcal/mol), 4-methyl-2,6-di-*tert*-butylphenol (80.5 kcal/mol) TBP-H (83.2 kcal/mol).[146] The O-H bond energy of Bn-TEMPOH is approximately 72 kcal/mol[104] and the reactivity depicted by the iron superoxo species towards these substrates (*vide supra*) could not be rationalized based on solely the bond strength of the O-H bonds. Further investigation is clearly needed to establish the reactivity pattern of the nascent iron-superoxo species.

The reaction energetics are clearly different for **2**. In this case, oxidative decarboxylation is favored both at 25 and – 40 °C and the corresponding peroxo intermediate is not observed to form at the lower temperature. This difference in reactivity from **1** suggests that the intramolecular attack of the superoxo moiety on the bound BF in **2** is much more facile at – 40 °C than the corresponding attack on the bound PRV in **1**, presumably resulting from the increased electrophilicity of the BF carbonyl carbon because of the more electron withdrawing phenyl group. As a result the superoxo intermediate derived from **2** is too short-lived to allow alternative intermolecular reaction pathways to occur.

Another factor to consider may be the relative basicities of the carboxylate ligands used in this study, as reflected by their aqueous pK_a values. They increase in the order: benzoylformic acid (1.39),[147] pyruvic acid (1.94),[148] benzoic acid (4.19).[149] The differing basicities of the bound carboxylate ligands will modulate the reducing power of the respective iron(II) centers and affect the equilibria that govern the initial O_2 binding step and the subsequent reaction of the O_2 adduct with a second molecule of $[Fe^{II}(Tp^{iPr2})(O_2CR)]$ to form the peroxo intermediate. Thus, formation of the peroxo intermediate should be most favorable for **3**. Indeed, unlike in the oxygenation of **1** at -40 °C, we found that the oxygenation of **3** cannot be prevented by the presence of TBP-H. The fact that the latter reaction occurs only in toluene solvent introduces another mechanistic variable to consider and details of the oxygenation mechanisms of **1** and **3** may differ. Clearly a more in-depth comparison of the oxygenation chemistry of **1** and **3** will be informative.

In conclusion we have described a set of three $Fe^{II}(Tp^{iPr2})$ complexes **1** – **3**, where the ancillary carboxylate or α-keto acid ligand significantly modulates the outcome of the reaction. In all three cases, the initial formation of a common iron(III)-superoxo intermediate is inferred. Under the appropriate conditions, this species derived from **1** can A) act as a nucleophile to initiate the oxidative decarboxylation of the bound α-ketocarboxylate, B) become reduced by another equivalent of iron(II) complex to form a diiron(III)-peroxo intermediate, or C) abstract a hydrogen atom from phenol. On the other hand, **2** reacts with O_2 and solely follows pathway A, while **3** follows only pathway B because of the differences in the electronic properties of the ancillary ligand. Iron(III)-superoxo species have also been implicated recently in the reactions of Fe^{II}(TMC) and

Fe^{II}(N4Py) (TMC = 1,4,8,11-tetramethyl-1,4,8,11-tetraaza-cyclotetradecane; N4Py = *N,N*-bis(2-pyridylmethyl)bis(2-pyridyl)methylamine) with O_2 in the presence of protons and reductants to form oxoiron(IV) and hydroperoxoiron(III) species respectively.[150,151] These reactions demonstrate the versatility of the iron(III)-superoxo moiety and support the mechanistic diversity illustrated in Scheme 3.4 for the various iron–O_2 adducts that must form in the catalytic cycles of nonheme iron oxidases and oxygenases.

Chapter 4

An Iron(II)-carboxylate Complex that Reacts with O_2 and Hydroxylates an Aliphatic C-H Bond

Compound Abbreviations:

1 = [$Fe^{II}(Tp^{iPr2})$(OBz]

2 = [$Fe^{II}(Tp^{iPr2})$(PRV)]

3 = [$Fe^{II}(Tp^{iPr2})$(BF)]

4 = [$Fe^{II}(Tp^{Ph2})$(OBz)]

5 = [$Fe^{II}(Tp^{iPr2*})$(OBz)]

4.1 Introduction

Oxygen activation, essential for many different physiological transformations, is performed in diverse mononuclear non-heme iron enzymes often with the help of the co-substrates like α-ketoglutarate, and tetrahydrobiopterin.[3,6] But how oxygen is activated at an iron center where these co-subtrates are absent is an open and intriguing question for chemists and bio-chemists to answer. Based on model studies two different mechanistic pathways have been proposed for oxygen activation at iron complexes without the co-substrates. In one class, oxygen activation occurs involving a hydroperoxo intermediate as proposed for the enzymes like Rieske dioxygenases.[3,152-154] In another pathway, the reaction is proposed to proceed with the help of another iron center, making a diiron peroxo intermediate, as proposed in the non-heme diiron enzymes like soluble methane mono-oxygenase (sMMO), ribonucleotide reductase (class 1a), toluene-mono-oxygenase.[116,155-157] In these enzymes the active site contain a di-iron center that is bridged by the carboxylate groups of the proteins. Even though in enzymes, oxygen is activated by a diiron center on a very fast time-scale, and oxygen activation can lead to oxidation of hydrocarbons, to date very few examples of model complexes are known that carry out the same chemistry.

In synthetic studies only two iron-carboxylate complexes are known that are able to hydroxylate the aromatic ring via oxygen activation. One example from the Que group, $[Fe^{II}(Tp^{Ph2})(OBz)]$, was shown to react with oxygen and perform hydroxylation of a phenyl ring of the ligand Tp^{Ph2}, albeit very slowly.[84] Although no intermediate has been observed, a dimeric peroxo intermediate has been proposed. The better characterized example comes from Suzuki's group.[158] Suzuki and coworkers were able to identify two diiron-peroxo-bridged intermediates supported by a heptacoordinated ligand and a carboxylate bridge. When complex $[Fe_2(L^{Ph4})(OOCCPh_3)]^{2+}$ was oxygenated at – 40 °C in dichloromethane, it formed an intense chromophore at 665 nm. The species associated with this chromophore was identified by ESI-MS and resonance Raman spectroscopy as a diferric-peroxo intermediate $[(\mu\text{-}1,2\text{-}O_2)Fe_2(L^{Ph4})(OOCCPh_3)]^{2+}$. Warming up the solution from – 40 °C to 25 °C resulted in decay of that chromophore and generation of a dark-blue chromophore. The ESI-MS characterization of the dark-blue solution suggested hydroxylation of the phenyl group of the ligand L^{Ph4}. The ligand recovery after decomposition of the complex, further established the hydroxylation of the phenyl group in 90% yield.[158] Both of the above mentioned reactions mimic the function of the enzyme toluene-mono-oxygenase, where a diferric-peroxo intermediate is invoked in the oxidation of an aromatic ring.[159,160] But oxidation of an aliphatic C-H bond, as in the primary reaction performed by soluble methane mono-oxygenase (sMMO), where a diferric-peroxo intermediate has been involved, has not been demonstrated in a synthetic system by oxygen activation.[116]

4.2 Experimental Section

Materials and methods

All reagents and solvents were purchased from commercial sources and used without further purification unless otherwise stated. Preparation and handling of air-sensitive materials were carried out under inert atmosphere using standard Schlenk techniques or a glovebox. The ligand K(Tp^{iPr2}) was generously provided by Prof. Kiyoshi Fujisawa and used without further purification. Sodium benzoate was purchased from Aldrich. The complex [Fe(Tp^{iPr2})(OBz)] was prepared as previously reported.[136]

Physical methods

UV-visible spectra were recorded on a Hewlett-Packard 8453A diode array spectrometer equipped with a cryostat from Unisoku Scientific Instruments. Electrospray ionization mass spectrometry experiments were carried out on a Bruker BioTOF II mass spectrometer using the following conditions: spray chamber voltage = 4000 V; gas carrier temperature = 200 °C. GC product analyses were performed on a Perkin-Elmer Sigma 3 gas chromatograph (AT-1701 column, 30 m) with a flame ionization detector.

4.3 Oxygen Activation by [$FeTp^{iPr2}$OBz] at Room Temperature:

As mentioned previously, [Fe^{II}(Tp^{Ph2})(OBz)] reacted with oxygen very slowly (2 to 3 days) relative to the corresponding α-ketocarboxylate complex [Fe^{II}(Tp^{Ph2})(BF)] and generated the ligand hydroxylated product [Fe(Tp^{Ph2*})(OBz)]. Our recent oxygenation studies with complex [Fe^{II}(Tp^{iPr2})(BF)] (**3**) showed that **3** was also able to activate oxygen at room temperature and perform hydroxylation of the *iso*-propyl group of the ligand.[113] This observation led us to investigate the oxygenation of complex

$[Fe^{II}(Tp^{iPr2})(OBz)]$ (**1**) at room temperature. The major difference between **3** and **1** is the ancillary ligand; **3** is supported by an α-ketocarboxylate (benzoylformate) whereas **1** is supported by the corresponding carboxylate (benzoate). Bubbling O_2 through the pale-yellow solution of **1** in toluene at 25 °C resulted in immediate spectral changes with the formation of an intense near-UV feature at 370 nm. The reaction was complete within 15 minutes, as observed for **3**. The similar reaction times for **1** and **3** were remarkable, as it suggested that in the case of oxygenation of $FeTp^{iPr2}$ complexes the ancillary α-ketocarboxylate ligand did not play a significant role, quite contrary to what was observed with the $[Fe^{II}(Tp^{Ph2})(BF)]$/$[Fe^{II}(Tp^{Ph2})(OBz)]$ pair. ESI-MS analysis of the intensely colored product solution suggested the formation of an alkoxoiron(III) product, as manifested by peaks at *m/z* = 536. The peak at *m/z* = 536 has a mass and an isotope distribution pattern that corresponds to an ion with the composition of $[[(Tp^{iPr2})Fe^{III}] + O - H]^+$(see Figure 4.2); that is, one ligand hydrogen atom has been replaced by an oxygen atom, suggesting the hydroxylation of the Tp^{iPr2} ligand in the course of the reaction to form the oxidation product $[Fe^{II}(Tp^{iPr2*})(OBz)]$ (**5**). The most likely hydroxylation site is at one of the 3-isopropyl methine carbons, as this is the weakest C–H bond present in the ligand and is also in the vicinity of the iron center. We thus assign the *m/z* = 536 peak as $[Fe(Tp^{iPr2*})]^+$ where Tp^{iPr2*} represents the Tp^{iPr2} ligand in which the 3° C–H bond of a 3-isopropyl group on the Tp^{iPr2} ligand has been hydroxylated. Based on the molar absorptivity of the 370 nm peak the amount of hydroxylation is estimated to be 70%.

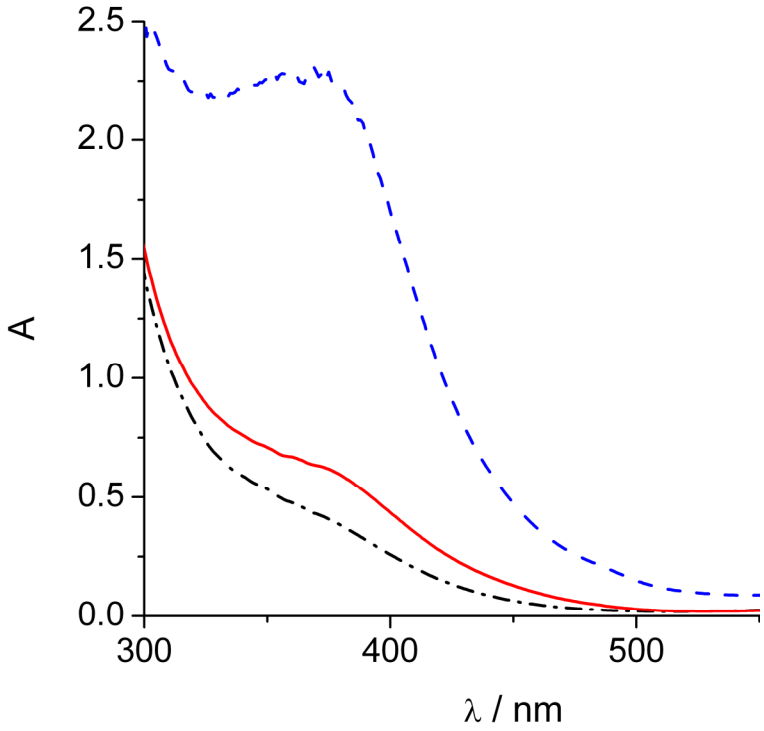

Figure 4.1. Reaction of **1** (1 mM in a 1-cm cell) with oxygen at room temperature. Black dashed-dotted line: **1** alone; blue dashed line: **1** + O_2; red solid line: **1** + THT +O_2.

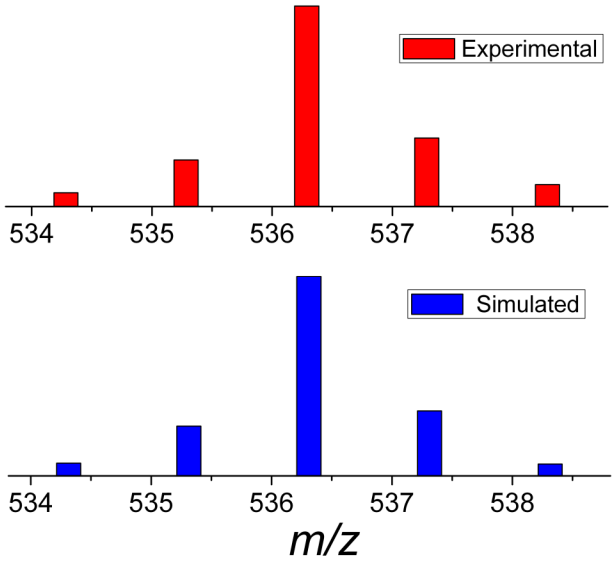

Figure 4.2. ESI-MS analysis of the end solution generated from reaction of **1** and oxygen at room temperature in toluene.

When the oxygenation of **1** was performed in the presence of 100 mM tetrahydrothiophene (THT), the intense yellow chromophore associated with $[Fe(Tp^{iPr2*})]^+$ did not form. ESI-MS analysis of this solution revealed only one major peak at *m/z* = 625, whose mass and isotope distribution pattern matched those for $[Fe^{II}(Tp^{iPr2})[(OS(CH_2)_4]]^+$. Tetramethylenesulfoxide was confirmed to be the oxidation product by GC analysis (65% yield with naphthalene as an internal standard).

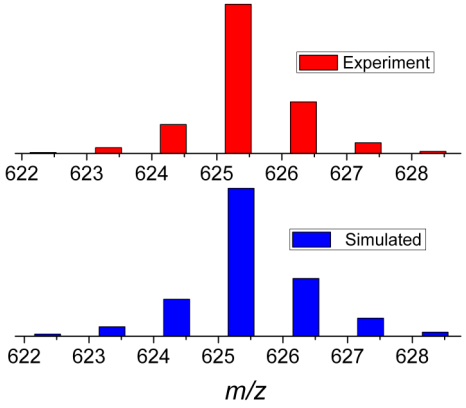

Figure 4.3. ESI-MS analysis of the solution at the end generated from reaction of **1** and oxygen in the presence of THT at room temperature in toluene.

4.4 Oxygen Activation by $FeTp^{iPr2}OBz$ at Low Temperature

When **1** was oxygenated at – 50 °C, a green chromophore was observed with λ_{max} = 680 nm, as reported by Kitajima.[136] The green chromophore was stable in toluene at – 50 °C, and it was characterized by resonance Raman spectroscopy and by EXAFS analysis to be a $[\mu\text{-}(1,2\text{-}O_2)Fe^{II}_2(Tp^{iPr2})_2(OBz)_2]$ intermediate (**1-P,** Scheme 4.1).

Scheme 4.1 Reaction of oxygen with [Fe(Tp^{iPr2})(OBz)] generated a μ-(η^1:η^1)-peroxo intermediate.

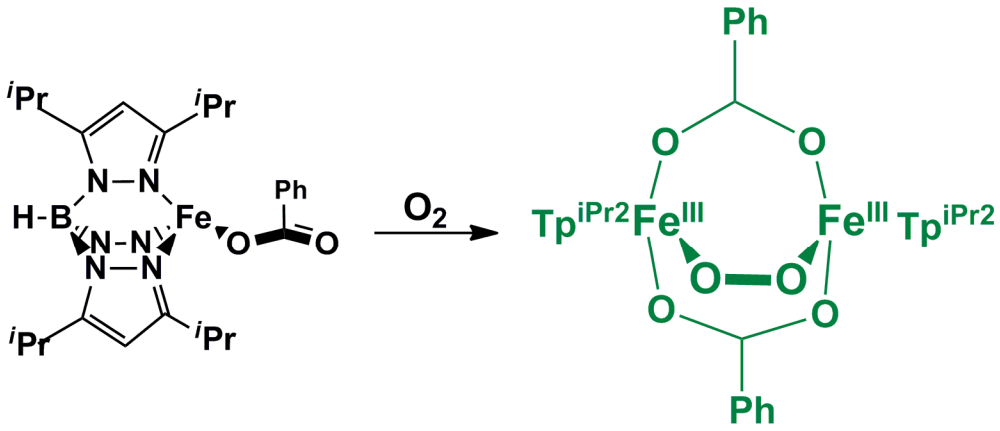

1 **1-P**

Interestingly, addition of 1 equivalent of a proton (pyridinium triflate) to a solution of **1-P** in toluene led to decay of the peroxo band even at – 50 °C within an hour. This decay trace is mono-phasic and can be fit by a single exponential with a rate constant of 7×10^{-4} s^{-1}.

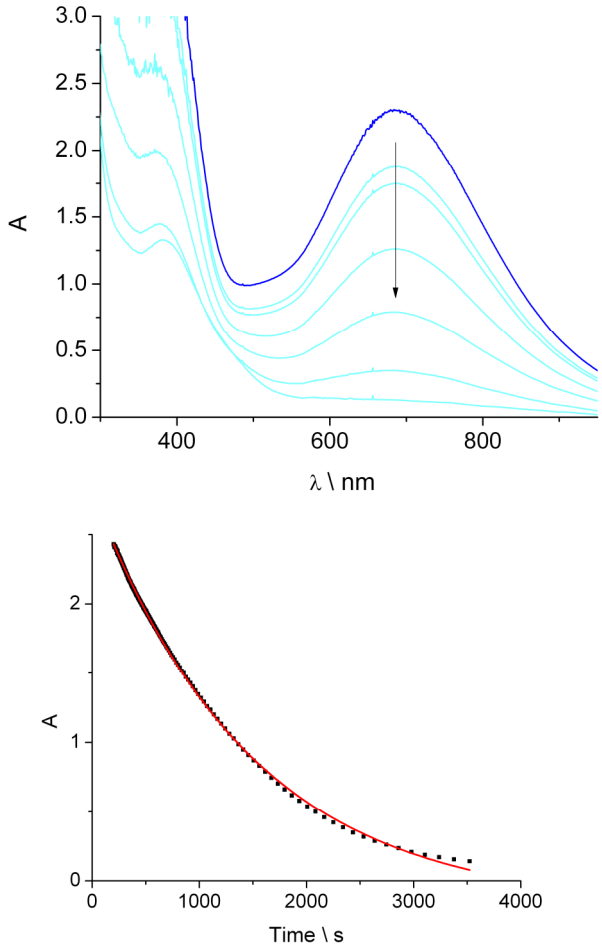

Figure 4.4. Top: Reaction of **1-P** (0.5 mM, l = 1 cm) with pyridinium triflate (1 equivalent with respect to **1-P**) at – 50 °C in toluene. Bottom: Decay trace of 680 nm.

When pyridinium triflate was added anaerobically to a solution of **1** in toluene at – 50 °C and oxygen was bubbled to this solution, **1-P** formation was not prevented; however the band at 680 nm disappeared after complete formation. Comparison of the rate of peroxo formation [4×10^{-2} s^{-1}] (Figure 4.6) to that of its decay [7×10^{-4} s^{-1}] explained why pre-addition of the proton did not have a significant effect on **1-P** formation.

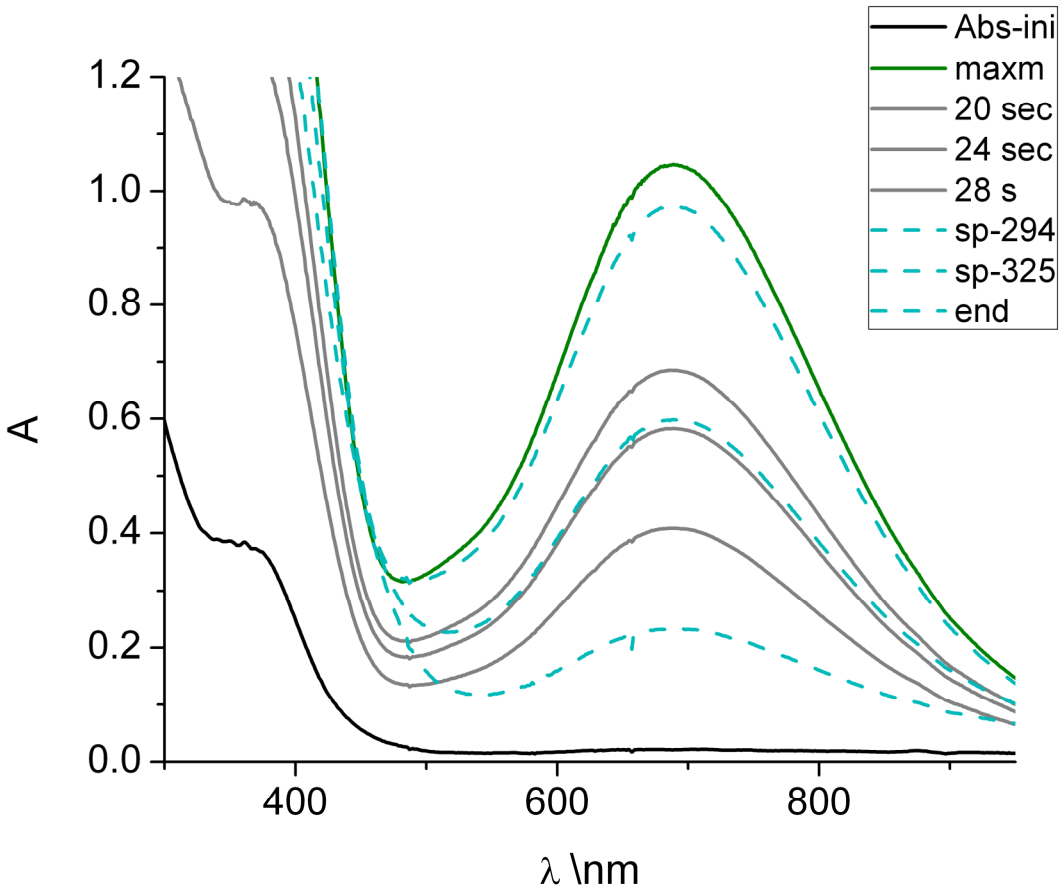

Figure 4.5. Reaction of **1** (0.5 mM in a 1-cm cell) with oxygen in the presence of pyridinium triflate (0.25 mM) in toluene at – 50 °C.

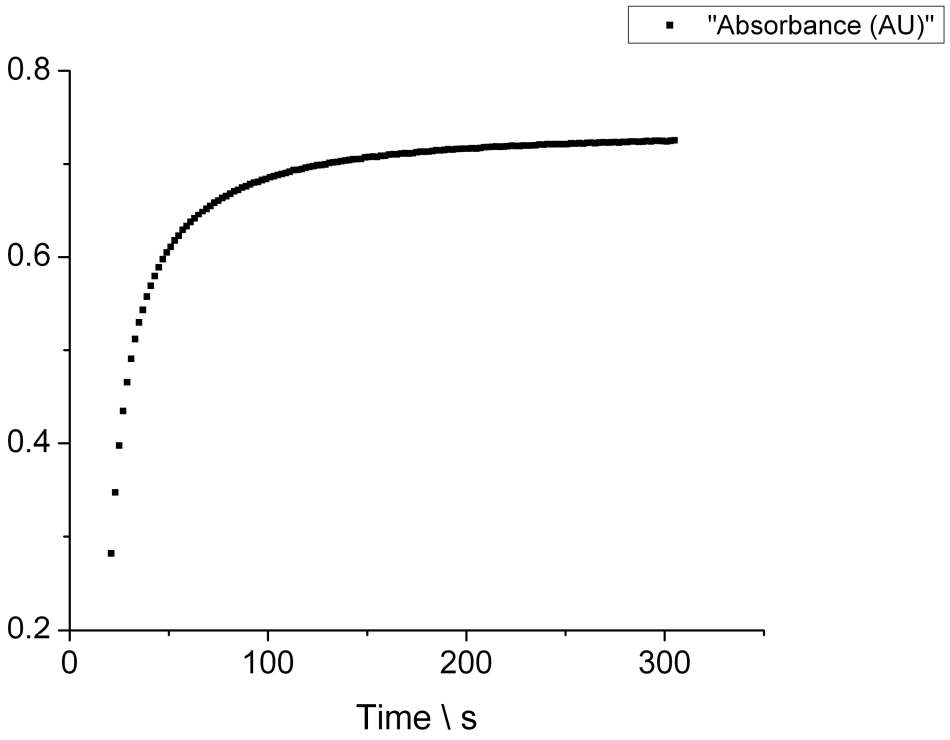

Figure 4.6. Formation trace of 680 nm (**1-P**) in toluene at – 50 °C.

Furthermore, when THT was added to the decay of this peroxo species, ESI-MS analysis at the end of the reaction showed the mass peak at *m/z* = 625. In the absence of THT, the product solution showed a major peak at *m/z* = 536. These two outcomes strongly suggested that the proton-assisted decay pathway of the peroxo species generated a high-valent intermediate that can transfer oxo group to a thioether or hydroxylate a ligand C-H bond. In order to rationalize the decay, two hypotheses can be proposed a) decay due to protonation of the **1-P** intermediate or 2) decay due to coordination of pyridine, the conjugate base of pyridinium triflate, to **1-P**. In order to test the latter, **1-P** was generated from **1** and oxygen, and to this solution was added pre-cooled solution of pyridine in toluene at – 50 °C. Addition of 1 equivalent pyridine also lead to decay of **1-P**, but the reaction was not complete within an hour and followed a

complex kinetic behavior. Therefore, it could be proposed that the decay monitored in the presence of pyridinium triflate could not solely arise from coordination of the pyridine to the **1-P** intermediate.

As the conjugate base of pyridinium triflate can coordinate to the iron center, in a different experiment, decay of **1-P** was investigated in the presence of HBF_4, an acid with a non-coordinating conjugate base. Similar behavior was noted; addition of 1 equivalent of HBF_4 to a preformed solution of **1-P** at – 50 °C led to complete decay of the peroxo intermediate. The product solution of the reaction showed a mass peak of *m/z* = 536. However, the decay trace of the **1-P** was complex and could not be fit by one exponential.

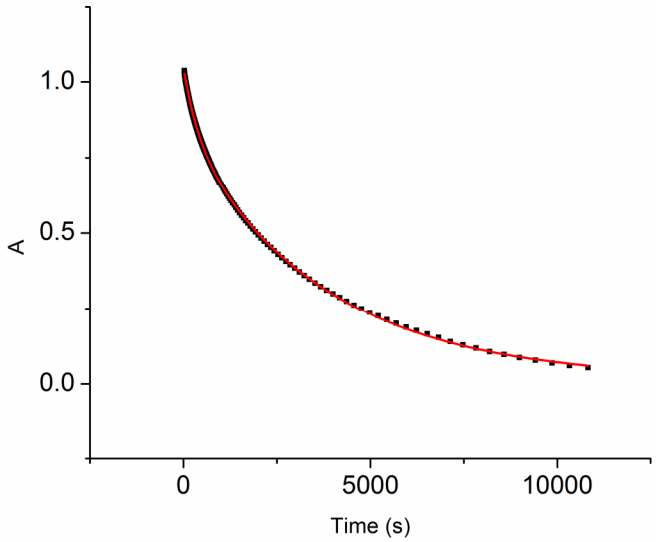

Figure 4.7 Decay trace of 680 nm and its fitting using a double exponential when HBF_4 was used as an acid.

The complex kinetic behavior of **1-P** in the presence of HBF_4 could be explained by considering the acidity of the HBF_4. Pyridinum triflate is a very weak acid with pK_a of 5 whereas HBF_4 is relatively strong acid with pK_a of – 0.4. The strong acidity of HBF_4 could result in additional pathways for **1-P** decay, complicating the kinetics. Therefore, further studies are clearly needed for establishing the mechanism of proton dependence of **1-P** decay.

Complete disappearance of the 680 nm band in the presence of the proton, even at – 50 °C, suggested that the proton was accelerating the decay pathway of the peroxo species by co-ordinating to the peroxo moiety. Protonation of a similar peroxo species, generated from [Fe(N-EtHPTB)(OBz)] and oxygen, has been recently reported by Lippard and coworkers.[161] But unlike **1**, the addition of acid to $[Fe_2(\mu\text{-}O_2)(\text{N-EtHPTB})(\mu\text{-}PhCO_2)]^{2+}$ leads to the shift of the peroxo band, and it was proposed that upon addition of acid, protonation and dissociation of the bridging carboxylate [Scheme 4.2b] instead of the peroxo moiety generated the red shift in the λ_{max}. Our results, on the other hand, suggested that, although **1-P** has bridging benzoate ligand, the proton in this case prefers coordination at a place such that the peroxo species could decay, whether by coordinating to the benzoate unit followed by an acid-assisted decay pathway or directly coordinating to the peroxo moiety (Scheme 4.2) is not clear yet. Nevertheless, the proton accelerated the decay of **1-P** such that formation of a high-valent oxidizing intermediate was facilitated.

Scheme 4.2 Possible sites for proton coordination to the peroxo moiety A) in the enzyme soluble methane monooxygenase B) Model complex $[Fe_2(\mu\text{-}O_2)(N\text{-}EtHPTB)(\mu\text{-}PhCO_2)]^{2+}$ C) **1-P**.

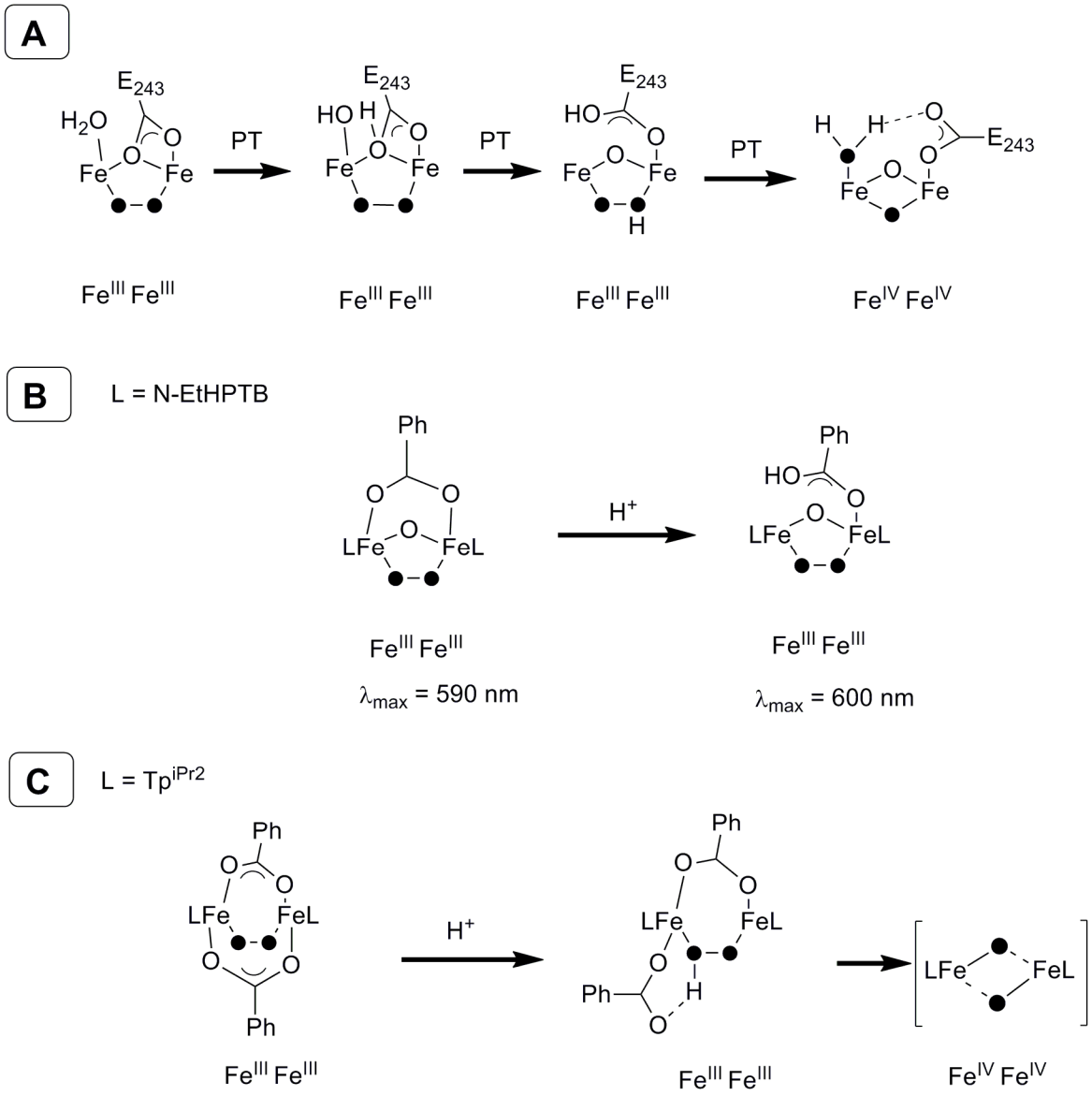

4.5 Discussion

Scheme 4.1 shows our current understanding of the mechanism of intramolecular ligand hydroxylation of **1**, which lacks the α-ketoacid. The rate constant calculated from the **1-P** formation kinetics confirmed that, upon introduction of oxygen to a solution of **1** in toluene, **1-P** was formed almost instantaneously even at – 50 °C. Intermediate **1-P** has been characterized by different spectroscopic means. The Fe-O and O-O vibrations of the intermediate **1-P** obtained from resonance Raman spectroscopy [418 cm^{-1} and 876 cm^{-1} respectively][136] along with the Fe-Fe distance of 3.5 Å calculated from a recent EXAFS analysis (unpublished data from the Que group) suggested the binding mode of the peroxo unit as [μ-η1:η1]. Important discoveries from the Que and Lippard groups had established the sluggish reactivity of the intermediates similar to **1-P**.[162,163] In this study it was observed that **1** can oxidize the ligand within 15 minutes at room temperature, suggesting the involvement of a strongly oxidizing intermediate. This intermediate could have a diamond core structure (Fe_2O_2) as proposed for the enzyme sMMO[164-166] or could have a monoferryl structure as observed in the mono-nuclear non-heme iron enzymes.[53,58] Thorough studies on a model complex of sMMO ($L_2Fe_2O_2$, where L is tris((4-methoxy-3,5-dimethyl-pyridine-2-yl)methyl)amine) from the Que group suggested that the high-valent intermediate with a diamond core structure oxidizes 9,10-dihydroanthracene two to three orders of magnitude slower than that observed for $[Fe^{IV}(O)(L)(MeCN)]^{2+}$, the corresponding mononuclear oxoiron(IV) complex supported by the same ligand.[167] Therefore, **1-P** might be converted to an open core oxoiron(IV) species that could abstract H-atom of the ligand within 15 minutes. Therefore, the ligand hydroxylation reaction and oxidation of tetrahydrothiophene performed by **1** and oxygen at room

temperature most likely involve a mononuclear oxoiron(IV) intermediate as shown in scheme 4.3 by breaking the O-O bond.

Scheme 4.3 Probable mechanism for the reaction of [$Fe^{II}(Tp^{iPr2})$(OBz)] (**1**) complex with dioxygen

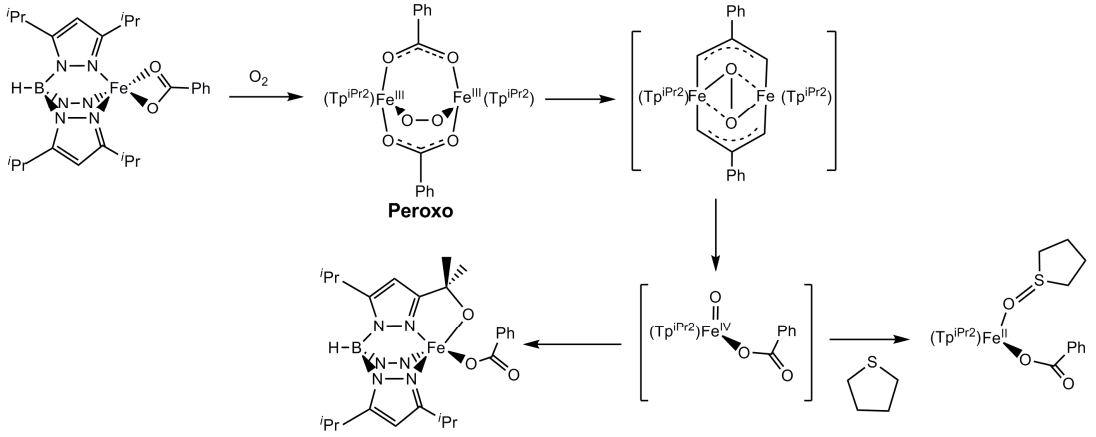

At this stage it is not clear how proton facilitates the decay of the **1-P** intermediate. Our ESI-MS analysis on THT oxidation suggested that proton-assisted decay of **1-P** in the presence of acid also generates the high-valent oxoiron intermediate, but how this is accomplished is not well-understood. Based on the enzyme mechanism[116] and also on recent model studies,[161] it can be proposed that the proton coordinates to the bridging carboxylate making it monodentate and that carboxylic acid shuttles the proton to the peroxo unit leading to its decay. In another pathway, it could be envisioned that the proton coordinates directly to the peroxo unit of **1-P**, facilitating its decay [Scheme 4.4]. Our current results are insufficient to prove or disprove any of the proposed pathways. We have also observed decay of **1-P** in the presence of pyridine, although reaction kinetics are entirely different. Having a co-ordinating conjugate base complicates our understanding of the mechanism. In order to extract the sole effect of the proton, HBF_4 was used, but change of pK_a from 5 of pyridinium triflate to – 0.4 of HBF_4 might lead to additional acid-assisted decay pathways, complicating the kinetics. Based on these results

it could be proposed that in order to extract the exclusive effect of the proton on the decay of the **1-P** intermediate, reaction should be carried out in the presence of 2,4,6-tri(t-Butyl)pyridinum triflate or collidinium triflate. Nevertheless, our observation of proton assisted decay of the intermediate **1-P** is unique and the nature of the decay product makes intermediate **1-P**, the first model compound, to mimic the function of the enzyme sMMO, where a high-valent intermediate generated from the decay of a peroxo intermediate is responsible for hydroxylation of a C-H bond.

Scheme 4.4 Probable sites for the proton-assisted decay of the intermediate **1-P**.

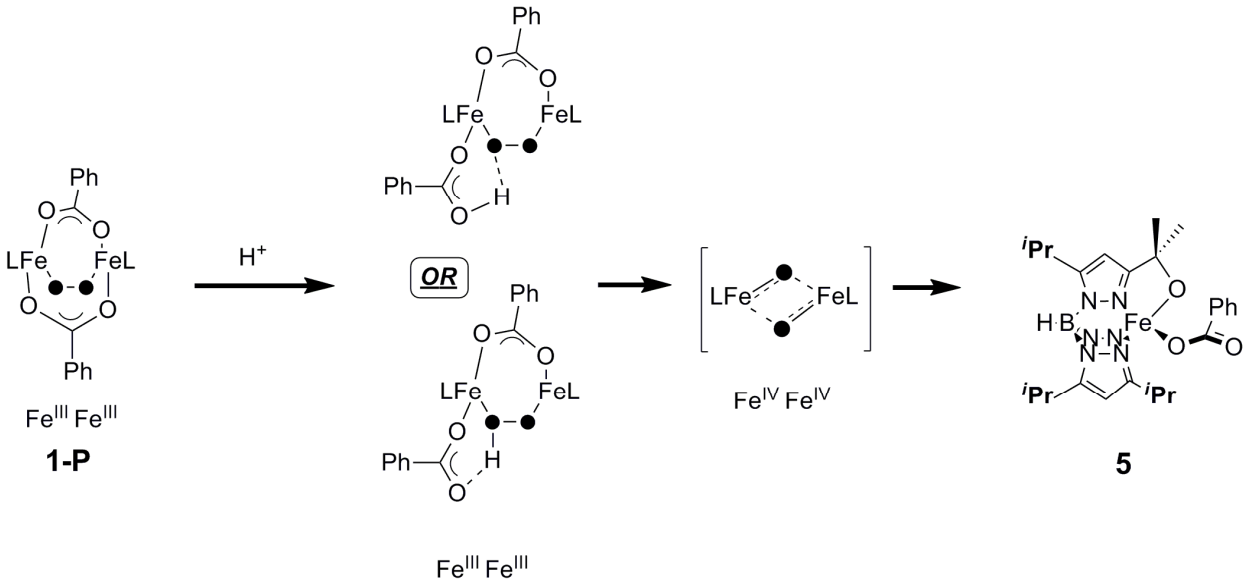

Chapter 5

Conclusions and Perspective

5.1. Introduction

This thesis has presented our current understanding of the mechanism of oxygen activation by functional model complexes of the α-KG-dependent enzymes, namely with [Fe(Tp^{R2})($O_2CC(O)R$)] complexes (where Tp is hydrotris(3,5-dialkylpyrazol-1-yl)borate, Scheme 5.1). The reactivity of these model complexes can be finely tuned by changing the substituents on the ligand framework and also by tuning electronic and steric properties of the ancillary α-ketocarboxylate. Chapter 3 describes how these changes allowed us to speculate intermediates generated at the very early stage of oxygen activation.[113] Chapter 2 described detailed reactivity studies of a functional model complex of the α-KG-dependent dioxygenases. For the first time, selective oxidation of added hydrocarbons has been achieved by an oxygen-derived iron-based oxidant.[101] This is a remarkable observation in the field of bio-inorganic chemistry, as previously oxidation of hydrocarbons in the presence of oxygen always showed loss of selectivity.[89] Oxygen activation by an iron complex without the ancillary α-ketocarboxylate ligand was reported in Chapter 4.

Scheme 5.1 Variations in the ligand and the ancillary ligand site.

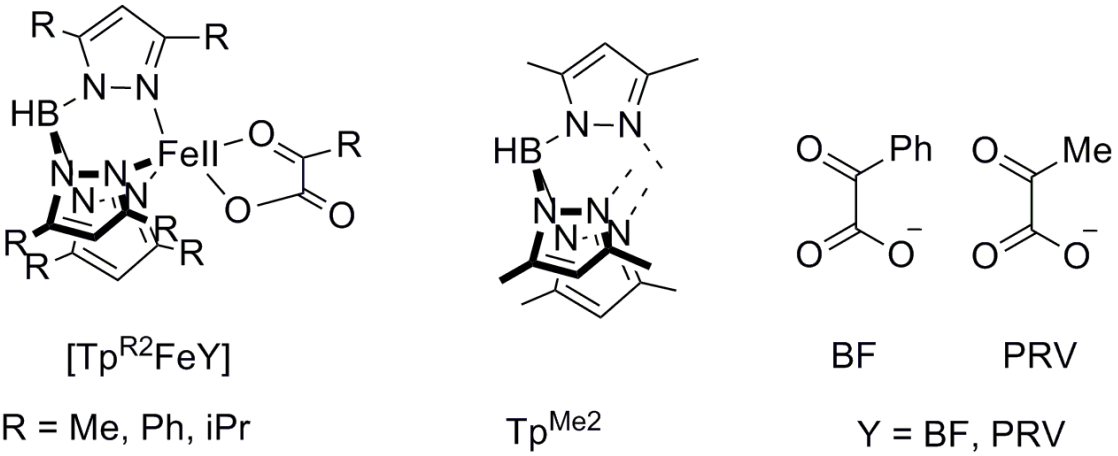

5.2. Reactivity of the Ferryl Intermediate

The oxygen-derived oxidant generated from the reaction of [Fe(Tp^{Ph2})(BF)] and oxygen showed remarkable reactivity.[101] The oxidant, presumably a ferryl intermediate, oxidized an array of added hydrocarbon substrates and did so with unique selectivity. Two types of selectivity have been observed: product selectivity where dehydrogenated products were repeatedly observed[101] and specificity towards the ω-position of the linear alkanes. The usual reactivity associated with the ferryl intermediates is the hydroxylation of a C-H bond, except for the substrates where desaturation will lead to added stabilization of the product (like cyclohexadiene conversion to benzene).[96,97,146,168] This work showed the less known example of the ferryl intermediate that performs selective desaturation of substrates. Even cyclohexene converts to form 1,3-cyclohexadiene rather than 2-cyclohexenol.[101] In various metalloenzymes, substrate hydroxylation and dehydrogenation are in fact related transformations that are controlled by the interactions of the substrate with the active site pocket.[29,169,170] DFT calculations indicate that the

outcome of the C-H bond oxidation depends on what happens after the rate determining C-H bond cleavage step.[62] Oxygen rebound from the iron center to the incipient alkyl radical generates the alcohol, while oxidation of the alkyl radical to a carbocation leads to dehydrogenation.[62] Desaturation can also happen if the ferric hydroxo intermediate abstracts the second hydrogen-atom from the vicinal C-H bond of the radical substrate.[63,64] According to DFT calculations the distance between the alkyl radical and the Fe-OH unit is the key factor that controls the outcome; the greater the distance, the less favored is the rebound step.[62] The experimental data clearly show that oxygen rebound does not occur in the oxidation of hydrocarbons in the reaction of [Fe(Tp^{Ph2})(BF)] with oxygen. This work is also important because of its oxidation source, oxygen. In the literature, there are very few examples of ferryl intermediates generated directly from oxygen. One of the examples includes generation of a ferryl intermediate from [Fe(TMC)($OTf)_2$] (where, TMC is 1,4,8,11-tetramethyl-1,4,8,11-tetraaza-cyclotetradecane) using oxygen, reductant, and the proton,[151,171] but this complex is less reactive perhaps due to its intermediate spin state (S = 1).[146] Our study described in Chapter 2 adds a great detail to the reactivity of mononuclear ferryl intermediates, particularly with respect to the cleavage of substrates with strong C-H bonds.

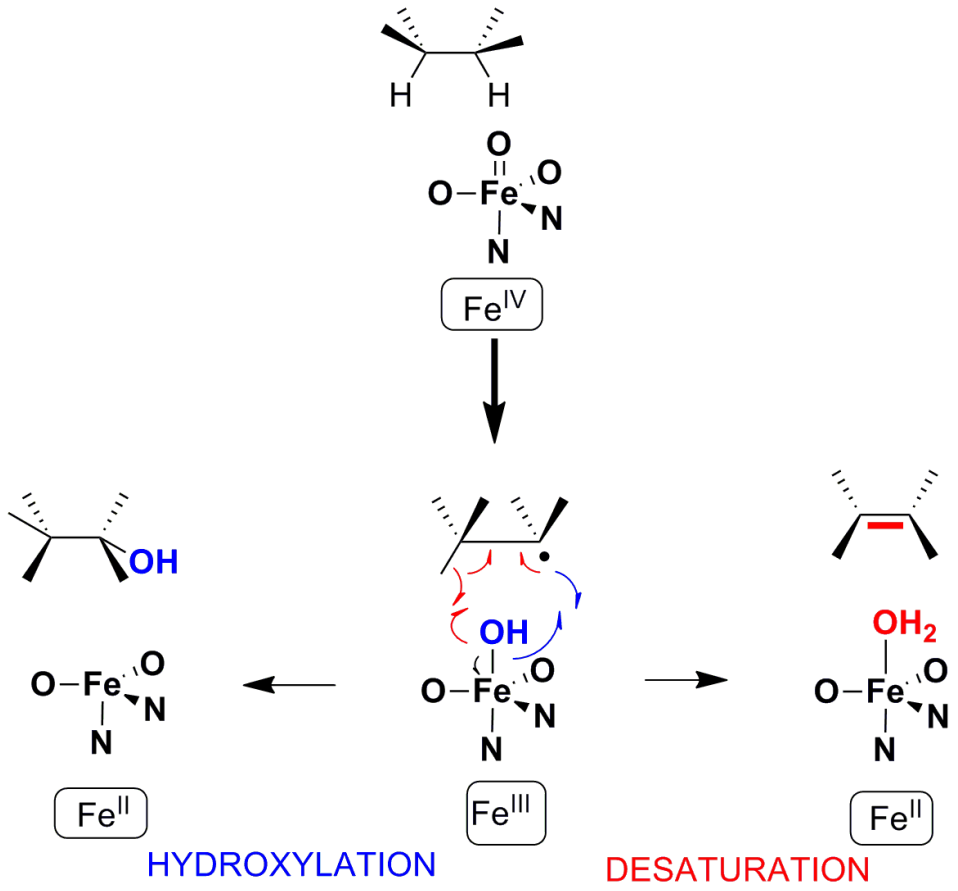

Figure 5.1. Schematic representation showing the mechanism of desaturation vs. hydroxylation from metal-centered oxidation. Blue half-arrows showed electron transfer for rebound whereas red half-arrows showed electron transfer for desaturation.

Another significant observation from the reactivity studies of [Fe(Tp^{Ph2})(BF)] with oxygen was its remarkable regioselectivity. For the first time specific ω-selectivity toward oxidation of n-alkanes was observed for a biomimetic complex. When a linear alkane was introduced as a substrate, the ferryl intermediate derived from [Fe(Tp^{Ph2})(BF)] specifically attacks the terminal methyl group over the internal methylene groups, which have weaker C-H bonds. Our current understanding speculates

that the ferryl intermediate is encumbered in a pocket made by the phenyl group of the ligand that dictates this selectivity. Apparently, only the terminal methyl group has access to the ferryl species and not the internal methylene groups. Thus the initial attack occurs only at the terminal position to generate the substrate radical that is further oxidized to product alkene.

5.3. Investigating Reactivities of 'Pre-Ferryl' Intermediates: First Non-heme Mononuclear Iron-Superoxo Intermediate

Chemical evidence for the involvement of a mononuclear iron-superoxo species was established for the first time in the oxygenation of [Fe(Tp^{iPr2})(PRV)] complex.[113] Earlier attempts to stabilize a non-heme iron-superoxo intermediate in a mononuclear species have been unsuccessful. The two previously documented examples of non-heme iron-superoxo species came from oxygen activation by diiron centers.[125,130] In Chapter 3 we showed evidence of an iron-superoxo intermediate generated from a mononuclear iron complex, using phenols as trapping agents.[113] This was accomplished in two ways, tuning the electronic and steric properties of the Tp ligand by replacing the flat phenyl group with the *iso*-propyl group, and by changing the electronic properties of the α-ketocarboxylate ligand by replacing the electron withdrawing phenyl group with a methyl group. These two changes made the iron-superoxo intermediate live long enough to be trapped by the intermolecular oxidant 2,4,6-TBP (TBP is tri-*tert*-butyl phenol). Chapter 4 describes reactivity of another type of 'pre-ferryl' iron-oxygen adduct, the [Fe^{III}_2(μ-1,2-O_2)] intermediate. Although the [Fe^{III}_2(μ-1,2-O_2)] intermediate by itself is stable at low temperature, it decays in the presence of acid and perform ligand oxidation. Although the mechanism of the decay of [Fe^{III}_2(μ-1,2-O_2)] species is not well-understood at this point, it has opened many possibilities to explore.

5.4. Future Challenges

Iron and oxygen, two benevolent chemicals, are abundant in nature. Therefore selective oxidation of hydrocarbons by iron-oxygen-based oxidants can have the wide scope of applications.[172] The results described in this thesis are unique in nature and they have opened many avenues to explore. In this thesis we have established involvement of a strongly oxidizing oxidant generated from [Fe(Tp^{Ph2})(BF)] and O_2 that selectively oxidizes added hydrocarbons.[101] Based on the evidence obtained from the DFT studies,[64,106] active species involved in these transformations must be a high-spin oxoiron(IV) species,[106] but how to trap this intermediate is a challenge worth pursuing for fundamental understanding.

5.4.1. Generation of Stable High-spin Oxoiron(IV) Intermediate from Oxygen

To date there have been only few examples of high-spin oxoiron(IV) complexes, two of them being stabilized in a trigonal-bi-pyramidal geometry.[78,173] The oxoiron(IV) intermediate generated from [Fe(Tp^{R2})(BF)] and O_2 might possess the similar trigonal-bi-pyramidal geometry and most likely be high-spin. The reactivity depicted by the oxoiron(IV) generated from [Fe(Tp^{Ph2})(BF)] clearly suggested that in order to stabilize the ferryl intermediate, ligand design will play a significant role. In order to support the high-spin environment, the Tp ligand framework might be used, but the ligand has to be modified to prevent ligand hydroxylation. To circumvent phenyl group oxidation of the Tp^{Ph2} ligand, the 4-NO_2-C_6H_4-group could be introduced in the Tp framework. In order to slow *iso*-propyl group oxidation of the Tp^{iPr2} ligand by the oxidant, deuteration on the methine position of the *iso*-propyl group could be performed (Scheme 5.3).

Scheme 5.2. Possible ligand variation to trap the oxoiron(IV) intermediate

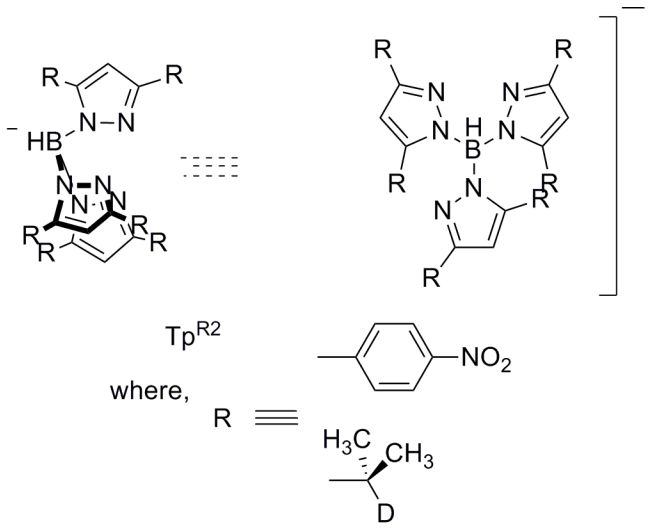

5.4.2. Understanding the Mechanism of Desaturation vs Hydroxylation by Studying Model Complexes

[Fe(Tp^{Ph2})(BF)] and O_2 generates an oxidant that exhibits unusual selectivity. The oxidant always preferred desaturation of hydrocarbons. Understanding this selectivity will also be very interesting for bio-inorganic chemists. Our current hypothesis ascribes this selectivity to the encumbered nature of the active oxidant ('cleft size'). This hypothesis can be easily verified by varying the steric bulk in the Tp ligand and ancillary α-ketocarboxylate ligand, and monitoring hydrocarbon oxidations. Relaxation of the 'cleft size' might also allow the carbon-centered radical to give hydroxylated product along with the desaturated product.

5.4.3. Trapping of the Iron-superoxo Intermediate

One of the challenging future projects would be to trap and characterize the iron-superoxo intermediate. One trick that worked in our favor to chemically trap the iron-superoxo species was the lower electrophilicity of the pyruvate. In order to trap the 'pre-ferryl' intermediate, the decay pathways of the iron-superoxo species have to be decelerated. In this system, the decay pathway of the iron-superoxo species involves nucleophilic attack of the superoxo unit to the carbonyl group of the α-ketoacid.[84] As this is a nucleophilic attack, making the carbonyl group less electrophilic might increase the lifetime of the iron-superoxo species. This could be achieved by introducing the *iso*-propyl or *tert*-butyl group in the α-ketoacid. Another pathway by which a mononuclear iron-superoxo species can decay is by reacting with another iron-center. In order to prevent the second pathway, Tp ligands with bulky alkyl substituents might be used. The steric properties of the Tp ligand and the ancillary ligand have to be tuned cautiously, as too much bulky group in the ligand can hinder oxygen coordination to the iron center.[82] Scheme 5.3 shows one probable complex worth investigating.

Scheme 5.3. Possible ligand/ancillary ligand variation to trap the 'pre-ferryl' intermediate

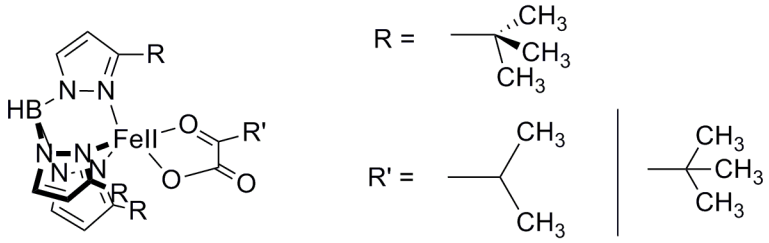

References:

(1) Que, L., Jr.; Tolman, W. B. *Nature* **2008**, *455*, 333-340.

(2) Feig, A. L.; Lippard, S. J. *Chem. Rev.* **1994**, *94*, 759-805.

(3) Bruijnincx, P. C. A.; Koten, G. v.; Gebbink, R. J. M. K. *Chem. Soc. Rev.* **2008**, *37*, 2716-2744.

(4) Solomon, E. I.; Brunold, T. C.; Davis, M. I.; Kemsley, J. N.; Lee, S.-K.; Lehnert, N.; Neese, F.; Skulan, A. J.; Yang, Y.-S.; Zhou, J. *Chem. Rev.* **2000**, *100*, 235-349.

(5) Abu-Omar, M. M.; Loaiza, A.; Hontzeas, N. *Chem. Rev.* **2005**, *105*, 2227-2252.

(6) Costas, M.; Mehn, M. P.; Jensen, M. P.; Que, L., Jr. *Chem. Rev.* **2004**, *104*, 939-986.

(7) Kovaleva, E. G.; Lipscomb, J. D. *Nat. Chem. Biol.* **2008**, *4*, 186-193.

(8) Solomon, E. I.; Sundaram, U. M.; Machonkin, T. E. *Chem. Rev.* **1996**, *96*, 2563-2605.

(9) Nam, W. *Acc. Chem. Res.* **2007**, *40*, 522–531.

(10) Denisov, I. G.; Makris, T. M.; Sligar, S. G.; Schlichting, I. *Chem. Rev.* **2005**, *105*, 2253-2278.

(11) Que, L., Jr. *Nat. Struct. Biol.* **2000**, *7*, 182-184.

(12) Kryatov, S. V.; Rybak-Akimova, E. V.; Schindler, S. *Chem. Rev.* **2005**, *105*, 2175-2226.

(13) Tshuva, E. Y.; Lippard, S. J. *Chem. Rev.* **2004**, *104*, 987-1012.

(14) Hegg, E. L.; Que, L., Jr. *Eur. J. Biochem.* **1997**, *250*, 625-629.

(15) Koehntop, K. D.; Marimanikkuppam, S.; Ryle, M. J.; Hausinger, R. P.; Que, L., Jr. *J. Biol. Inorg. Chem.* **2006**, *11*, 63-72.

(16) Hausinger, R. P. *Crit. Rev. Biochem. Mol. Biol.* **2004**, *39*, 21-68.

(17) Clifton, I. J.; McDonough, M. A.; Ehrismann, D.; Kershaw, N. J.; Granatino, N.; Schofield, C. J. *J. Inorg. Biochem.* **2007**, *100*, 644-669

(18) Kivirikko, K. I.; Myllylä, R.; Pihlajaniemi, T. *FASEB J.* **1989**, *3*, 1609-1617.

(19) Stenflo, J.; Holme, E.; Lindstedt, S.; Chandramouli, N.; Huang, L. H. T.; Tam, J. P.; Merrifield, R. B. *Proc. Natl Acad. Sci U. S. A* **1989**, *86*, 444-447.

(20) Ivan, M.; Kondo, K.; Yang, H.; Kim, W.; Valiando, J.; Ohh, M.; Salic, A.; Asara, J. M.; Lane, W. S.; Kaelin, W. G., Jr. *Science* **2001**, *292*, 464-468.

(21) Jaakkola, P.; Mole, D. R.; Tian, Y.-M.; Wilson, M. I.; Gielbert, J.; Gaskell, S. J.; von Kriegsheim, A.; Hebestreit, H. F.; Mukherji, M.; Schofield, C. J.; Maxwell, P. H.; Pugh, C. W.; Ratcliffe, P. J. *Science* **2001**, *292*, 468-472.

(22) Hewitson, K. S.; McNeill, L. A.; Elkins, J. M.; Schofield, C. J. *Biochem. Soc. Trans.* **2003**, *31*, 510-515.

(23) Hewitson, K. S.; McNeill, L. A.; Schofield, C. J. *Curr. Pharm. Des.* **2004**, *10*, 821-833.

(24) McNeill, L. A.; Hewitson, K. S.; Gleadle, J. M.; Horsfall, L. E.; Oldham, N. J.; Maxwell, P. H.; Pugh, C. W.; Ratcliffe, P. J.; Schofield, C. J. *Bioorg. Med. Chem. Lett.* **2002**, *12*, 1547-1550.

(25) Yu, B.; Edstrom, W. C.; Benach, J.; Hamuro, Y.; Weber, P. C.; Gibney, B. R.; Hunt, J. F. *Nature* **2006**, *439*, 879-884.

(26) Aas, P. A.; Otterlei, M.; Falnes, P. Ø.; Vågbø, C. B.; Skorpen, F.; Akbari, M.; Sundheim, O.; Bjørås, M.; Slupphaug, G.; Seeberg, E.; Krokan, H. E. *Nature* **2003**, *421*, 859-796.

(27) Mishina, Y.; Yang, C.-G.; He, C. *J. Am. Chem. Soc.* **2005**, *127*, 14592-14593.

(28) Baldwin, J. E.; Abraham, E. *Nat. Prod. Rep.* **1988**, *5*, 129-145.

(29) Baldwin, J. E.; Adlington, R. M.; Crouch, N. P.; Schofield, C. J.; Turner, N. J.; Aplin, R. T. *Tetrahedron* **1991**, *47*, 9881-9900.

(30) Lloyd, M. D.; Merritt, K. D.; Lee, V.; Sewell, T. J.; Wha-Son, B.; Baldwin, J. E.; Schofield, C. J.; Elson, S. W.; Baggaley, K. H.; Nicholson, N. H. *Tetrahedron* **1999**, *55*, 10201-10220.

(31) Clifton, I. J.; Doan, L. X.; Sleeman, M. C.; Topf, M.; Suzuki, H.; Wilmouth, R. C.; Schofield, C. J. *J. Biol. Chem.* **2003**, *278*, 20843-20850.

(32) Blasiak, L. C.; Vaillancourt, F. H.; Walsh, C. T.; Drennan, C. L. *Nature* **2006**, *440*, 368-371.

(33) Vaillancourt, F. H.; Yeh, E.; Vosburg, D. A.; Garneau-Tsodikova, S.; Walsh, C. T. *Chem. Rev.* **2006**, *106*, 3364-3378.

(34) Galonic, D. P.; Barr, E. W.; Walsh, C. T.; Bollinger, J. M., Jr.; Krebs, C. *Nature Chem. Biol.* **2007**, *3*, 113-116.

(35) Que, L., Jr.; Ho, R. Y. N. *Chem. Rev.* **1996**, *96*, 2607-2624.

(36) Hanauske-Abel, H. M.; Günzler, V. *J. Theor. Biol.* **1982**, *94*, 421-455.

(37) Hanauske-Abel, H. M.; Popowicz, A. M. *Curr. Med. Chem.* **2003**, *10*, 1005-1019.

(38) Lloyd, M. D.; Lee, H.-J.; Harlos, K.; Zhang, Z.-H.; Baldwin, J. E.; Schofield, C. J.; Charnock, J. M.; Garner, C. D.; Hara, T.; van Scheltinga, A. C. T.; Valegård, K.; Viklund, J. A. C.; Hajdu, J.; Andersson, I.; Danielsson, Å.; Bhikhabhai, R. *J. Mol. Biol.* **1999**, *287*, 943-960.

(39) Cosper, N. J.; Stålhandske, C. M. V.; Saari, R. E.; Hausinger, R. P.; Scott, R. A. *J. Biol. Inorg. Chem.* **1999**, *4*, 122-129.

(40) Purpero, V.; Moran, G. R. *JBIC, J. Biol. Inorg. Chem.* **2007**, *12*, 587-601.

(41) Ho, R. Y. N.; Mehn, M. P.; Hegg, E. L.; Liu, A.; Ryle, M. J.; Hausinger, R. P.; Que, L., Jr. *J. Am. Chem. Soc.* **2001**, *123*, 5022-5029.

(42) Valegård, K.; vanScheltinga, A. C. T.; Lloyd, M. D.; Hara, T.; Ramaswamy, S.; Perrakis, A.; Thompson, A.; Lee, H.-J.; Baldwin, J. E.; Schofield, C. J.; Hajdu, J.; Andersson, I. *Nature* **1998**, *394*, 805-809.

(43) Zhang, Z.; Ren, J.; Stammers, D. K.; Baldwin, J. E.; Harlos, K.; Schofield, C. J. *Nat. Struct. Biol.* **2000**, *7*, 127-133.

(44) Wilmouth, R. C.; Turnbull, J. J.; Welford, R. W. D.; Clifton, I. J.; Prescott, A. G.; Schofield, C. J. *Structure* **2002**, *10*, 93-103.

(45) Ryle, M. J.; Padmakumar, R.; Hausinger, R. P. *Biochemistry* **1999**, *38*, 15278-15286.

(46) Elkins, J. M.; Ryle, M. J.; Clifton, I. J.; Hotopp, J. C. D.; Lloyd, J. S.; Burzlaff, N. I.; Baldwin, J. E.; Hausinger, R. P.; Roach, P. L. *Biochemistry* **2002**, *41*, 5185-5192.

(47) Pavel, E. G.; Zhou, J.; Busby, R. W.; Gunsior, M.; Townsend, C. A.; Solomon, E. I. *J. Am. Chem. Soc.* **1998**, *120*, 743-753.

(48) Borowski, T.; Bassan, A.; Siegbahn, P. E. M. *Chem. Eur. J.* **2004**, *10*, 1031-1041.

(49) Bassan, A.; Borowski, T.; Siegbahn, P. E. M. *Dalton Trans.* **2004**, 3153-3162.

(50) Price, J. C.; Barr, E. W.; Tirupati, B.; Bollinger, J. M., Jr.; Krebs, C. *Biochemistry* **2003**, *42*, 7497-7508.

(51) Riggs-Gelasco, P. J.; Price, J. C.; Guyer, R. B.; Brehm, J. H.; Barr, E. W.; Bollinger, J. M., Jr.; Krebs, C. *J. Am. Chem. Soc.* **2004**, *126*, 8108-8109.

(52) Proshlyakov, D. A.; Henshaw, T. F.; Monterosso, G. R.; Ryle, M. J.; Hausinger, R. P. *J. Am. Chem. Soc.* **2004**, *126*, 1022-1023.

(53) Price, J. C.; Barr, E. W.; Glass, T. E.; Krebs, C.; Bollinger, J. M., Jr. *J. Am. Chem. Soc.* **2003**, *125*, 13008-13009.

(54) Price, J. C.; Barr, E. W.; Hoffart, L. M.; Krebs, C.; Bollinger, J. M., Jr. *Biochemistry* **2005**, *44*, 8138-8147.

(55) Bollinger, J. M., Jr.; Price, J. C.; Hoffart, L. M.; Barr, E. W.; Krebs, C. *Eur. J. Inorg. Chem.* **2005**, 4245-4254.

(56) Hoffart, L. M.; Barr, E. W.; Guyer, R. B.; Bollinger, J. M., Jr.; Krebs, C. *Proc. Natl. Acad. Sci. U. S. A.* **2006**, *103*, 14738-14743.

(57) Sinnecker, S.; Svensen, N.; Barr, E. W.; Ye, S.; Bollinger, J. M., Jr.; Neese, F.; Krebs, C. *J. Am. Chem. Soc.* **2007**, *129*, 6168-6179.

(58) Krebs, C.; Galonić Fujimori, D.; Walsh, C. T.; Bollinger, J. M., Jr. *Acc. Chem. Res.* **2007**, *40*, 484-492.

(59) Groves, J. T.; Han, Y.-Z. In *Cytochrome P450: Structure, Mechanism, and Biochemistry*; 2nd ed.; Ortiz de Montellano, P. R., Ed.; Plenum Press: New York, 1995, p 3-48.

(60) Galonic Fujimori, D.; Barr, E. W.; Matthews, M. L.; Koch, G. M.; Yonce, J. R.; Walsh, C. T.; Bollinger, J. M., Jr.; Krebs, C.; Riggs-Gelasco, P. J. *J. Am. Chem. Soc.* **2007**, *129*, 13408-13409.

(61) Vaillancourt, F. H.; Vosburg, D. A.; Walsh, C. T. *Chem. Bio. Chem.* **2006**, *7*, 748-752.

(62) Kumar, D.; de Visser, S. P.; Shaik, S. *J. Am. Chem. Soc.* **2004**, *126*, 5072-5073.

(63) Hull, J. F.; Balcells, D.; Sauer, E. L. O.; Raynaud, C.; Brudvig, G. W.; Crabtree, R. H.; Eisenstein, O. *J. Am. Chem. Soc.* **2010**, *132*, 7605-7616.

(64) Usharani, D.; Janardanan, D.; Shaik, S. *J. Am. Chem. Soc.* **2011**, *133*, 176-179.

(65) Beck, A.; Weibert, B.; Burzlaff, N. I. *Eur. J. Inorg. Chem.* **2001**, 521-527.

(66) Beck, A.; Barth, A.; Hu1bner, E.; Burzlaff, N. *Inorg. Chem.* **2003**, *42*, 7182-7188.

(67) Müller, R.; Hübner, E.; Burzlaff, N. *Eur. J. Inorg. Chem.* **2004**, *2004*, 2151-2159.

(68) Bruijnincx, P. C. A.; Buurmans, I. L. C.; Gosiewska, S.; Moelands, M. A. H.; Lutz, M.; Spek, A. L.; Koten, G. v.; Klein Gebbink, R. J. M. *Chem. Eur. J.* **2008**, *14*, 1228-1237.

(69) Bruijnincx, P. C. A.; Lutz, M.; Spek, A. L.; Faassen, E. E. v.; Weckhuysen, B. M.; Koten, G. v.; Klein Gebbink, R. J. M. *Eur. J. Inorg. Chem.* **2005**, 779-787.

(70) Que, L., Jr. *Acc. Chem. Res.* **2007**, *40*, 493-500.

(71) Grapperhaus, C. A.; Mienert, B.; Bill, E.; Weyhermüller, T.; Wieghardt, K. *Inorg. Chem.* **2000**, *39*, 5306-5317.

(72) Rohde, J.-U.; In, J.-H.; Lim, M. H.; Brennessel, W. W.; Bukowski, M. R.; Stubna, A.; Münck, E.; Nam, W.; Que, L., Jr. *Science* **2003**, *299*, 1037-1039.

(73) England, J.; Guo, Y.; Farquhar, E. R.; Young, V. G., Jr.; Munck, E.; Que, L., Jr. *J. Am. Chem. Soc.* **2010**, *132*, 8635-8644.

(74) Pestovsky, O.; Stoian, S.; Bominaar, E. L.; Shan, X.; Münck, E.; Que, L., Jr.; Bakac, A. *Angew. Chem. Int. Ed.* **2005**, *44*, 6871-6874.

(75) Hirao, H.; Kumar, D.; Que, L., Jr.; Shaik, S. *J. Am. Chem. Soc.* **2006**, *128*, 8590-8606.

(76) Decker, A.; Rohde, J.-U.; Klinker, E. J.; Wong, S. D.; Que, L., Jr.; Solomon, E. I. *J. Am. Chem. Soc.* **2007**, *129*, 15983-15996.

(77) Ye, S.; Neese, F. *Curr. Op. Chem. Biol.* **2009**, *13*, 89-98.

(78) England, J.; Martinho, M.; Farquhar, E. R.; Frisch, J. R.; Bominaar, E. L.; Münck, E.; Que, L., Jr. *Angew. Chem. Int. Ed.* **2009**, *48*, 3622-3626.

(79) Chiou, Y.-M.; Que, L., Jr. *J. Am. Chem. Soc.* **1992**, *114*, 7567-7568.

(80) Chiou, Y.-M.; Que, L., Jr. *J. Am. Chem. Soc.* **1995**, *117*, 3999-4013.

(81) Ha, E. H.; Ho, R. Y. N.; Kesiel, J. F.; Valentine, J. S. *Inorg. Chem.* **1995**, *34*, 2265-2266.

(82) Hikichi, S.; Ogihara, T.; Fujisawa, K.; Kitajima, N.; Akita, M.; Moro-Oka, Y. *Inorg. Chem.* **1997**, *36*, 4539-4547.

(83) Hegg, E. L.; Ho, R. Y. N.; Que, L., Jr. *J. Am. Chem. Soc.* **1999**, *121*, 1972-1973.

(84) Mehn, M. P.; Fujisawa, K.; Hegg, E. L.; Que, L., Jr. *J. Am. Chem. Soc.* **2003**, *125*, 7828-7842.

(85) Lunsford, J. H. *Catal. Today* **2000**, *63*, 165-174.

(86) Neumann, R.; Abu-Gnim, C. *Chem. Commun.* **1989**, 1324-5.

(87) Conley, B. L.; Tenn, W. J.; Young, K. J. H.; Ganesh, S. K.; Meier, S. K.; Ziatdinov, V. R.; Mironov, O.; Oxgaard, J.; Gonzales, J.; Goddard, W. A.; Periana, R. A. *J. Mol. Catal. A: Chem.* **2006**, *251*, 8-23.

(88) Cook, B. R.; Reinert, T. J.; Suslick, K. S. *J. Am. Chem. Soc.* **1986**, *108*, 7281-6.

(89) Collman, J. P.; Zhang, X.; Lee, V. J.; Uffelman, E. S.; Brauman, J. I. *Science* **1993**, *261*, 1404-1411.

(90) Bhyrappa, P.; Young, J. K.; Moore, J. S.; Suslick, K. S. *J. Am. Chem. Soc.* **1996**, *118*, 5708-5711.

(91) Groves, J. T.; Nemo, T. E. *J. Am. Chem. Soc.* **1983**, *105*, 5786-91.

(92) Groves, J. T.; Myers, R. S. *J. Am. Chem. Soc.* **1983**, *105*, 5791-5796.

(93) Groves, J. T.; Nemo, T. E. *J. Am. Chem. Soc.* **1983**, *105*, 6243-6248.

(94) Nappa, M. J.; Tolman, C. A. *Inorg. Chem.* **1985**, *24*, 4711-4719.

(95) Mansuy, D.; Bartoli, J. F.; Momenteau, M. *Tetrahedron Lett.* **1982**, *23*, 2781-4.

(96) Chen, M. S.; White, M. C. *Science* **2007**, *318*, 783-787.

(97) Kaizer, J.; Klinker, E. J.; Oh, N. Y.; Rohde, J.-U.; Song, W. J.; Stubna, A.; Kim, J.; Münck, E.; Nam, W.; Que, L., Jr. *J. Am. Chem. Soc.* **2004**, *126*, 472-473.

(98) Wang, D.; Farquhar, E. R.; Stubna, A.; Muenck, E.; Que, L., Jr. *Nat. Chem.* **2009**, *1*, 145-150, S145/1-S145/15.

(99) Trofimenko, S. *Chem. Rev.* **1993**, *93*, 943-980.

(100) Armarego, W. L. F.; Perrin, D. D. *Purification of Laboratory Chemicals*; Butterworth-Heinemann: Oxford, 1997.

(101) Mukherjee, A.; Martinho, M. é.; Bominaar, E. L.; M ünck, E.; Que, L., Jr. *Angew. Chem. Int. Ed.* **2009**, *48*, 1780-1783.

(102) Bryant, J. R.; Mayer, J. M. *J. Am. Chem. Soc.* **2003**, *125*, 10351-10361.

(103) Schofield, C. J.; Zhang, Z. *Curr. Opin. Struct. Biol.* **1999**, *9*, 722-731.

(104) Luo, Y.-R. *Comprehensive Handbook of Chemical Bond Energies*; Taylor & Francis: Boca Raton;, 2007.

(105) Borowski, T.; Bassan, A.; Siegbahn, P. E. M. *Inorg. Chem.* **2004**, *43*, 3277-3291.

(106) Janardanan, D.; Wang, Y.; Schyman, P.; Que, L.; Shaik, S. *Angew. Chem., Int. Ed.* **2010**, *49*, 3342-3345.

(107) Bigi, M. A.; Reed, S. A.; White, M. C. *Nat. Chem.* **2011**, *3*, 216-222.

(108) Kitajima, N.; Tolman, W. B. *Prog. Inorg. Chem.* **1995**, *43*, 419-531.

(109) Das, S.; Brudvig, G. W.; Crabtree, R. H. *Chem. Commun.* **2008**, 413-424.

(110) Shanklin, J.; Achim, C.; Schmidt, H.; Fox, B. G.; Münck, E. *Proc. Natl. Acad. Sci. USA* **1997**, *94*, 2981-2986.

(111) Khenkin, A. M.; Shteinman, A. A. *J. Chem. Soc., Chem. Commun.* **1984**, 1219-1220.

(112) Das, S.; Incarvito, C. D.; Crabtree, R. H.; Brudvig, G. W. *Science* **2006**, *3112*, 1941-1943.

(113) Mukherjee, A.; Cranswick, M. A.; Chakrabarti, M.; Paine, T. K.; Fujisawa, K.; MuÌˆnck, E.; Que, L. *Inorg. Chem.* **2010**, *49*, 3618-3628.

(114) van, d. D. W. A.; Krebs, C.; Bollinger, J. M., Jr. *Curr. Opin. Struct. Biol.* **2010**, *20*, 673-683.

(115) Bollinger, J. M., Jr.; Krebs, C. *Curr. Opin. Chem. Biol.* **2007**, *11*, 151-158.

(116) Tinberg, C. E.; Lippard, S. J. *Acc. Chem. Res.* **2011**, *44*, 280-288.

(117) Cicchillo, R. M.; Zhang, H.; Blodgett, J. A. V.; Whitteck, J. T.; Li, G.; Nair, S. K.; van der Donk, W. A.; Metcalf, W. W. *Nature* **2009**, *459*, 871-874.

(118) Paine, T. K.; Paria, S.; Que Jr, L. *Chemical Communications* **2010**, *46*, 1830-1832.

(119) Kovaleva, E. G.; Lipscomb, J. D. *Science* **2007**, *316*, 453-457.

(120) Mbughuni, M. M.; Chakrabarti, M.; Hayden, J. A.; Bominaar, E. L.; Hendrich, M. P.; Münck, E.; Lipscomb, J. D. *Proc. Natl. Acad. Sci. U. S. A.* **2010**, *107*, 16788-16793, S16788/1-S16788/7.

(121) Bollinger, J. M., Jr.; Diao, Y.; Matthews, M. L.; Xing, G.; Krebs, C. *Dalton Trans.* **2009**, 905-914.

(122) Brown, P. M.; Caradoc-Davies, T. T.; Dickson, J. M. J.; Cooper, G. J. S.; Loomes, K. M.; Baker, E. N. *Proc. Natl. Acad. Sci. USA* **2006**, *103*, 15032-15037.

(123) Xing, G.; Barr, E. W.; Diao, Y.; Hoffart, L. M.; Prabhu, K. S.; Arner, R. J.; Reddy, C. C.; Krebs, C.; Bollinger, J. M., Jr. *Biochemistry* **2006**, *45*, 5402-5412.

(124) Xing, G.; Diao, Y.; Hoffart, L. M.; Barr, E. W.; Prabhu, K. S.; Arner, R. J.; Reddy, C. C.; Krebs, C.; Bollinger, J. M., Jr. *Proc. Natl. Acad. Sci. U. S. A.* **2006**, *103*, 6130-6135.

(125) Shan, X.; Que, L., Jr. *Proc. Natl. Acad. Sci. U. S. A.* **2005**, *102*, 5340-5345.

(126) Würtele, C.; Gaoutchenova, E.; Harms, K.; Holthausen, M. C.; Sundermeyer, J.; Schindler, S. *Angew. Chem. Int. Ed.* **2006**, *45*, 3867-3869.

(127) Maiti, D.; Fry, H. C.; Woertink, J. S.; Vance, M. A.; Solomon, E. I.; Karlin, K. D. *J. Am. Chem. Soc.* **2007**, *129*, 264-265.

(128) Maiti, D.; Lee, D.-H.; Gaoutchenova, K.; Würtele, C.; Holthausen, M. C.; Sarjeant, A. A. N.; Sundermeyer, J.; Schindler, S.; Karlin, K. D. *Angew. Chem. Int. Ed.* **2008**, *47*, 82-85.

(129) Kunishita, A.; Kubo, M.; Sugimoto, H.; Ogura, T.; Sato, K.; Takui, T.; Itoh, S. *J. Am. Chem. Soc.* **2009**, *131*, 2788-2789.

(130) Zhao, M.; Helms, B.; Slonkina, E.; Friedle, S.; Lee, D.; DuBois, J.; Hedman, B.; Hodgson, K. O.; Fréchet, J. M. J.; Lippard, S. J. *J. Am. Chem. Soc.* **2008**, *130*, 4352-4363.

(131) Kitajima, N.; Fukui, H.; Moro-oka, Y.; Mizutani, Y.; Kitagawa, T. *J. Am. Chem. Soc.* **1990**, *112*, 6402-6403.

(132) Blessing, R. *Acta.. Cryst.* **1995**, *A51*, 33-38.

(133) SAINT+ V6.45; Bruker Analytical X-Ray Systems: Madison, WI, 2003.

(134) SHELXTL V6.14; Bruker Analytical X-Ray Systems: Madison, WI, 2000.

(135) Paine, T. K.; Zheng, H.; Que, L., Jr. *Inorg. Chem.* **2005**, *44*, 474-476.

(136) Kitajima, N.; Tamura, N.; Amagai, H.; Fukui, H.; Moro-oka, Y.; Mizutani, Y.; Kitagawa, T.; Mathur, R.; Heerwegh, K.; Reed, C. A.; Randall, C. R.; Que, L., Jr.; Tatsumi, K. *J. Am. Chem. Soc.* **1994**, *116*, 9071-9085.

(137) Kitajima, N.; Osawa, M.; Tanaka, M.; Moro-oka, Y. *J. Am. Chem. Soc.* **1991**, *113*, 8952-8953.

(138) Reinaud, O. M.; Theopold, K. H. *J. Am. Chem. Soc.* **1994**, *116*, 6979-6980.

(139) Goldsmith, C. R.; Jonas, R. T.; Stack, T. D. P. *J. Am. Chem. Soc.* **2002**, *124*, 83-96.

(140) Roelfes, G.; Lubben, M.; Chen, K.; Ho, R. Y. N.; Meetsma, A.; Genseberger, S.; Hermant, R. M.; Hage, R.; Mandal, S. K.; Young, V. G., Jr.; Zang, Y.; Kooijman, H.; Spek, A. L.; Que, L., Jr.; Feringa, B. L. *Inorg. Chem.* **1999**, *38*, 1929-1936.

(141) Kim, K.; Lippard, S. J. *J. Am. Chem. Soc.* **1996**, *118*, 4914-4915.

(142) Girerd, J.-J.; Banse, F.; Simaan, A. J. *Struct. Bonding* **2000**, *97*, 145-177.

(143) Fiedler, A. T.; Shan, X.; Mehn, M. P.; Kaizer, J.; Torelli, S.; Frisch, J. R.; Kodera, M.; Que, L., Jr. *J. Phys. Chem. A* **2008**, *112*.

(144) Zhang, X.; Furutachi, H.; Fujinami, S.; Nagatomo, S.; Maeda, Y.; Watanabe, Y.; Kitagawa, T.; Suzuki, M. *J. Am. Chem. Soc.* **2005**, *127*, 826-827.

(145) Modarelli, D. A.; Rossitto, F. C.; Lahti, P. M. *Tetrahedron Lett.* **1989**, *30*, 4473-6.

(146) Sastri, C. V.; Lee, J.; Oh, K.; Lee, Y. J.; Lee, J.; Jackson, T. A.; Ray, K.; Hirao, H.; Shin, W.; Halfen, J. A.; Kim, J.; Que, L., Jr.; Shaik, S.; Nam, W. *Proc. Natl. Acad. Sci. U. S. A.* **2007**, *104*, 19181-19186.

(147) Wheatley, M. S. *Experientia* **1956**, *12*, 339-340.

(148) Chiang, Y.; Kresge, A. J.; Pruszynski, P. *J. Am. Chem. Soc.* **1992**, *114*, 3103-3107.

(149) Lide, D. R. In *CRC Handbook of Chemistry and Physics*; 73rd ed. ed.; CRC Press:: Boca Raton, FL, 1992, p 8-39.

(150) Lee, Y.-M.; Hong, S.; Morimoto, Y.; Shin, W.; Fukuzumi, S.; Nam, W. *J. Am. Chem. Soc.* **2010**, *132*, 10668-10670.

(151) Hong, S.; Lee, Y.-M.; Shin, W.; Fukuzumi, S.; Nam, W. *J. Am. Chem. Soc.* **2009**, *131*, 13910-13911.

(152) Kovaleva, E. G.; Neibergall, M. B.; Chakrabarty, S.; Lipscomb, J. D. *Acc. Chem. Res.* **2007**, *40*, 475-483.

(153) Neibergall, M. B.; Stubna, A.; Mekmouche, Y.; Munck, E.; Lipscomb, J. D. *Biochemistry* **2007**, *46*, 8004-8016.

(154) Wolfe, M. D.; Altier, D. J.; Stubna, A.; Popescu, C. V.; Münck, E.; Lipscomb, J. D. *Biochemistry* **2002**, *41*, 9611-9626.

(155) Bochevarov, A. D.; Li, J.; Song, W. J.; Friesner, R. A.; Lippard, S. J. *J. Am. Chem. Soc.* **2011**, *133*, 7384-7397.

(156) Wallar, B. J.; Lipscomb, J. D. *Chem. Rev.* **1996**, *96*, 2625-2658.

(157) Stubbe, J. *J. Biol. Chem.* **1990**, *265*, 5329-5332.

(158) Yamashita, M.; Furutachi, H.; Tosha, T.; Fujinami, S.; Saito, W.; Maeda, Y.; Takahashi, K.; Tanaka, K.; Kitagawa, T.; Suzuki, M. *J. Am. Chem. Soc.* **2007**, *129*, 2-3.

(159) Murray, L. J.; Garcia-Serres, R.; Naik, S.; Huynh, B. H.; Lippard, S. J. *J. Am. Chem. Soc.* **2006**, *128*, 7458-7459.

(160) Murray, L. J.; Naik, S. G.; Ortillo, D. O.; Garca-Serres, R.; Lee, J. K.; Huynh, B. H.; Lippard, S. J. *J. Am. Chem. Soc.* **2007**, *129*, 14500-14510.

(161) Do, L. H.; Hayashi, T.; Moenne-Loccoz, P.; Lippard, S. J. *J. Am. Chem. Soc.* **2010**, *132*, 1273-1275.

(162) LeCloux, D. D.; Barrios, A. M.; Lippard, S. J. *Bioorg. Med. Chem.* **1999**, *7*, 763-772.

(163) Xue, G.; Fiedler, A. T.; Martinho, M.; Münck, E.; Que, L., Jr. *Proc. Natl. Acad. Sci. USA* **2008**, *105*, 20615-20620.

(164) Lee, S.-K.; Nesheim, J. C.; Lipscomb, J. D. *J. Biol. Chem.* **1993**, *268*, 21569-21577.

(165) Liu, K. E.; Wang, D.; Huynh, B. H.; Edmondson, D. E.; Salifoglou, A.; Lippard, S. J. *J. Am. Chem. Soc.* **1994**, *116*, 7465-7466.

(166) Lee, S.-K.; Fox, B. G.; Froland, W. A.; Lipscomb, J. D.; Münck, E. *J. Am. Chem. Soc.* **1993**, *115*, 6450-6451.

(167) Xue, G.; De, H. R.; Münck, E.; Que, L., Jr. *Nat. Chem.* **2010**, *2*, 400-405.

(168) Chen, K.; Que, L., Jr. *J. Am. Chem. Soc.* **2001**, *123*, 6327-6337.

(169) Kartha, J. S.; Skordos, K. W.; Sun, H.; Hall, C.; Easterwood, L. M.; Reilly, C. A.; Johnson, E. F.; Yost, G. S. *Biochemistry* **2008**, *47*, 9756-9770.

(170) Jin, Y.; Lipscomb, J. D. *J. Biol. Inorg. Chem.* **2001**, *6*, 717-725.

(171) Thibon, A.; England, J.; Martinho, M.; Young, V. G., Jr.; Frisch, J. R.; Guillot, R.; Girerd, J.-J.; Münck, E.; Que, L., Jr.; Banse, F. *Angew. Chem. Int. Ed.* **2008**, *47*, 7064-7067.

(172) Enthaler, S.; Junge, K.; Beller, M. *Angew. Chem. Int. Ed.* **2008**, *47*, 3317-3321.

(173) Lacy, D. C.; Gupta, R.; Stone, K. L.; Greaves, J.; Ziller, J. W.; Hendrich, M. P.; Borovik, A. S. *J. Am. Chem. Soc.* **2010**, *132*, 12188-12190.

Appendix I

We noted that addition of hydrocarbons did not significantly affect the one hour reaction time between complex **1** and oxygen. In fact, the rate determining step likely leads to the formation of the putative Fe^{IV}=O oxidant, so the relative amounts of **2** and interception product observed would then reflect the relative rates of intramolecular and intermolecular interception of the oxidant. Therefore the yield of interception must provide an indirect method to calculate the relative rate of substrate oxidation with respect to ligand hydroxylation. As rate determining step was the oxygen binding, ligand hydroxylation rate was not possible to calculate but semi-empirical calculation provided the factor to which substrate oxidation was favored over ligand hydroxylation at room temperature

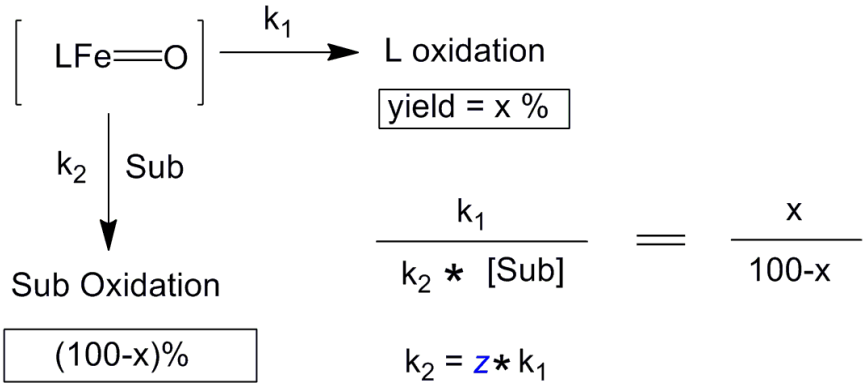

Table A2.1 Summarizes the factor z for diverse substrates.

Substrate	Concentration of substrate [M]	% of interception	'z' corrected with equivalent hydrogen atoms
c-Hexene	0.001	40	170
9,10-DHA	0.05	70	10
1,2-DHN	0.002	45	100
THF	0.05	55	6
c-Octane	0.2	40	2×10^{-1}
c-Hexane	1	30	4×10^{-2}
n-Heptane	0.5	55	4×10^{-1}
n-Octane	0.5	55	4×10^{-1}
TMS	1	25	3×10^{-2}
c-Hexene-d_{10}	0.001	40	170
THF-d_8	0.2	45	1
n-Octane-d_6	1	0	
c-Hexane-d_{12}	1	0	

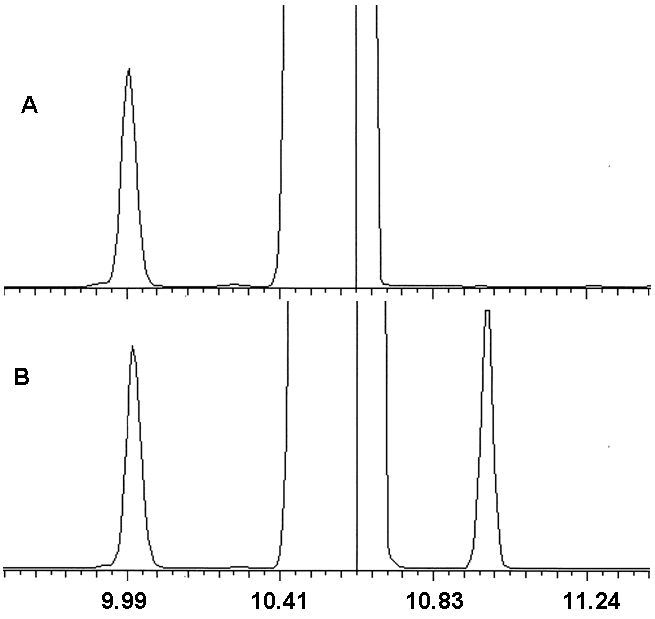

Figure A1. GC analysis of n-octane reaction, X-axis shows retention time in min. A) Analysis of the product solution, showing 1-octene at 10 min. B) Analysis of the product solution doped with *cis*-2-octene (10.95 min). Huge peak corresponds to substrate octane.

Appendix II

Bibliography

Publications

- **Anusree Mukherjee**, Matthew A. Cranswick, Mrinmoy Chakrabarti, Tapan Paine, Kiyoshi Fujisawa, Eckard Münck, Lawrence Que Jr., "Oxygen Activation at Mononuclear Nonheme Iron Centers: A Superoxo Perspective" *Inorg. Chem.* **2010,** *49,* 3618-3628 (***Most Accesssed Article*** in Q2 of Inorganic Chemistry)
- **Anusree Mukherjee,** Marlène Martinho, Emile L. Bominaar, Eckard Münck, Lawrence Que Jr., "Shape-selective Interception by Hydrocarbons of the O_2-Derived Oxidant of a Bio-mimetic Nonheme Iron Complex"; *Angew. Chem. Int Ed*. 2009, *48*, 1780-1783 (Selected as ***Very Important Paper*** by Reviewers)

Selective Presentations

- **Anusree Mukherjee**, Marlène Martinho, Emile L. Bominaar, Eckard Münck, Lawrence Que Jr., "A Bio-inspired Iron Complex that Oxidizes Hydrocarbons Shape-selectively" presented at 239th ACS National Meeting, San Francisco, CA, March 21-25, 2010 (Oral Presentation)
- **Anusree Mukherjee,** Matthew A. Cranswick, Tapan Paine, Kiyoshi Fujisawa, Lawrence Que Jr., "Modeling Nonheme Iron Enzymes: Indirect Evidence of a Putative Iron-superoxo Intermediate" presented at 239th ACS National Meeting, San Francisco, CA, March 21-25, 2010 (Poster Presentation, this poster was also selected for the presentation in SCI-MIX)
- **Anusree Mukherjee**, Marlène Martinho, Emile L. Bominaar, Eckard Münck, Lawrence Que Jr., "Shape-selective Oxidation of Hydrocarbons by a Nonheme Bio-mimetic Iron Complex" presented at Student Scholar Showcase, Minneapolis, University of Minnesota, January 2009 (invited seminar, Poster Presentation)
- **Anusree Mukherjee**, Marlène Martinho, Eckard Münck, Lawrence Que Jr., "Modeling α-KG dependent Enzymes using Tp Ligands" presented at CBITG Symposium, St. Paul, University of Minnesota, May 2009 (Poster Presentation)
- **Anusree Mukherjee**, Marlène Martinho, Eckard Münck, Lawrence Que Jr., "Hydrocarbon Oxidation by a Functional Model of α-KG dependent Enzymes" presented at 235th ACS National Meeting, New Orleans, LA, April 6-10, 2008 (Poster Presentation)